

**Investigation into the dynamic
nature of the pyrenoid of
*Chlamydomonas reinhardtii***

Eleanor Fletcher

MSc by Research
University of York
Biology

September 2020

Abstract

Our rising global population requires innovation to increase crop yields and provide food security. One promising solution is to improve the performance of Rubisco, an important enzyme which fixes CO_2 into organic matter. In our current atmosphere, O_2 competes with CO_2 at the active site of Rubisco, leading to the energetically wasteful process of photorespiration. To overcome this problem, single-celled photosynthetic eukaryotes have evolved a biophysical CO_2 -concentrating mechanism (CCM) to concentrate CO_2 around Rubisco. Critical to CCM function is the assembly of Rubisco into a liquid-liquid phase separated (LLPS) organelle called the pyrenoid. Rubisco is packaged with its linker protein Essential Pyrenoid Component 1 (EPYC1) to form the pyrenoid matrix, which is surrounded by a starch sheath. This study aims to investigate the mobility of pyrenoid components including Rubisco under different growth conditions, using Fluorescence Recovery After Photobleaching (FRAP). A dual-tagged Rubisco-starch line was created to simultaneously observe Rubisco and starch movement during cell division, using time-lapse confocal microscopy. The modification of the starch sheath during pyrenoid division was further investigated using a bioinformatics approach, revealing potential candidates involved in pyrenoid starch degradation and synthesis. It is hypothesised that HCO_3^- delivery to the pyrenoid matrix requires conversion from CO_2 by low- CO_2 -inducible proteins LCIB/C, and transport across thylakoids by Bestrophin-like proteins (BST1-3). The role of these complexes in recycling escaping CO_2 is explored. Preliminary results allow further investigation into the dynamic nature of the pyrenoid, which will help guide current efforts to engineer a pyrenoid into higher plants.

Table of Contents

Abstract.....	2
Table of Contents.....	3
List of Tables.....	5
List of Figures.....	6
Acknowledgements.....	7
Declaration.....	8
Chapter 1: Introduction.....	9
Efficient photosynthesis can be achieved by utilising CO ₂ -concentrating mechanisms.....	9
The CCM in Chlamydomonas involves an organelle called the pyrenoid.....	11
C _i transporters and carbonic anhydrases are needed for a functional CCM.....	12
The pyrenoid is further categorised into substructures which have individual roles in the CCM.....	14
The Chlamydomonas CCM may be engineered into higher plants to increase crop yields.....	16
Project aims.....	16
Chapter 2: Preliminary investigation into the mobilities of Rubisco, LCIB and LC19.....	17
Chapter summary.....	17
Introduction.....	17
Methods.....	21
Results.....	22
Discussion.....	26
Chapter 3: Pyrenoid starch sheath dynamics during division.....	31
Chapter summary.....	31
Introduction.....	31
Methods.....	37
Results.....	40
Discussion.....	53
Chapter 4: LCIB/C and BST1-3 may interact to aid inorganic carbon recycling.....	61
Chapter summary.....	61
Introduction.....	61
Methods.....	66
Results.....	68

Discussion.....	70
Chapter 5: Final conclusions and future perspectives.....	73
Insights revealed into the dynamic nature of the pyrenoid and progress made in this study.....	73
The work in this study enables future investigation into the dynamic nature of the pyrenoid.....	74
The work in this study may aid engineering of the pyrenoid into higher plants.....	76
Final conclusion.....	77
Supplementary materials.....	78
References.....	86

List of Tables

Table 1. Proteins involved in starch synthesis in <i>Arabidopsis thaliana</i> showed homology to starch synthesis proteins in <i>Chlamydomonas reinhardtii</i>	44
Table 2. Disorder profiles, PFAM annotations and coiled-coil probabilities for Chlamydomonas candidates potentially involved in starch synthesis during or after division.....	47
Table 3. Proteins involved in starch degradation in <i>Arabidopsis thaliana</i> showed homology to starch degradation proteins in <i>Chlamydomonas reinhardtii</i>	50
Table 4. Proposed combinations of Chlamydomonas transformations using already available Chlamydomonas lines and recombineered plasmids from this study.....	70

List of Figures

Figure 1. Schematic depiction of competing reactions of CO ₂ and O ₂ with Rubisco.....	10
Figure 2. Schematic depiction of key structures in Chlamydomonas and key pyrenoid proteinaceous structures.....	11
Figure 3. Schematic depiction of C _i transport to Rubisco under very low-CO ₂ conditions and low-CO ₂ conditions.....	12
Figure 4. Rubisco-Venus mobility was similar between photoautotrophic and heterotrophic growth conditions.....	23
Figure 5. Re-homogenisation of LC19 occurred after FRAP however recovery was subtle...25	
Figure 6. Overview of Chlamydomonas life cycle and key steps in starch synthesis and degradation.....	33
Figure 7. Rubisco-Venus disperses and <i>de novo</i> -formed puncta fuse during division.....	41
Figure 8. Representative stages of cell division with dual tagged Rubisco-Venus and STA2-mCherry.....	42
Figure 9. mRNA abundance profiles for proteins known to be involved in chloroplast division.....	45
Figure 10. Chlamydomonas proteins proposed to be involved in starch synthesis with peak normalised mRNA abundance during the dark phase.....	46
Figure 11. CBM-containing proteins with peak normalised mRNA abundance during the division window.....	49
Figure 12. Chlamydomonas proteins potentially involved in starch degradation with peak normalised mRNA abundance during the division window.....	52
Figure 13. mRNA abundance profiles of CCM genes and previously characterised pyrenoid starch-associated proteins.....	53
Figure 14. Hypothetical models of pyrenoid starch dynamics during pyrenoid fission.....	59
Figure 15. C _i recycling by LCIB/C, BST1-3 and CAH3 allows CO ₂ to be released in close proximity to Rubisco whilst preventing CO ₂ escape from the pyrenoid matrix.....	63
Figure 16. Visual representation of recombineering method for LCIB-mScarlet-i.....	68
Figure 17. DNA gel electrophoresis of LCIB-mScarlet-i and BST1-mScarlet-i after restriction enzyme digest using SacI.....	69

Acknowledgements

I would like to thank everyone in the Mackinder lab for their support during my MSc by Research. In particular, I would like to thank my supervisor Dr. Luke Mackinder for his unending enthusiasm and encouragement throughout the project. Despite the isolation that 2020 brought, Luke continued to make me feel part of a team and provided fantastic advice and support in unprecedented times. I am extremely grateful for the skills he taught me, and for giving me this opportunity.

I want to thank the post-docs in the lab, whose guidance went beyond science. Thank you to Dr. Charlotte Walker for her patient teaching and her words of wisdom: "it's a marathon, not a sprint!" Thank you also to Dr. Gary Yates who taught me the value of absorbing 'espresso shots' of relevant information, and for being equally as excited at getting some great microscopy images. Thank you both for your pep-talks, they were a source of great encouragement. Thank you also to Dr. Irina Grouneva for always pointing me in the right direction in the lab, and to Dr. Philipp Girr for sharing your interesting plans.

The students in the lab also deserve my thanks. It was great to exchange ideas with James who never ceased to amaze me with his curiosity. Thank you to my bench buddy Christine for teaching me about recombineering, and to Max who always seemed to have a smile on his face.

To my friends and family, I could not have done this without you. In particular, my friends Kate, Claudia and Leah who were always there for me and for my mum and step-mum for their encouragement. Finally, I would like to thank my Dad for his unwavering support, without whom the completion of this project would not have been possible.

Declaration

I declare that this thesis is a presentation of original work and I am the sole author. This work has not previously been presented for an award at this, or any other, University. All sources are acknowledged as References.

Chapter 1: Introduction

Efficient photosynthesis can be achieved by utilising CO₂-concentrating mechanisms

Carbon fixation by photosynthesis contributes to almost all organic matter production in the biosphere (Field *et al.*, 1998). Oxygenic photosynthesis, the process of converting CO₂, H₂O and sunlight to organic matter and O₂ evolved over 2.8 billion years ago (De Marais, 2000). An important and abundant enzyme responsible for the fixation of CO₂ is Ribulose-1,5-bisphosphate carboxylase/oxygenase, known as Rubisco (Ellis, 1979). Three forms of Rubisco have been identified (I, II and III), which along with Rubisco-like proteins (form IV) have been proposed to evolve from a common ancestor, a methanogenic archaeon (Tabita *et al.*, 2008). Form I is the most abundant form of Rubisco, and is found in vascular plants, cyanobacteria and algae (Whitney *et al.*, 2011). Rubiscos in form I are found in a hexadecameric complex (L₈S₈), where two groups of four small subunits cap a core of eight large subunits (Taylor *et al.*, 2001; Whitney *et al.*, 2011). Rubisco carboxylates its substrate, Ribulose-1,5-bisphosphate to return two molecules of 3-phosphoglycerate (3PGA) in the Calvin-Benson-Bassham cycle (Bassham and Calvin, 1962; Taylor *et al.*, 2001). The reduction of 3PGA returns glyceraldehyde-3-phosphate (G3P), leading to the production of important sugars such as sucrose for growth (Stein and Granot, 2019) and glucose which is stored as starch (Smith and Zeeman, 2020) (Fig. 1).

However, photosynthesis is limited by Rubisco: its slow catalytic rate and low affinity for CO₂ mean Rubisco can only work at 25% of its catalytic capacity in C₃ plants (Caemmerer *et al.*, 1981; Sage *et al.*, 1987). Photosynthesis is also limited by photorespiration, a process whereby O₂ competes with CO₂ at the active site of Rubisco (Bauwe *et al.*, 2010). The evolution of oxygen-producing photosynthesis causing atmospheric levels of O₂ to rise is therefore an unfavourable paradox (Dismukes *et al.*, 2001). Photorespiration uses energy (adenosine triphosphate (ATP)) and reducing power (NADPH), whilst causing CO₂ losses of roughly 20% of net C₃ plant photosynthesis (Keys *et al.*, 1986; Cegelski and Schaefer, 2006; Peterhansel *et al.*, 2010) (Fig. 1). Therefore, photosynthetic organisms have subsequently evolved mechanisms to limit this wasteful process. C₄ plants have evolved to concentrate CO₂ around Rubisco by spatial separation of key processes; CO₂ is fixed to produce dicarboxylic acids in the cytosol of mesophyll cells, which are transported and decarboxylated in the location of Rubisco (Moroney and Ynalvez, 2007). This saturates the active site of Rubisco with CO₂, decreasing the likelihood of reaction with O₂ and photorespiration (Gowik *et al.*, 2011).

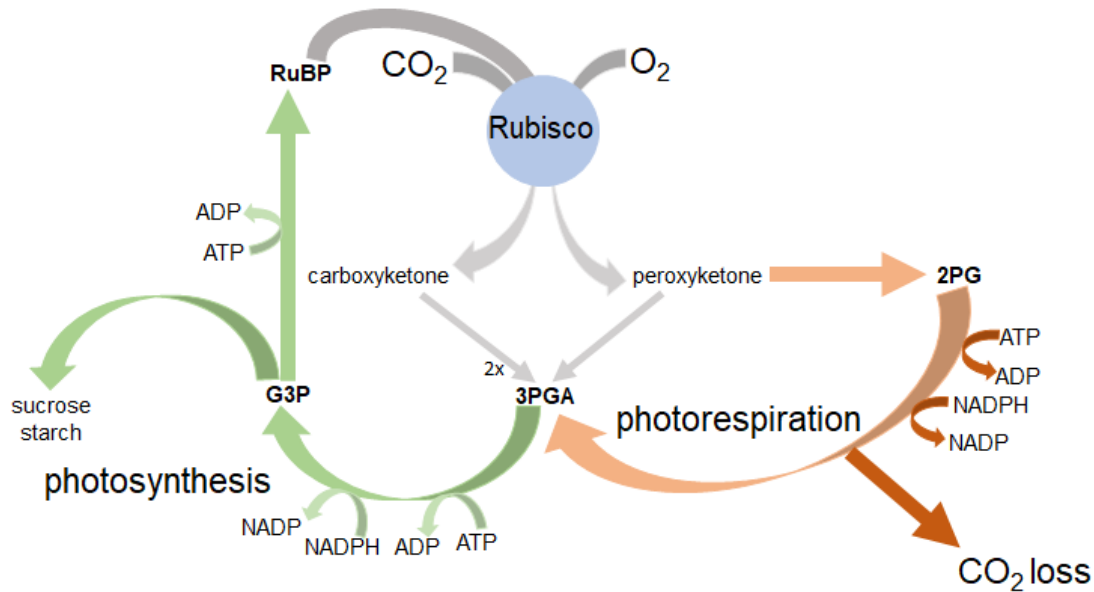


Figure 1. Schematic depiction of competing reactions of CO₂ and O₂ with Rubisco. The photosynthetic Calvin-Benson-Bassham cycle (green) involves the reaction of Rubisco with its substrates CO₂ and Ribulose-1,5-bisphosphate (RuBP). 2 molecules of 3-phosphoglycerate (3PGA) are produced and reduced to glyceraldehyde-3-phosphate (G3P) which is needed for the production for sucrose, glucose and starch or recycled back to RuBP. The wasteful process of photorespiration (orange) regenerates 3PGA via 2-phosphoglycerate (2PG), which utilises ATP and NADPH and causes CO₂ loss. Adapted from Whitney *et al.*, (2011).

Single-celled marine phototrophs, such as eukaryotic algae, have also evolved CO₂-concentrating mechanisms (CCMs) to increase the concentration of CO₂ around Rubisco (Meyer *et al.*, 2017). In addition to the limitations of Rubisco, CCMs are required in aquatic environments because inorganic carbon ($C_i = CO_2 + HCO_3^-$) levels fluctuate. Also, CO₂ diffuses 10,000 times slower in water than in air (Moroney and Ynalvez, 2007) and CO₂ concentrations vary with changing pH (Colman, 1989). Cyanobacteria, which also have CCMs, can accumulate internal C_i 500-1000-fold the concentration of external C_i (Colman, 1989) whilst the unicellular green alga *Chlamydomonas reinhardtii* (hereafter *Chlamydomonas*) has been shown to accumulate internal CO₂ by up to 40-fold compared to external concentrations (Badger *et al.*, 1980). This highly efficient photosynthetic strategy results in a significant contribution to global CO₂ fixation by eukaryotic algae, in the range of 30%-40% (Mackinder *et al.*, 2016).

The CCM in *Chlamydomonas* involves an organelle called the pyrenoid

The CCM in eukaryotic algae comprises a series of C_i transporters, conversion of C_i species by carbonic anhydrases and a mechanism to aggregate Rubisco. Central to the CCM in *Chlamydomonas* is a membrane-less organelle called the pyrenoid. The pyrenoid contains a proteinaceous matrix surrounded by a starch sheath, with traversing thylakoids which are continuous with thylakoids in the chloroplast stroma (Fig. 2A). Additional punctate and mesh-like layers are present at the periphery of the pyrenoid (Mackinder *et al.*, 2017) (Fig. 2B). *Chlamydomonas* induces its CCM and acclimatizes to two CO_2 conditions, low- CO_2 (LC=0.03-0.5% volume) and very low- CO_2 (VLC<0.02% volume (Wang and Spalding, 2014)). CCM candidate genes have been identified through forward and reverse genetics screens carried out in limiting CO_2 conditions, which include microarrays and transcriptomic analysis (Miura *et al.*, 2004; Yamano *et al.*, 2008; Brueggeman *et al.*, 2012; Fang *et al.*, 2012) or isolating mutants with reduced growth, C_i affinity or accumulation (Spalding *et al.*, 1983b; Colombo *et al.*, 2002; Thyssen *et al.*, 2003; Mitchell *et al.*, 2014).

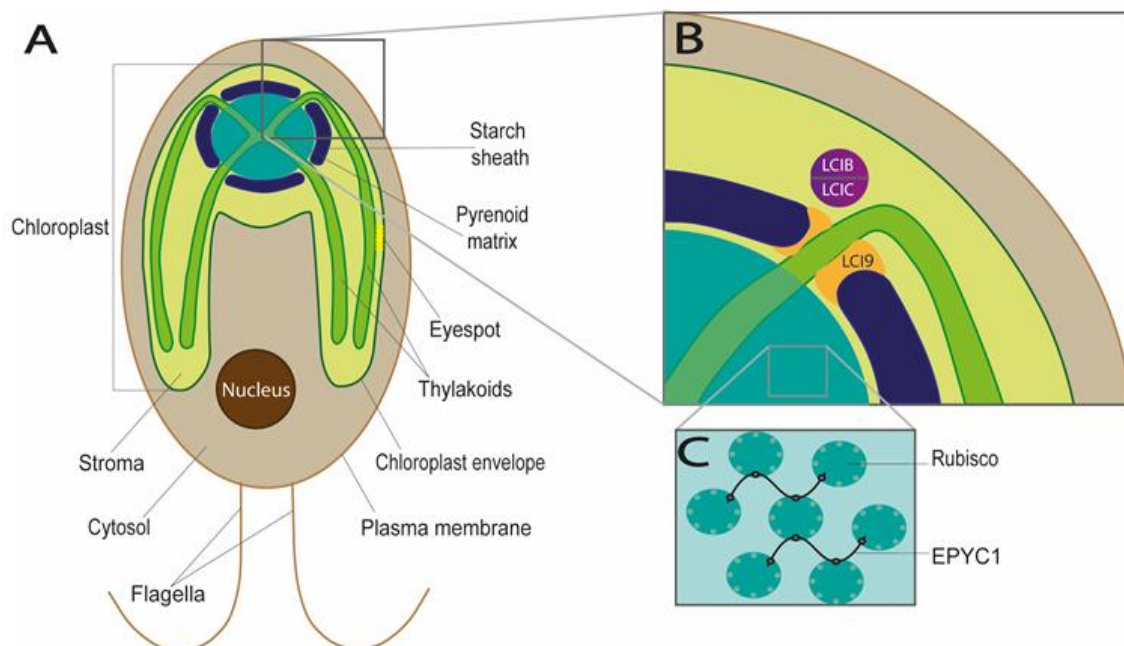


Figure 2. Schematic depiction of A) key structures in *Chlamydomonas* and B) key pyrenoid proteinaceous structures including LCIB-puncta and LCI9-mesh and C) the pyrenoid matrix consisting of Rubisco and its linker protein EPYC1.

C_i transporters and carbonic anhydrases are needed for a functional CCM

Under VLC conditions active transport of inorganic Carbon (C_i) from the extracellular environment to the site of Rubisco occurs through a series of transporters, which reside in the plasma, chloroplast and thylakoid membranes (Fig. 3A). In the plasma membrane, the proteins proposed to be involved in C_i transport are HLA3 and LCI1 (Im and Grossman, 2002; Kono *et al.*, 2020). HLA3 is an ATP-binding cassette (ABC) transporter responsible for HCO₃⁻ transport (Im and Grossman, 2002) whilst LCI1 is proposed to be a unidirectional (periplasm to cytoplasm) CO₂ pump (Kono *et al.*, 2020). Once in the cytosol, HCO₃⁻ is transported into the stroma across the chloroplast membrane by LCIA, which belongs to a formate-nitrite transporter family (Wang and Spalding, 2014; Yamano *et al.*, 2015). It is proposed that LCIA cooperates with HLA3 to allow coordinated HCO₃⁻ transport from the extracellular space into the chloroplast (Yamano *et al.*, 2015). Finally, three Bestrophin-like proteins (BST1-3) have been proposed to transport HCO₃⁻ across the thylakoid membrane (Mukherjee *et al.*, 2019) (Fig. 3A).

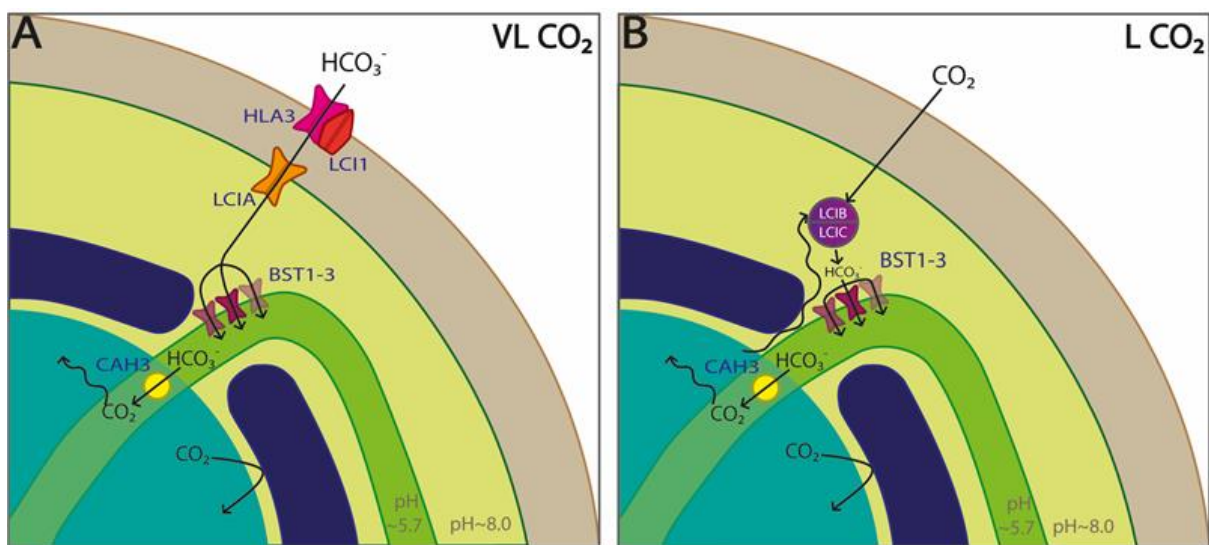


Figure 3. Schematic depiction of C_i transport to Rubisco under A) very low-CO₂ conditions and B) low-CO₂ conditions. A) HCO₃⁻ is transported into the stroma by the co-operative action of HLA3 and LCIA. B) LCIB/LCIC puncta are required for CO₂ conversion to HCO₃⁻ in low-CO₂ conditions. In both conditions, BST1-3 are required for HCO₃⁻ transport into the thylakoid lumen, where HCO₃⁻ is converted to CO₂ by CAH3 in close proximity to Rubisco.

To convert HCO_3^- into CO_2 for fixation by Rubisco, carbonic anhydrases are required. Carbonic anhydrases are zinc metalloenzymes, in three families (α , β and γ), which reversibly convert CO_2 and HCO_3^- (Momayyezi *et al.*, 2020) (Eq. 1).



This interconversion of C_i species is also driven by the pH of the environment. Acidification of the thylakoid lumen (pH ~5.7) by the light-dependent reactions creates a pH gradient across the thylakoid membrane to the stroma (pH ~8.0 (Takizawa *et al.*, 2007)). The conversion of C_i from HCO_3^- to CO_2 occurs in more acidic environments ($\text{pK}_a = 6.3$), in this case, the thylakoid lumen (Moroney and Ynalvez, 2007). This requires an α -type carbonic anhydrase 3 (CAH3) which speeds up the conversion of HCO_3^- to CO_2 in the thylakoid lumen (Spalding *et al.*, 1983a; Karlsson *et al.*, 1998). The lumenal localisation and activity of CAH3 is proposed to be controlled by phosphorylation under LC conditions (Blanco-Rivero *et al.*, 2012). CO_2 then diffuses across the thylakoid membrane to the pool of Rubisco in the pyrenoid matrix (Sinetova *et al.*, 2012). The morphology of the pyrenoid thylakoids traversing the matrix further increases the efficiency of the CCM. As thylakoids enter the matrix, they fuse to form tubules containing ~5 mini-tubules, which have lumens continuous with the stroma (Engel *et al.*, 2015; Meyer *et al.*, 2016). This allows direct stroma-pyrenoid matrix exchange of the substrates and products of Rubisco.

Under LC conditions, a different C_i transport system is proposed. The predominant form of C_i influx is in the form CO_2 , not HCO_3^- , and an additional carbonic anhydrase called limiting- CO_2 -inducible B (LCIB) is required (Fig. 3B). LCIB is critical for the CCM in LC conditions because *LCIB* mutants have an 'air-dier' phenotype (Spalding *et al.*, 1983b; Wang and Spalding, 2006). Interestingly, LCIB changes in localisation under different CO_2 conditions, from a diffuse localisation in the chloroplast stroma under high CO_2 (HC) conditions, to puncta localising to the pyrenoid periphery under VLC conditions (Yamano *et al.*, 2010). LCIB forms a complex with limiting- CO_2 inducible C (LCIC), which is also upregulated under LC conditions (Miura *et al.*, 2004; Yamano *et al.*, 2010) (Fig. 2B). We do not yet know how the LCIB/C puncta localise to this region and whether the puncta mix internally. Whilst the function of LCIB as a carbonic anhydrase has not been confirmed, LCIB is proposed to be in a family of β -carbonic anhydrases to act as a CO_2 trap, converting CO_2 which escapes the pyrenoid matrix into HCO_3^- (Jin *et al.*, 2016) (Fig. 3B). This recycled HCO_3^- contributes to the HCO_3^- stromal pool, is transported by BST1-3 proteins into the thylakoid lumen and converted back to CO_2 by CAH3 in proximity to Rubisco (Mukherjee *et al.*, 2019). Analysis of CCM component interactions by immunoprecipitation coupled to mass

spectrometry has indicated that LCIB/C may interact with BST1-3 in order to recycle C_i (Mackinder *et al.*, 2017; Mukherjee *et al.*, 2019) however further analysis is required to corroborate these findings.

The pyrenoid is further categorised into substructures which have individual roles in the CCM

Under LC conditions, 90% of Rubisco is found within the pyrenoid matrix (Borkhsenius *et al.*, 1998). Rubisco is aggregated by Essential Pyrenoid Component 1 (EPYC1), an intrinsically disordered linker protein (Mackinder *et al.*, 2016). EPYC1 is essential for CCM function (as shown by O_2 evolution and C_i affinity) and for maintaining correct pyrenoid number, size and matrix density (Mackinder *et al.*, 2016). EPYC1 has four disordered repeats of ~60 amino acids, with a Rubisco-binding motif (RBM) on each repeat, meaning each EPYC1 may bind four Rubisco holoenzymes (Mackinder *et al.*, 2016; Meyer *et al.*, 2020) (Fig. 2C). An additional EPYC1 Rubisco binding site on the C-terminus has been revealed (Atkinson *et al.*, 2019), and the hypothesis that EPYC1 may interact with α -helices on the small subunit of Rubisco (Mackinder *et al.*, 2016) has been recently supported experimentally (Atkinson *et al.*, 2019). EPYC1 contains Rubisco-binding motifs (RBMs) which mediate targeting to the pyrenoid matrix (Meyer *et al.*, 2020).

The pyrenoid matrix was originally thought to be crystalline (Holdsworth, 1968) and whilst cryoelectron tomography suggested the matrix is arranged into a hexagonal close-packed lattice (Engel *et al.*, 2015), evidence for the matrix having liquid properties has been put forward (Freeman Rosenzweig *et al.*, 2017). It is now understood that the interaction of Rubisco with EPYC1 causes the matrix to undergo a biophysical phenomenon called liquid-liquid phase separation (LLPS) (Freeman Rosenzweig *et al.*, 2017). LLPS is a process where two liquids de-mix, much like oil in water, when components reach a critical concentration-dependent threshold (Mitrea and Kriwacki, 2016). LLPS is advantageous because it allows compartmentalisation of biochemical processes in a membrane-less compartment (Cuevas-Velazquez and Dinneny, 2018). The liquid nature of the pyrenoid matrix has been demonstrated by time-lapse imaging of dividing cells, where puncta fuse and larger puncta grow at the expense of smaller puncta (known as Ostwald ripening) (Freeman Rosenzweig *et al.*, 2017). Furthermore, evidence for the matrix mixing internally has been shown *in vivo* (Freeman Rosenzweig *et al.*, 2017) and *in vitro* (Wunder *et al.*, 2018). *In vitro* analysis has shown that the interaction of Rubisco and EPYC1 alone is sufficient to cause the formation of liquid droplets, and that phase-separated Rubisco is catalytically active (Wunder *et al.*, 2018). However, further investigation is needed to understand how LLPS of the pyrenoid matrix changes under different growth conditions.

LLPS of the pyrenoid matrix enables CO₂ fixation in the absence of a surrounding membrane. However, the pyrenoid matrix is traversed by thylakoid membranes and is encapsulated by a starch sheath (Fig. 2B). The organisation of the traversing thylakoids and the starch sheath around the matrix is proposed to be mediated by RBM-containing thylakoid and starch-associated proteins (Meyer *et al.*, 2020). The starch sheath forms under LC conditions and has therefore been proposed to correlate with CCM induction (Ramazanov *et al.*, 1994). However, starchless mutants are still able to induce a functional CCM (Villarejo *et al.*, 1996). It has been suggested that the starch may act as a barrier to escaping CO₂ (Ramazanov *et al.*, 1994) (Fig. 3) but evidence for the functional role of starch for the CCM has been lacking until recently. Starch-sheathless mutants *Isoamylase1* and *sta11-1* were unable to correctly localise LCIB, suggesting the starch sheath may play a role in localising puncta containing key CCM components to the pyrenoid periphery (Toyokawa *et al.*, 2020). By gaining understanding of the effect of mutations in starch-associated proteins, the role of starch is becoming clearer. A Granule Bound Starch Synthase, called GBSSI or STA2, and RBM-containing StArch Granules Abnormal 1 (SAGA1) are needed for correct starch sheath morphology (Izumo *et al.*, 2011; Itakura *et al.*, 2019; Meyer *et al.*, 2020). A *saga1* mutant was shown to have multiple pyrenoids (Itakura *et al.*, 2019), suggesting SAGA1 may be involved in the natural tendency to form one large pyrenoid, which must be overcome when pyrenoids divide. Whilst matrix dynamics have been reported during cell division (Freeman Rosenzweig *et al.*, 2017), the movement or role of the starch sheath during pyrenoid division has yet to be observed. Gaps between the starch plates making up the starch sheath are proposed to be filled with a mesh-layer of a protein called LCI9, a glucan 1,4- α -glucosidase potentially involved in starch breakdown (Mackinder *et al.*, 2017) (Fig. 2B). However, the mesh or gel-like nature of LCI9 has not been confirmed. This could be further explored by studying the recovery of fluorescently-labelled LCI9 after photobleaching (see introduction to Chapter 2 for description of fluorescence recovery after photobleaching (FRAP) microscopy technique). Slow recovery may help to confirm the hypothesis that LCI9 plays a structural role in gluing starch plates together.

Starch sheath formation and the induction of the CCM must be regulated to respond to varying CO₂ levels. The acclimation of *Chlamydomonas* to LC for LCIB-dependent CO₂ recapture and to VLC for HLA3 and LCIA cooperative uptake of HCO₃⁻ (Wang and Spalding, 2014) requires a C_i sensing mechanism. The current mechanism by which *Chlamydomonas* senses changes in C_i is unknown, however the induction and transcription of CCM genes is proposed to be controlled by CCM1, a transcription factor, in LC conditions (Fukuzawa *et al.*, 2001). Additionally, CCM induction appears to require retrograde calcium signalling from the pyrenoid to nucleus involving CAS, a Ca²⁺-binding protein (Wang *et al.*, 2016). Light is also

an important part of CCM regulation as cells synchronised to a light/dark cycle undergo CCM induction during the dark-to-light transition (Mitchell *et al.*, 2014).

The *Chlamydomonas* CCM may be engineered into higher plants to increase crop yields

The human population is predicted to increase by 2.3 billion people between 2009 and 2050 (FAO 2009). To sustain our growing population, we will need to double food production by 2050 (Tilman *et al.*, 2011). This is a target which is not currently being met (Ray *et al.*, 2013), therefore innovative solutions to improve crop production and food security are required. Introducing a functional CCM into crop plants has been predicted to increase photosynthesis by up to 60% (Long *et al.*, 2015). Cumulative work to understand the function of proteins within the algal CCM has enabled targeting of key components, including HLA3 and LCIA, to appropriate intracellular locations in *Nicotiana benthamiana* and *Arabidopsis thaliana* (hereafter *Arabidopsis*) (Atkinson *et al.*, 2016). Although it was shown that HLA3 and LCIA could transport C_i across *Xenopus* oocyte plasma membranes, no growth advantage was shown for expressing HLA3 and LCIA in *Arabidopsis* (Atkinson *et al.*, 2016), therefore further work to understand the functional components of the CCM is required. More specifically, by gaining further understanding of the dynamic nature of the pyrenoid, and interactions of key CCM components, we may better understand the requirements for engineering pyrenoids into higher plants (Mackinder, 2017).

Project aims

Many questions remain unanswered regarding the dynamic nature of key pyrenoid components. The first aim of this study is to capture Rubisco, LCIB and LC19 mobility using a method called Fluorescence Recovery After Photobleaching (FRAP) (Chapter 2). The role of the starch sheath, particularly the movement and inheritance of starch during the key cellular process of division, is also not well understood. The second aim of this study is to use time-lapse imaging to capture this process, which requires development of a dual-tagged line, allowing observation of Rubisco and starch movement simultaneously (Chapter 3). In addition, elucidation of potential starch synthesis and degradation candidates by bioinformatics is required to gain understanding into starch remodelling during division (Chapter 3). The interaction of key pyrenoid components involved in C_i conversion and transport also requires further investigation. The recycling of escaping CO_2 via LCIB/C and BST1-3 is a particularly interesting avenue to explore. The third aim of this study is to facilitate investigation into the proximity of key CCM component via Fluorescence Resonance Energy Transfer (FRET), by developing appropriate FRET-pair tagged proteins (Chapter 4).

Chapter 2: Preliminary investigation into the mobilities of Rubisco, LCIB and LCI9

Chapter summary

Rubisco in the pyrenoid matrix undergoes a biophysical phenomenon called liquid-liquid phase separation (LLPS) with its linker protein Essential Pyrenoid Component 1 (EPYC1). Surrounding the pyrenoid matrix are several structures, including a starch plate-like layer whose gaps are proposed to be filled with a LCI9-mesh and surrounded by a punctate-layer of LCIB/C. The ability of Rubisco to undergo LLPS depends on the growth condition of *Chlamydomonas*, where component concentration and post-translational modifications may play a role. The mobility of Rubisco, and other important CCM components (LCIB and LCI9) can be tested using Fluorescence Recovery After Photobleaching (FRAP). This study highlights progress made on optimisation of FRAP and sample preparation, with preliminary results revealing Rubisco mobility is not dependent on growth condition, and LCI9 re-homogenisation is slow. This work enables future investigation into CCM component mobilities, especially in high and low-CO₂ conditions. Progress in understanding the mobility of CCM components will help guide successful engineering of a CCM into higher plants.

Introduction

Cellular components require compartmentalisation to carry out key processes, either in membrane-bound or membraneless organelles (Choi *et al.*, 2020). The pyrenoid, a membraneless organelle, compartmentalises the CO₂ fixing enzyme Rubisco via interaction with a linker protein, Essential Pyrenoid Component 1 (EPYC1) (Mackinder *et al.*, 2016). Rubisco and EPYC1 are integral components of the pyrenoid matrix (Borkhsenius *et al.*, 1998; Mackinder *et al.*, 2016), which was previously thought to be crystalline (Holdsworth, 1968). However, recent work has shown that the pyrenoid matrix has liquid properties and the pyrenoid is now characterised as a liquid-liquid phase separated (LLPS) organelle (Freeman Rosenzweig *et al.*, 2017).

LLPS is a biophysical phenomenon whereby two liquids can de-mix (like oil in water) (Hyman *et al.*, 2014). A polymer-enriched and polymer-depleted phase forms due to favourable interactions between components, meaning the entropic tendency to stay mixed is overcome (Hyman *et al.*, 2014; Wheeler and Hyman, 2018; Wunder *et al.*, 2019). LLPS requires 'scaffold' proteins which allow multivalent interactions and may contain low

complexity domains (LCD's) (Wheeler and Hyman, 2018). LCD's are found interspersed in 'scaffold' proteins and are called spacers, between which reside sticker regions of the 'scaffold' that mediate interactions (Choi *et al.*, 2020). For LLPS to occur, interacting components must have appropriate interaction strength, range and valency (Hyman *et al.*, 2014) and several conditions must be satisfied, including component concentration, pH and temperature (Wheeler and Hyman, 2018). Despite this, LLPS is found in a wide range of organisms and cell types, including nucleoli in *Xenopus laevis*, mammalian stress granules and the P-granules of the model worm *Caenorhabditis elegans* (Brangwynne *et al.*, 2011; Elbaum-Garfinkle *et al.*, 2015; Kroschwald *et al.*, 2015).

LLPS of the pyrenoid matrix is possible due to the strength, valency and range of EPYC1-Rubisco interactions. Over 80% of EPYC1 consists of four ~60 amino acid repeats, which each have a large disordered 'spacer' region, and an α -helix 'sticker' region orchestrating binding to the Rubisco small subunit (SSU) (Mackinder *et al.*, 2016; Atkinson *et al.*, 2019). Simultaneously, the *Chlamydomonas* Rubisco SSU contains 2 α -helices which are important for pyrenoid formation (Meyer *et al.*, 2012) as they enable interaction with EPYC1 (Atkinson *et al.*, 2019). The multivalency of the Rubisco-EPYC1 interaction has been further demonstrated, as an additional SSU interaction site on the C-terminus of EPYC1 has been identified (Atkinson *et al.*, 2019), meaning each EPYC1 may interact with five Rubisco holoenzymes and it is possible that Rubisco may bind 8 EPYC1 proteins (Mackinder *et al.*, 2016). The length of EPYC1 is suitable for bridging the 1-4 nm gap between Rubisco holoenzymes, and different mobilities of EPYC1 and Rubisco suggest their interaction is transient (Freeman Rosenzweig *et al.*, 2017). Rubisco and EPYC1 are proposed to interact with low affinity (Freeman Rosenzweig *et al.*, 2017) and undergo LLPS through a process of complex coacervation, where polymers with positive charge (EPYC1) and negative charge (Rubisco) form a dense droplet phase through electrostatic interactions (Brangwynne *et al.*, 2015; Wunder *et al.*, 2018). Further support for the pyrenoid matrix as a LLPS organelle comes from *in vitro* reconstitution of liquid droplets with Rubisco and EPYC1 (Wunder *et al.*, 2018).

Compartmentalisation of key processes requires separation of components from their surroundings and the ability of components to freely diffuse to undertake chemical reactions (Hyman *et al.*, 2014). A technique called Fluorescence Recovery After Photobleaching (FRAP) has been used to show that components mix internally within LLPS organelles, such as mammalian stress granules (Kedersha *et al.*, 2000), P granules from *C. elegans* (Brangwynne *et al.*, 2009) and P-bodies from yeast (Kroschwald *et al.*, 2015). To understand the dynamic nature of a protein of interest by measuring its mobility using FRAP, a fluorescently-tagged version of the protein must be introduced into a cell (Phair *et al.*, 2004), for example by fusing the protein to a Yellow Fluorescent Protein, Venus (Rekas *et al.*,

2002). Within the area of fluorescence, a region of interest (ROI) then receives a short pulse from a high-powered focused laser to irreversibly photobleach the fluorophores, making proteins 'invisible' without changing their concentration or chemistry (Reits and Neefjes, 2001; Phair *et al.*, 2004). Time-lapse imaging with a low laser power is then used to monitor fluorescence 'recovery' within this ROI, which can be plotted to acquire a recovery curve (Reits and Neefjes, 2001). If proteins are mobile, unbleached molecules outside the region of interest will move into the bleached region, and fluorescence will be seen to increase; if the proteins are not mobile 'recovery' will not occur (Phair *et al.*, 2004). Recovery curves allow the calculation of mobile and immobile pools of protein by comparing final and initial fluorescence intensities, and the speed of recovery is calculated as half the plateau intensity ($T_{1/2}$) (Ishikawa-Ankerhold *et al.*, 2012).

In *Chlamydomonas*, FRAP has been used to investigate the mobility of Rubisco-Venus, EPYC1-Venus and RCA1-Venus (Rubisco activase) *in vivo* (Freeman Rosenzweig *et al.*, 2017). In photoautotrophic conditions, it was shown that Rubisco-Venus mixes within the pyrenoid; a 'wave' of Rubisco-Venus signal moved from the unbleached to bleached half of the pyrenoid and the Rubisco-Venus signal re-homogenised after 20s (Freeman Rosenzweig *et al.*, 2017). However, questions still remain regarding the nature of Rubisco mobility *in vivo* under different growth conditions, including in the light and dark. It has been shown that the localisation and abundance of Rubisco changes through the dark-light transition where two hours before dawn ~75% of labelled Rubisco was found in the pyrenoid whilst ~90% of Rubisco localised to the pyrenoid in the light period (Mitchell *et al.*, 2014). Whilst *Chlamydomonas* is a photosynthetic organism, it is able to grow using acetate as the sole carbon source (Sueoka, 1960) via the glyoxylate cycle (Kunze *et al.*, 2006) and therefore can also be grown in the dark. By growing cells with acetate, it has been shown that the distribution of Rubisco changes; a greater proportion of Rubisco localises to the stroma compared to cells grown in photoautotrophic conditions (Borkhsenius *et al.*, 1998). It has been hypothesised that changes in Rubisco distribution under different growth conditions requires a phase transition (aggregation to dissolution of components or *vice versa*) (Wunder *et al.*, 2019). Phase transitions may be controlled by the concentration of components (Wunder *et al.*, 2018), valency (Li *et al.*, 2012), post-translational modifications (Owen and Shewmaker, 2019) and/or metabolites (Patel *et al.*, 2017). Investigation into changes of Rubisco mobility under different distributions may aid our understanding of EPYC1-Rubisco packing through phase transitions.

Whilst FRAP has been carried out on components within the pyrenoid matrix, the pyrenoid contains at least 3 additional layers including a plate-like layer, a mesh-layer and a punctate-layer which have yet to be explored with this technique (Mackinder *et al.*, 2017). Like Rubisco, the putative β -carbonic anhydrase LCIB (Jin *et al.*, 2016), which forms a 350

kDa hexamer complex with LCIC (Yamano *et al.*, 2010) spatially reorganises under different growth conditions. Under HC and LC conditions, LCIB localises to the chloroplast stroma (Duanmu *et al.*, 2009; Yamano *et al.*, 2010; Wang and Spalding, 2014) whereas under VLC conditions, LCIB is localised to the pyrenoid periphery as puncta in a ring-like structure (Yamano *et al.*, 2010; Wang and Spalding, 2014). Similarly to the HC and LC conditions, dark-grown cells have a diffuse localisation of LCIB in the stroma (Yamano *et al.*, 2010), therefore both CO₂ availability and light are required for dynamic relocalisation. It has recently been shown that LCIB may be dependent on the starch sheath for localisation to the pyrenoid periphery (Toyokawa *et al.*, 2020). The starch sheath, which makes up the plate-like layer, has gaps between the plates which are proposed to be filled with a mesh-like layer of a protein with unknown function, LCI9 (Mackinder *et al.*, 2017). FRAP can be used to investigate the mobility of LCIB/C when differentially distributed and could test the hypothesis that LCI9 is largely immobile and behaves as a structural mesh.

To investigate the mobility of CCM components, appropriate sample preparation and microscope settings for FRAP needed to be optimised, and preliminary results were collected. To undertake preliminary investigations in Rubisco mobility, *Chlamydomonas* with Venus-tagged Rubisco was grown in TP media in the light (photoautotrophically), and in TAP media (containing acetate) in the dark (heterotrophically). The use of FRAP to investigate the mobility of LCIB and LCI9 in addition to Rubisco mobility under different growth conditions may reveal insights into the dynamic nature of the pyrenoid. An initial attempt to reconstitute the pyrenoid matrix in higher plants was unsuccessful (Atkinson *et al.*, 2019). Future attempts may benefit from gaining understanding of the drivers of phase transitions, how the dynamics of additional CCM components contribute to pyrenoid formation, and how growth conditions may affect pyrenoid maintenance in algae and higher plants.

Methods

Growth conditions:

All strains used were maintained on TAP-agar containing paromomycin ($20 \mu\text{g mL}^{-1}$) and then streaked out onto fresh plates to acquire a single colony for liquid growth. Cultures of *Chlamydomonas* cells for testing Rubisco-Venus mobility (RBCS1-Venus, with the native copy present) were grown in Tris-minimal (TP) media in the light, and Tris-Acetate-Phosphate (TAP) media in the dark. These cultures were named photoautotrophic and heterotrophic respectively. TP and TAP media at pH 7.4 was used (Gorman and Levine, 1965) which was optimised with a revised nutrient supplement (Kropat *et al.*, 2011). Cells containing LCIB-Venus and LCI9-Venus (with the native copy present) were grown in TP-light conditions. All cultures were grown on shakers in 25 mL volumes in 100 mL conical flasks, with paromomycin ($5 \mu\text{g mL}^{-1}$). Cultures were grown at air levels of CO_2 with a light intensity of $150 \mu\text{mol photons m}^{-2}\text{s}^{-1}$.

Microscopy preparation:

Colonies with Venus-tagged proteins were grown until they reached a concentration of $2\text{-}4 \times 10^6 \text{ cells mL}^{-1}$. $40 \mu\text{L}$ of each culture was pipetted into individual wells in a poly-L-lysine coated Ibidi plate and allowed to dry for 5 minutes. For Rubisco-Venus and LCIB-Venus, $160 \mu\text{L}$ of 1.5% (w/v) low melting point Agar was pipetted into each well and allowed to dry for 5 minutes. For LCI9-Venus, 3% (w/v) low melting point Agar was used.

Image acquisition:

Confocal images were acquired using a Zeiss LSM780, with a 63x/1.4 numerical aperture. The 514 nm laser was used to excite Venus-tagged proteins. For Rubisco-Venus, acquisition laser power was set to 0.3% for photoautotrophic and heterotrophic cultures, and 0.05% for LCI9-Venus. For Rubisco-Venus and LCI9-Venus, after 10 pre-bleach images were taken, 100% laser power for 10 iterations was directed to one half of each pyrenoid. Images were taken every 0.9700s for 120s for Rubisco-Venus and every 0.9700s for 300s for LCI9-Venus.

Image analysis:

All images were analysed using ImageJ after exporting the bleached region of interest from Zeiss. Movement was corrected using the StackReg plugin, or FRAP traces were removed from the analysis if correction for movement was not possible. For Rubisco-Venus two different analysis methods were attempted.

1) Intrapyreoid homogeneity was calculated as the ratio between the fluorescence intensity of the bleached and unbleached regions (bleached intensity divided by unbleached intensity) at each time point (Freeman Rosenzweig *et al.*, 2017). All values were then normalised to between 0 and 1.

2) A double normalisation was carried out as described in Phair *et al.*, (2004), by using the FRAP Norm Plugin on ImageJ.

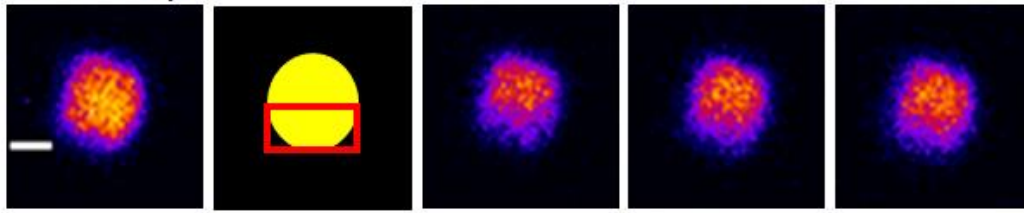
FRAP curves were created using Excel, and for each condition, a mean FRAP curve with standard error bars was plotted.

For LCI9-Venus, the mean gray value was plotted over time for the bleached and unbleached halves of the pyrenoid, the whole pyrenoid and a control pyrenoid.

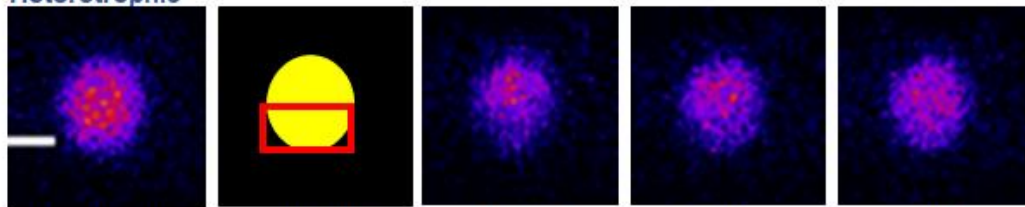
Results

To investigate the mobility of Rubisco under different growth conditions, *Chlamydomonas* was grown photoautotrophically and heterotrophically and FRAP experiments were carried out. Images were taken over 120s, and a high-powered laser was directed to $\frac{1}{2}$ of each pyrenoid after 10s of acquisition (Fig. 4A). Rubisco-Venus signal was analysed by the intrapyrenoid homogeneity method (Fig. 4B) and the double normalisation method (Fig. 4C). Pre-bleach images indicate that heterotrophically grown cells contained smaller pyrenoids, and the stromal Rubisco-Venus signal was increased comparatively to the photoautotrophic condition (Fig. 4A). Whilst the Rubisco-Venus signal appeared to be lower in heterotrophic pyrenoids (Fig. 4A) recovery after photobleaching appeared to be similar to the photoautotrophic condition, for both analysis methods (Fig. 4B, C). However, for the photoautotrophic condition, the FRAP curves appeared to continue to increase up until 120s (Fig. 4B, C), whilst for the heterotrophic condition, the FRAP curves plateaued at ~70s (Fig. 4B, C).

A Photoautotrophic



Heterotrophic



Pre-bleach

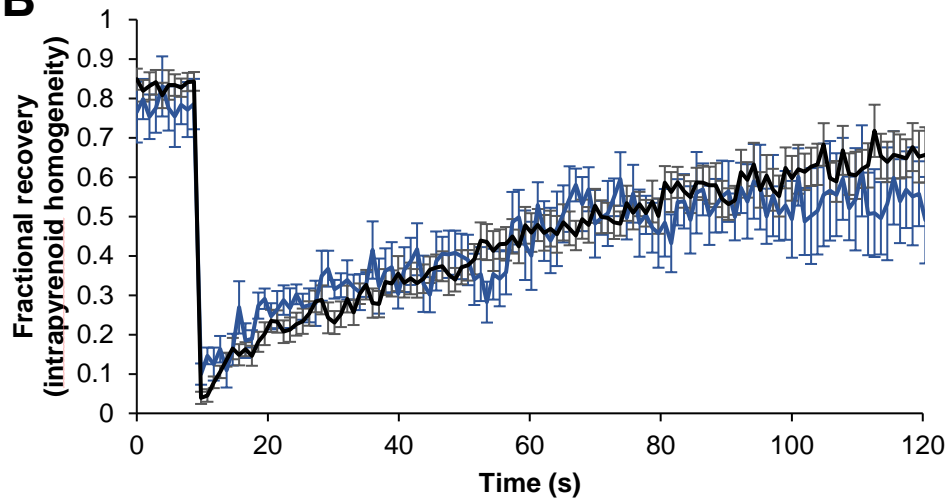
Bleach
diagram

Bleach
event

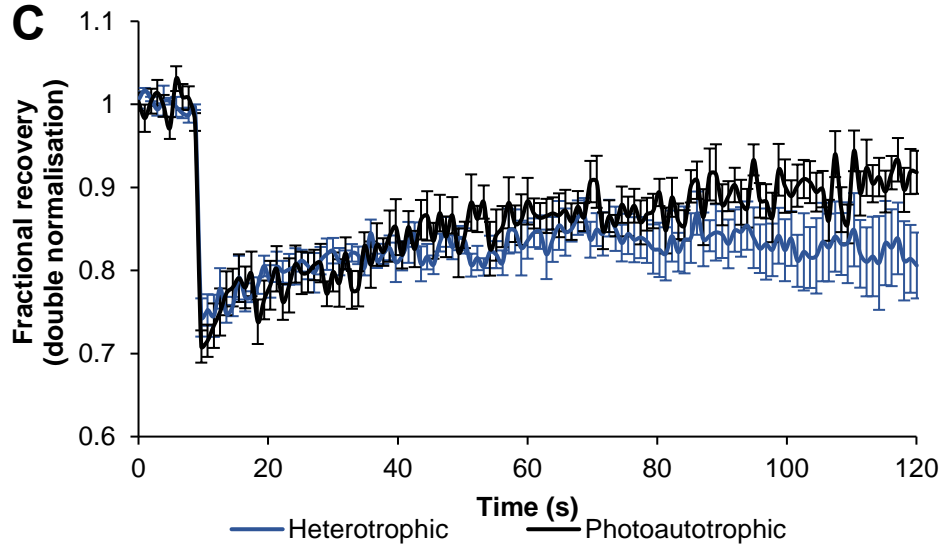
30s

90s

B



C



— Heterotrophic

— Photoautotrophic

Figure 4. Rubisco-Venus mobility was similar between photoautotrophic (n=11) and heterotrophic (n=5) growth conditions. The bleach event occurred 10s into image acquisition.

- A. Representative images for a single FRAP experiment in photoautotrophic and heterotrophic conditions. Images of pyrenoids before bleaching occurred (pre-bleach), when bleaching occurred (bleach event), and 30s and 90s after the bleach event are shown. A bleaching diagram indicates the area of the pyrenoid (yellow) that was bleached (red box). Scale bar = 1 μm .
- B. The intrapyrenoid homogeneity analysis method (Freeman Rosenzweig *et al.*, 2017) was used to produce FRAP curves for each condition, with standard error bars shown.
- C. The double normalisation analysis method (Phair *et al.*, 2004) was used to produce FRAP curves for each condition, with standard error bars shown.

To investigate the mobility of proteins outside of the pyrenoid matrix, FRAP was carried out on LCIB-Venus and LCI9-Venus. Due to cell movement, quantitative results for LCIB-Venus could not be obtained. 3% (w/v) low melting point Agar was trialled for sample preparation of LCI9-Venus tagged cells which led to a reduction of cell movement. However only one FRAP experiment could be performed meaning the result was very preliminary. This FRAP experiment showed LCI9-Venus appeared to re-homogenise after 150s (Fig. 5A) indicating recovery was slow. Minimal recovery for plotted LCI9-Venus fluorescence intensity was observed (Fig. 5B), however an initial increase of LCI9-Venus recovery occurred between 10-50s (Fig. 5B).

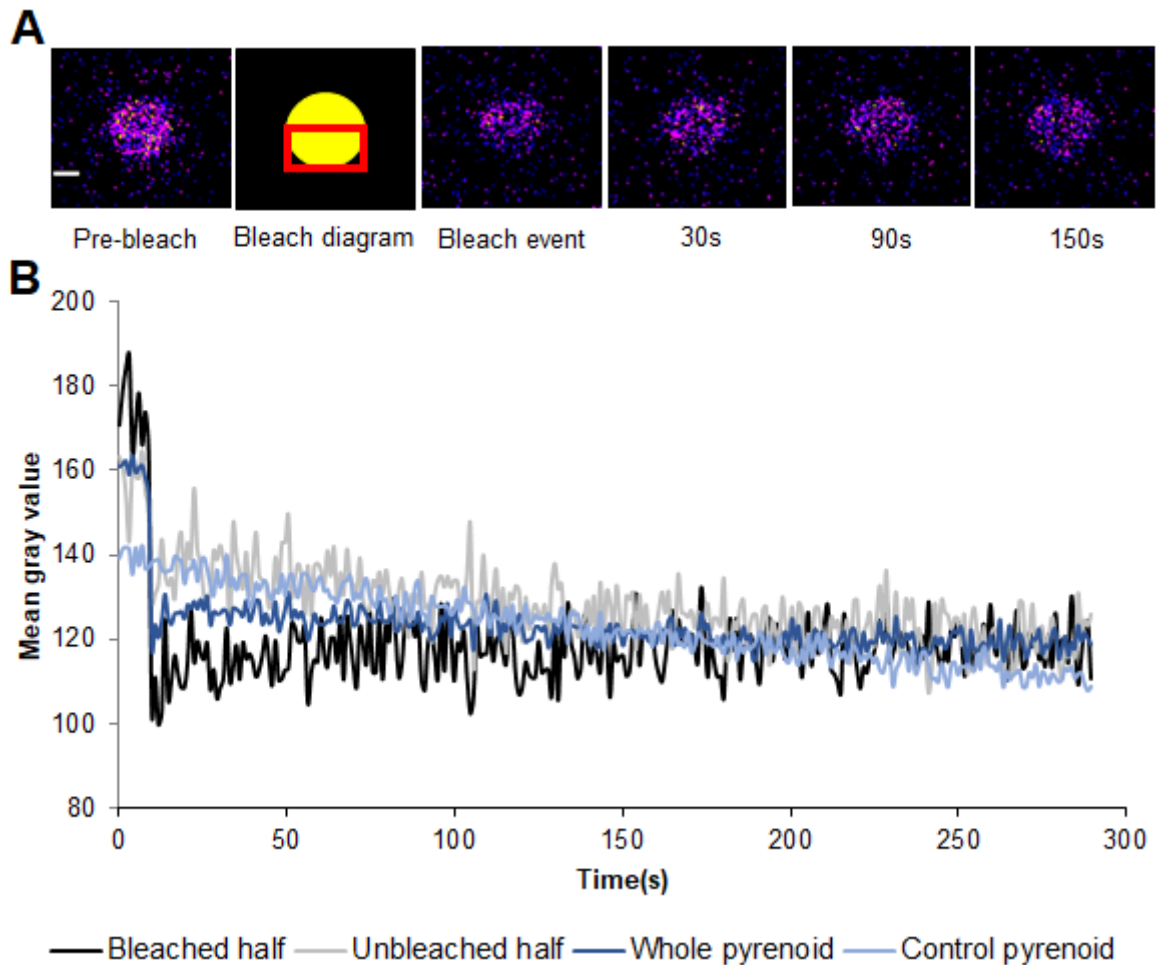


Figure 5. Re-homogenisation of LCI9 occurred after FRAP however recovery was subtle. Image acquisition was possible using 3% (w/v) low melting point TP Agar which reduced cell movement.

- A. Representative images for a single FRAP experiment. Images of pyrenoids before bleaching occurred (pre-bleach), when bleaching occurred (bleach event), and 30s, 90s and 150s after the bleach event are shown. A bleaching diagram indicates the area of the pyrenoid (yellow) that was bleached (red box). Scale bar = 1 μ m.
- B. The mean gray value for LCI9-Venus was plotted for the corresponding pyrenoid in A); ROIs for the bleached and unbleached halves of the pyrenoid, the whole pyrenoid and a control pyrenoid were plotted over time. The bleach event occurred 10s into image acquisition.

Discussion

Pre-bleach Rubisco-Venus images suggest there is less Rubisco in the pyrenoid under heterotrophic conditions

The observation of smaller pyrenoids with a simultaneously increased stromal signal in heterotrophic grown cells (Fig. 4A) agrees with past observations that when *Chlamydomonas* was grown on acetate and in the dark, ~80% (Borkhsenius *et al.*, 1998) and ~75% (Mitchell *et al.*, 2014) of Rubisco was localised to the pyrenoid respectively. The inability to fully partition Rubisco under these growth conditions may be explained by the concentration of EPYC1, as partitioning of Rubisco has been shown to be dependent on EPYC1 concentration *in vitro* (Wunder *et al.*, 2018) and up-regulation of EPYC1 transcription and translation occurs at LC and in the light (Turkina *et al.*, 2006; Mackinder *et al.*, 2016). Reduced brightness of the Rubisco-Venus signal in the pre-bleach heterotrophic condition (Fig. 4A) may be attributed to increased observed changes in Rubisco LSU abundance during the day/night cycle, where LSU abundance increased in the light and at the end of the dark phase (Recuenco-Muñoz *et al.*, 2015). This agrees with *in vitro* investigations which surmised that the size of the pyrenoid matrix is likely to be component limited (Wunder *et al.*, 2018). Whilst our preliminary data does not show differences in Rubisco mobility under different growth conditions (Fig. 4B, C), the slight dissolution of the pyrenoid matrix in dark and acetate-grown cells suggests a phase transition occurs in this condition, and therefore further understanding of the driving factors of LLPS is needed.

Preliminary results confirm internal mixing of Rubisco-Venus in the pyrenoid matrix under both heterotrophic and photoautotrophic conditions, and offer avenues for improvement for future FRAP acquisition

Preliminary results show recovery of Rubisco-Venus signal using FRAP in both photoautotrophic and heterotrophic conditions (Fig. 4), confirming that Rubisco in the pyrenoid matrix is mobile under different growth conditions and cellular metabolic states (Freeman Rosenzweig *et al.*, 2017). LLPS organelles facilitate the aggregation of components, whilst retaining the ability to allow components to freely diffuse for chemical reactions (Hyman *et al.*, 2014). *Chlamydomonas* benefits from this because the less abundant chaperone RCA1 is able to access the active sites of Rubisco holoenzymes to remove inhibitory sugar phosphates (Portis, 2003; Freeman Rosenzweig *et al.*, 2017). In this study, whilst it was possible to reconstitute previously reported Rubisco dynamics (Freeman Rosenzweig *et al.*, 2017), no difference in Rubisco mobility was observed between different growth conditions (Fig. 4), possibly due to the preliminary nature of the data collected. Due

to the optimisation of FRAP in this study, it is now possible to collect further FRAP data which may show differences in Rubisco mobility under different growth conditions.

An insufficient bleach depth was an issue for the double normalisation analysis method where the Rubisco-Venus signal appeared to only decrease by 30% of its original value after bleaching (Fig. 4C). Future FRAP experiments should aim to increase the bleach depth in the bleached ROI; it is advised to reduce the fluorescent signal by more than 70% (Phair *et al.*, 2004). A moderate bleach depth of 40-50% may be observed if a fraction of the tagged-protein population undergoes rapid diffusion before collection of the first post-bleach image (Phair *et al.*, 2004). However, re-homogenisation was previously reported to take ~20s (Freeman Rosenzweig *et al.*, 2017) and bleaching was not visually obvious for the heterotrophic condition (Fig. 4A). Therefore, bleach depth should be increased by increasing laser iterations, however to avoid 'spill over' bleaching in adjacent areas, a smaller bleaching ROI may be needed.

In addition to unintentional bleaching of adjacent areas, unwanted bleaching through acquisition should also be minimised. Ideally a control pyrenoid should be included within the image frame, and less than ~10% of signal dimming from 50-100 images should take place (Phair *et al.*, 2004). Another complication can arise from data noise due to cell movement (Phair *et al.*, 2004). This can be improved through taking results from small areas inside large bleach areas, or by allowing cells to equilibrate to the temperature of the microscope for some time (>30 min) before imaging (Phair *et al.*, 2004). Both of these techniques were implemented for the gathering of results in this study, however if cells are left to acclimatise for considerable time, it would be advisable to use anti-evaporation oil (Ibidi) on top of the loaded sample. In this study, no additional light (mounted onto the microscope stage) was used, however this would be recommended to ensure the CCM remains induced during imaging. After further optimisation of sample loading and acquisition, an appropriate analysis method should be chosen with care. Whilst intrapyrenoid homogeneity was used previously to measure re-homogenisation of Rubisco-Venus in the pyrenoid after FRAP (Freeman Rosenzweig *et al.*, 2017), this analysis method is not suitable for investigation of Rubisco (or LCIB) mobility when dispersed in the stroma. Whilst it was not possible to observe differences in Rubisco-Venus mobility under this experimental set-up, there is much evidence to suggest growth conditions may play a role in LLPS.

Under different growth conditions, metabolic pathways and ATP availability varies. A study on the green alga *Chlorella pyrenoidosa* revealed that in heterotrophic conditions, the theoretical ATP yield is higher (19.3 g/mol) than in autotrophic conditions (3.11 g/mol), as ATP is utilised in the Calvin cycle (Yang *et al.*, 2000). ATP acts as a hydrotrope, meaning it can solubilize hydrophobic molecules, preventing LLPS (Patel *et al.*, 2017). Energy availability depending on growth condition may therefore contribute to or prevent formation

of LLPS droplets but may also affect the mobility of components. The viscosity of LLPS nucleoli in *Xenopus laevis* oocytes was proposed to be dependent on metabolic activity, where ATP depletion led to ~10-fold increase in viscosity (Brangwynne *et al.*, 2011). In yeast, it has been shown that nutrient depletion can cause assembly and disassembly of foci; adenine subtraction caused the purine biosynthetic enzyme Ade4-GFP to form puncta, and glutamine synthase (Gln1-GFP) puncta formed reversibly in response to glucose fluctuations (Narayanaswamy *et al.*, 2009). Further examination of ATP and other metabolites as contributors to LLPS in *Chlamydomonas* is required, as understanding how different metabolic pathways under varying growth conditions contribute to LLPS could be vital when engineering a pyrenoid into higher plants.

Concentration-dependence and post-translational modifications may contribute to LLPS

LLPS is dependent on several factors, including the concentrations of components, temperature and pH (Wheeler and Hyman, 2018). To undergo phase separation, a threshold concentration of associating components must be reached (Choi *et al.*, 2020). *In vitro* phase separation of CCM components was possible with 1 μM EPYC1 and 0.5 μM Rubisco (Wunder *et al.*, 2018). The concentration of Rubisco in plant chloroplasts (~500 μM (Harris and Königer, 1997)) is similar to in *Chlamydomonas* (~628 μM (Freeman Rosenzweig *et al.*, 2017)) meaning the concentration of EPYC1 needed for higher plant Rubisco de-mixing could be similar to *Chlamydomonas* concentrations. However, whilst the estimated stoichiometry of EPYC1 to Rubisco LSU in *Chlamydomonas* under LC is ~1:6 (Mackinder *et al.*, 2016), and *in vitro* one to four EPYC1 proteins interacted with eight Rubisco LSUs (Wunder *et al.*, 2018), reconstitution of droplets *in planta* was not possible due to the low concentration of EPYC1 to Rubisco LSU (~1:84 (Atkinson *et al.*, 2019)). This low EPYC1 concentration was attributed to proteolytic degradation in the chloroplast of *Arabidopsis* (Nishimura *et al.*, 2017; Atkinson *et al.*, 2019) suggesting further knowledge of EPYC1 regulation is needed. It could be speculated that increased concentrations of EPYC1 under a particular growth condition may lead to increased Rubisco-EPYC1 binding and increased packing of Rubisco, leading to decreased Rubisco mobility. To study the effect of EPYC1 concentration on the mobility of Rubisco, FRAP could be carried out using an *in vitro* system (Wunder *et al.*, 2018) with addition of different concentrations of EPYC1.

Regulation of EPYC1-Rubisco binding affinity may occur post-translationally through phosphorylation of EPYC1, or Rubisco methylation (Turkina *et al.*, 2006; Wang *et al.*, 2014a; Mackinder *et al.*, 2016). In *C. elegans* it has been proposed that phosphorylation of highly disordered proteins involved in droplet formation (MEG proteins) causes disassembly of P granules (Wang *et al.*, 2014b). Alternatively, phosphorylation can cause assembly of

mammalian stress granules (Kedersha *et al.*, 2016), and may allow incorporation of additional components into the droplet (Kwon *et al.*, 2013). Regulation of phase transitions through phosphorylation (Li *et al.*, 2012) may suggest the importance of kinase activity for LLPS. EPYC1 phosphorylation may initiate interaction with phosphoprotein-binding 14-3-3 proteins FTT1 and FTT2, possibly leading to changes in EPYC1 activity or EPYC1-Rubisco binding (Chevalier *et al.*, 2009; Mackinder *et al.*, 2017). Alternatively, methylation, particularly of arginine residues, may play a role in mediating protein-protein interactions (Hughes and Waters, 2006). Methylation of *Chlamydomonas* Rubisco has been reported (Taylor *et al.*, 2001) and may be carried out by the putative methyltransferase CIA6 (Ma *et al.*, 2011). EPYC1 was shown to be phosphorylated in LC conditions (Turkina *et al.*, 2006), therefore different growth conditions may influence post-translational modifications of Rubisco and EPYC1. Perturbations of phosphorylation sites in EPYC1 (Turkina *et al.*, 2006; Wang *et al.*, 2014a) followed by attempted *in vitro* reconstitution of droplets (Wunder *et al.*, 2018) and FRAP may elucidate the role of EPYC1 phosphorylation on Rubisco mobility.

Optimisation of FRAP for LCIB and LCI9-Venus allows further investigation of the mobility of peripheral pyrenoid components

Successful optimisation of sample loading for FRAP in this study enables future investigation into the mobility of proteins which form structures smaller than the pyrenoid matrix (~1-2 μm). 3% (w/v) low melting point TP Agar reduced movement of cells tagged with LCI9-Venus (Fig. 5). After FRAP, LCI9-Venus recovery occurred, however re-homogenisation was slow (Fig. 5A) and was not obvious from quantitative measurement (Fig. 5B). However, recovery may appear to be reduced due to acquisition photobleaching, as a 21% decrease in the control pyrenoid signal was observed (Fig. 5B). These preliminary results may provide evidence for the hypothesis that LCI9 acts as a mesh, filling the gaps between starch plates (Mackinder *et al.*, 2017). However, the LCI9-Venus signal appeared to recover between 10-50s (Fig. 5B), which may suggest there is more than one fraction of LCI9: an immobile fraction which acts as a structural mesh, and a mobile fraction which recovers quickly after photobleaching. Slow visual re-homogenisation suggests that if there is a mobile fraction, it is probably smaller than the immobile fraction (Fig. 5A). LCI9 may be involved in re-modelling the starch sheath at plate junctions, as LCI9 contains two carbohydrate-binding module (CBM) 20 domains, and may act as a glucan 1,4- α -glucosidase (Mackinder *et al.*, 2017).

Whilst the results for LCI9-Venus mobility are preliminary, optimisation of FRAP for future experiments was achieved. Using 3% (w/v) low melting point TP agar on LCIB-Venus tagged cells may overcome previous problems of cell movement. There is much evidence supporting the mobility of LCIB under different CO₂ and light conditions (Duanmu *et al.*,

2009; Yamano *et al.*, 2010; Wang and Spalding, 2014), therefore LCIB would be an interesting target for FRAP. Recently, the localisation of LCIB has been shown to be dependent on the starch sheath (Toyokawa *et al.*, 2020), therefore it would also be interesting to investigate the mobility of LCIB when it is both localised to the pyrenoid periphery and starch sheath and while it is diffuse in the stroma (Yamano *et al.*, 2010). The mechanism which underlies the movement of LCIB under different conditions is unknown, however it could be hypothesised that its complex-forming partner LCIC carries out this function. It would be interesting to use FRAP to investigate the mobility of LCIC alongside LCIB, which presumably have similar mobilities. LCIB is able to form puncta both at the pyrenoid periphery and in the stroma (Yamano *et al.*, 2010), which are reminiscent of LLPS droplets. Whilst puncta are too small to test internal mixing with the FRAP set-up in this study, time-lapse imaging using LCIB-Venus tagged cells may indicate if puncta can undergo fusion and dissolution like the pyrenoid matrix and other LLPS organelles (Brangwynne *et al.*, 2011; Freeman Rosenzweig *et al.*, 2017). Carbonic anhydrase activity of LCIB has yet to be experimentally determined, however LCIB shares a similar structure to a family of β -carbonic anhydrases (Jin *et al.*, 2016). In Arabidopsis the cytoplasmic β -carbonic anhydrases CAH2 and CAH4 have been shown to be important for plant growth at low CO₂ (DiMario *et al.*, 2016). Therefore, whilst further investigation into the importance of LCIB/C mobility and function is required in *Chlamydomonas*, future FRAP results may aid CCM engineering into higher plants. Overall, future experimentation has been enabled with the optimisation of FRAP in this study.

Chapter 3: Pyrenoid starch sheath dynamics during division

Chapter summary

During cell division, organelles and organellar components must be partitioned for inheritance by daughter cells. It is not yet known how the starch sheath surrounding the pyrenoid matrix of *Chlamydomonas* is inherited during division. To gain insight into this process, previously published matrix division dynamics were re-produced using time-lapse imaging of lines expressing fluorescently-tagged Rubisco. Characteristics commonly seen in LLPS organelles were observed, including a phase transition, followed by formation of puncta *de novo* which coalesced. The creation of dual-tagged Rubisco-starch lines allowed hypotheses to be put forward for the involvement of the starch sheath during pyrenoid division: a passive role for starch association with the matrix, an active role for starch “pinching off” matrix, sequential starch degradation and synthesis, and dissociation of the starch to allow matrix “escape”. Further exploration of the starch degradation and synthesis hypothesis was carried out using known *Arabidopsis* starch modifying enzymes to BLAST for *Chlamydomonas* homologs. Previously published mRNA expression data was then used to find candidates with peak mRNA abundance during the division window. This further refined candidates that may be involved in starch granule initiation (Cre10.g457500), starch synthesis (the coiled-coil containing soluble starch synthases 2 and 6), and degradation (including PHO2 and STA4) during division. Proteins with AMPK1 carbohydrate-binding modules (CBMs) within the CBM48 family, and phosphofructokinases 1 and 2 may also be involved in modifying starch during division. By furthering our understanding of the involvement of the starch sheath during a vital cellular process, we hope to gain insight into the requirements needed to engineer a pyrenoid into higher plants.

Introduction

Plant cell division requires controlled partitioning of cellular components, including organelles, into each daughter cell (Sheahan *et al.*, 2004). Whilst most eukaryotes carry out binary division, *Chlamydomonas* undergoes multiple fission events (Heldt *et al.*, 2020). This is enabled by a prolonged G1 phase causing cell size to increase by more than 2-fold followed by alternating phases of DNA synthesis and mitosis (Cross and Umen, 2015). The volume of the mother cell determines the number of divisions per cell cycle, producing 2, 4, 8, 16 or 32 cells, with daughter cells having uniform size (Lien and Knutsen, 1979; Craigie and Cavalier-Smith, 1982). *Chlamydomonas* grows during the day and carries out DNA

synthesis and division at night (Cross and Umen, 2015). Division is controlled by light intensity, growth rate and starch reserves which supply energy (Vítová *et al.*, 2011). Similar to *Arabidopsis*, *Chlamydomonas* accumulates starch during the day, which is then degraded at night, when grown autotrophically (Levi and Gibbs, 1984; Klein, 1987; Thyssen *et al.*, 2001; Graf *et al.*, 2010; Zones *et al.*, 2015).

In *Chlamydomonas*, there are two fractions of starch, the pyrenoid starch sheath which forms under LC conditions and the stromal starch which accumulates under HC conditions (Kuchitsu *et al.*, 1988). The stromal and pyrenoid starch pools are structurally distinct, as seen by their absorbance spectra, with pyrenoid starch suggested to have more amylopectin (Kuchitsu *et al.*, 1988). Pyrenoid starch sheath granules are 'contorted' in order to form a close fit around the pyrenoid matrix and therefore pose a challenge to starch granule morphogenesis (Izumo *et al.*, 2011). It has been postulated that starch (along with cell size) plays a critical role in division, as it may be needed to pass a commitment point (Vítová *et al.*, 2011). However, how the stromal and pyrenoid pools of starch contribute to division is not yet known. Pyrenoid fission (which takes ~7 min) occurs at the end of chloroplast division (which takes ~30-80 min) and is driven by the chloroplast cleavage furrow (Johnson and Porter, 1968; Goodenough, 1970; Freeman Rosenzweig *et al.*, 2017). FTSZ proteins mediate chloroplast cleavage by forming a contractile ring at the chloroplast midpoint (Vitha *et al.*, 2001), and have circadian expression along with MIND and MINE1 proteins which are proposed to be involved in FTSZ ring positioning (Colletti *et al.*, 2000; Hu *et al.*, 2008).

The movement of Rubisco within the pyrenoid matrix during division has been characterised and shows that the pyrenoid matrix is inherited by elongation and fission (Goodenough, 1970) or by *de novo* synthesis (Freeman Rosenzweig *et al.*, 2017). For the former, it was shown that when a mother pyrenoid divides, matrix material elongates forming a dumbbell shape, with two puncta joined by a bridge of matrix material. The puncta then separate to form two daughter pyrenoids (Freeman Rosenzweig *et al.*, 2017). It is not clear how the starch sheath is involved when the matrix elongates and forms a bridge between daughter pyrenoids before fission (Freeman Rosenzweig *et al.*, 2017). For either inheritance pattern, Rubisco was shown to disperse and undergo a partial phase transition from aggregated to partially soluble (Freeman Rosenzweig *et al.*, 2017). However, the crystalline starch sheath surrounding the matrix presumably restricts the movement of Rubisco from the matrix into the stroma during this phase transition. The aim of this study was to generate a dual-tagged Rubisco-starch line to observe Rubisco and starch dynamics simultaneously in dividing cells. By growing *Chlamydomonas* in a 12 h light/12 h dark cycle, cell division can be synchronised to ~1 hour after transition to the dark phase for time-lapse imaging (Fig. 6A) (Cross and Umen, 2015; Onishi *et al.*, 2019).

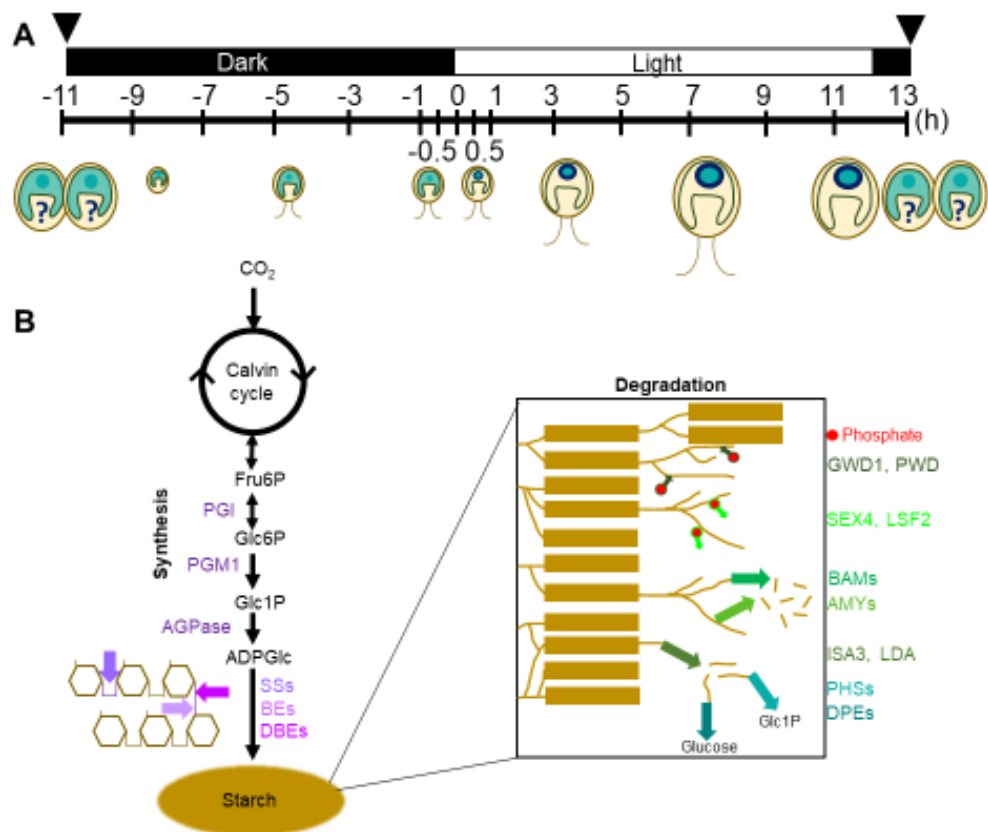


Figure 6. Overview of the life cycle of *Chlamydomonas* and key steps in starch synthesis and degradation.

A. Timeline of mRNA sampling frequency over a 24 h cycle, with a 12 h light/12 h dark regime. The timing of cell division is indicated with black arrows. Respective diagrams of *Chlamydomonas* cells at key stages are shown, with cell division and dispersal of Rubisco into the stroma occurring at -11h and 13h. Cell growth and pyrenoid starch sheath formation occurs during the light phase. The pyrenoid matrix is indicated with cyan and the starch sheath is indicated with dark blue. Adapted from Strenkert *et al.*, (2019).

B. Overview of key enzymes involved in starch synthesis and degradation, adapted from Streb and Zeeman (2012). The conversion of Fructose-6-phosphate (Fru6P), Glucose-6-phosphate (Glu6P), Glucose-1-Phosphate and Adenosine di-phosphate-glucose (ADPGlc) to starch requires phosphoglucose isomerase (PGI), phosphoglucomutase 1 (PGM1), ADPGlc-pyrophosphorylase (AGPase), starch synthases (SSs), starch branching enzymes (SBEs) and debranching enzymes (DBEs). Starch degradation involves a network of kinases (α -glucan, dikinase (GWD1) and phosphoglucan, water dikinase (PWD)), dephosphorylases (Starch Excess 4 (SEX4) and Like Sex Four 2 (LSF2)), β -amylases (BAMs), α -amylases (AMYs), debranching enzymes (isoamylase 3 (ISA3) and limit dextrinase (LDA)), starch phosphorylases (PHSs) and disproportionating enzymes (DPEs).

Starch is an important storage polysaccharide for photosynthetic green algae and plants (Ball and Morell, 2003) and is synthesised from ADP-glucose monomers into amylose and amylopectin polymers. Amylose is mostly unbranched and made from long chains of α -1,4-linked glucose. Amylopectin, which is the more abundant polysaccharide, also contains α -1,6-linked glucose which leads to the formation of branches. Branching allows adjacent chains of α -1,4-linked glucose to form a double helical structure. This leads to the formation of ordered, semi-crystalline starch granules (Ball and Morell, 2003; Smith and Zeeman, 2020).

In photosynthetic organisms, the substrates required for starch synthesis are produced through the Calvin-Benson-Bassham cycle (Smith and Zeeman, 2020). In microalgae, enzymes involved in starch synthesis are exclusively localised inside the chloroplast (Kombrink and Wöber, 1980; Levi and Gibbs, 1984). Phosphoglucose isomerase (PGI) is responsible for reversible isomerisation of Fructose-6-phosphate (Fru6P) and Glucose-6-phosphate (Glu6P) (Smith and Doolittle, 1992), which is then reversibly converted to Glucose-1-phosphate (Glc1P) by phosphoglucomutase (Caspar *et al.*, 1985; Streb *et al.*, 2009). The synthesis of adenosine di-phosphate (ADP)-glucose monomers requires ADP-glucose pyrophosphorylase (AGPase) (Espada, 1962; Smith *et al.*, 1997).

ADP-glucose is then synthesised into polysaccharides through the action of starch synthases, starch branching and debranching enzymes (Fig. 6B) (Smith and Zeeman, 2020). Starch synthases (SSs) use AGPGlc to elongate glucan chains by catalysing the formation of α -1,4 glycosidic bonds, and can be soluble or granule bound (GBSSI). Starch branching enzymes (SBEs/glucanotransferases) make α -1,6-linkages (branch points) by cutting α -1,4-linked glucose chains (Dumez *et al.*, 2006; Streb and Zeeman, 2012). Debranching enzymes (DBEs/mostly isoamylases) hydrolyse α -1,6-linkages which are needed to maintain correct amylopectin branching patterns (Delatte *et al.*, 2005; Streb *et al.*, 2008; Streb and Zeeman, 2012). In *Arabidopsis* starch granule initiation involves starch synthases (SS4 and SS5), the coiled-coil containing proteins MYOSIN-RESEMBLING CHLOROPLAST PROTEIN (MRC) and MAR BINDING FILAMENT-LIKE PROTEIN1 (MFP1), and PROTEIN TARGETING TO STARCH proteins (PTST2 and 3) (Roldán *et al.*, 2007; Ragel *et al.*, 2013; Seung *et al.*, 2017, Seung *et al.*, 2018; Abt *et al.*, 2020). *Arabidopsis* PTST1 is required to localise GBSSI to starch granules (Seung *et al.*, 2015).

Granule-bound starch synthase (GBSSI), named STA2 in *Chlamydomonas*, has been reported to be important for amylose synthesis, either by addition of amylose to pre-existing amylopectin, or by *de novo* synthesis (Delrue *et al.*, 1992; Wattedled *et al.*, 2002). GBSSI requires pre-existing amylopectin to extend amylose chains (Dauvillee *et al.*, 1999) but it has also been suggested that GBSSI synthesises amylopectin itself (Delrue *et al.*, 1992; Maddelein *et al.*, 1994). GBSSI has been identified in a range of plant species,

however the *Chlamydomonas* homolog STA2 has been shown to have 10-50 fold higher activity than vascular plant GBSSI activity (van de Wal, 2000; Wattedled *et al.*, 2002). STA2 has been proposed to contribute to the fusion of starch granules (Wattedled *et al.*, 2002) which may help to keep the starch plates contorted into a tight fit around the pyrenoid (Izumo *et al.*, 2011). STA2 has also been implicated in the CCM, as STA2 mRNA abundance increases (Miura *et al.*, 2004) in conjunction with starch sheath formation under LC (Kuchitsu *et al.*, 1988).

Unlike starch synthesis, which requires a linear pathway, starch degradation in the chloroplasts of plants involves a network of enzymes (Fig. 6B) (Streb and Zeeman, 2012), which lead to the production of Glc1P, glucose and maltose (Lloyd *et al.*, 2005). Phosphorylation of starch is required for degradation, which is carried out by α -glucan, dikinase (GWD1) and phosphoglucan, water dikinase (PWD) (Ritte *et al.*, 2006). Phosphorylation disrupts the packing of amylopectin, leading to destabilisation of double helices (Hansen *et al.*, 2009), meaning the starch granule surface becomes more soluble and available for attack by other enzymes (Hejazi *et al.*, 2008). Conversely the dephosphorylases Starch Excess 4 (SEX4) and Like Sex Four 2 (LSF2) are required to release phosphate from amylopectin (Hejazi *et al.*, 2010; Santelia *et al.*, 2011). Dephosphorylation is required for the function of β -amylases (BAMs), which hydrolyse linear chains at non-reducing ends (Tabata *et al.*, 1978; Lao *et al.*, 1999; Fulton *et al.*, 2008). The hydrolysis of internal α -1,4-bonds is carried out by α -amylases (AMs) (Stanley *et al.*, 2002) whilst the starch debranching enzymes isoamylase 3 (ISA3) and limit dextrinase (LDA) act on α -1,6-linkages (Wattedled *et al.*, 2005; Delatte *et al.*, 2006). Arabidopsis α -glucan starch phosphorylases (PHSs (or PHOs in *Chlamydomonas*)) catalyse the breakdown of starch by releasing Glc1P from the non-reducing ends of α -1,4-linked polysaccharides (Dauvillée *et al.*, 2006). Disproportionating enzymes (DPEs) degrade starch by transferring glucose to an acceptor, releasing a glucan moiety at the non-reducing end (Critchley *et al.*, 2001; Streb and Zeeman, 2012; O'Neill *et al.*, 2015).

The identification of starchless mutants in *Chlamydomonas* with functional CCMs (Villarejo *et al.*, 1996) may suggest that the starch sheath is merely a consequence of high pyrenoid metabolic activity causing an accumulation of adjacent metabolites, such as ADP-glucose and 3PGA (Ball *et al.*, 1991; Izumo *et al.*, 2011). However the starch sheath is hypothesised to act as a barrier to CO₂ escaping the pyrenoid matrix (Ramazanov *et al.*, 1994). Carboxysomes, which play a role in the CCMs of cyanobacteria, are surrounded by a proteinaceous shell which has also been implicated in trapping CO₂ (Dou *et al.*, 2008). Additionally, the carboxysome shell is suggested to sequester Rubisco for protection from O₂, and therefore the wasteful process of photorespiration (Colman, 1989), suggesting pyrenoid starch may also have this role. Recently, it has been shown that starch sheath-less

mutants with defective CCMs (*Isoamylase1* and *sta11-1*) have aberrant LCIB localisation (Toyokawa *et al.*, 2020), which is also suggested to trap CO₂ (Yamano *et al.*, 2010), suggesting the starch sheath may be involved in anchoring additional CO₂ recapture components to the pyrenoid periphery.

The green alga *Ostreococcus tauri* has a single centrally-located starch granule which elongates, divides and partitions into daughter cells during plastid division (Ral *et al.*, 2004), however little is known about starch-partitioning in *Chlamydomonas*. A previous observation suggested the starch sheath remains associated with the pyrenoid matrix during pyrenoid fission (Goodenough, 1970). StArch Granules Abnormal 1 (SAGA1), a protein found at the interface of the pyrenoid matrix and the starch sheath (Itakura *et al.*, 2019), may serve as a linker between the starch sheath and the matrix during division. Alternatively, starch sheath degradation may occur as is suggested for starch granule partitioning at the plastid constriction site in *O. tauri* (Ral *et al.*, 2004), which may be followed by sequential pyrenoid starch synthesis in daughter cells. Depending on the extent of degradation, new starch granules may need to be initiated, however little is known about the proteins involved in starch granule initiation in algae (Seung *et al.*, 2017, Seung *et al.*, 2018; Seung and Smith, 2019). Alternatively, movement of the thylakoids may be involved in pyrenoid starch sheath dynamics during division. For initial investigation of these hypotheses, time-lapse microscopy was carried out to image starch sheath movement (via mCherry-tagged STA2) whilst simultaneously capturing Rubisco movement (via Venus-tagged Rubisco), and compared to already published Rubisco dynamics (Freeman Rosenzweig *et al.*, 2017).

To investigate the role of starch synthesis and degradation during pyrenoid division, a bioinformatics approach was used. Genes which carry out similar functions in *Chlamydomonas* cluster their expression together (Strenkert *et al.*, 2019), including many CCM genes which are co-expressed in the middle of the day (Strenkert *et al.*, 2019) and chloroplast division genes which have peak expression during the light-dark transition (Hu *et al.*, 2008; Zones *et al.*, 2015). The diurnal rhythm of transitory starch synthesis and degradation, with the former occurring during the day, and the latter at night (Lu *et al.*, 2005) may also be controlled by diurnal oscillations in expression of key starch modifying genes (Strenkert *et al.*, 2019). The aim of this bioinformatics approach was to firstly identify genes in *Chlamydomonas* involved in starch modification. This was followed by analysis of mRNA expression data for these genes during the division window, with a goal to elucidate players in synthesis and/or degradation during pyrenoid division. Recent work suggests proteins which contain disorder, coiled-coil and carbohydrate-binding module (CBM) 20 domains are important for the starch sheath surrounding the pyrenoid (Itakura *et al.*, 2019). Therefore, starch modifying candidates with mRNA abundance coinciding with the division window were analysed for these properties. By gaining insight into the role of starch during the division of

the pyrenoid, we may better understand the starch-related requirements for engineering a pyrenoid into higher plants.

Methods

The methods used to gather preliminary data and proposed methods for gathering additional data are outlined below.

Chlamydomonas transformation:

The STA2-mCherry containing plasmid (with hygromycin resistance, available from the Chlamydomonas Resource Center) was extracted (Plasmid Mini Kit, QIAGEN) and linearised by restriction enzyme digest with EcoRV. 10 μL of the linearised plasmid, at a concentration of 14.5 ng kb⁻¹ was prepared. Chlamydomonas wild type and single-tagged Rubisco-Venus (RBCS1-Venus) cells were grown up to concentrations of 5 x 10⁶ mL⁻¹ in a 100 mL volume of TAP and for the tagged cells, with paromomycin (5 $\mu\text{g mL}^{-1}$). Cells were grown with 50 $\mu\text{mol photons m}^{-2} \text{s}^{-1}$ light and stirred at 125 rpm. Cultures were transferred to 50 mL screw-cap plastic tubes and centrifuged at 1000 g for 4 min at room temperature. The supernatant was removed, and pellets were resuspended in TAP-sucrose (40 mM) to make a concentration of 5 x 10⁷ mL⁻¹. 250 μL of each cell suspension was transferred to a 0.4 cm gap electroporation cuvette. Cells were incubated at 16°C for 5 min and 10 μL of the linearised plasmid was pipetted into each cuvette. Cells were electroporated at 800 V and 20 μF with a Gene Pulser II (Bio-Rad). Cells were immediately recovered by transfer to 8 mL of TAP-sucrose in screw-cap plastic tubes. These screw-cap plastic tubes were shaken horizontally at 125 rpm for 16 hours, in the dark. Cells were then centrifuged for 4 min at 1000 g, the supernatant was removed retaining ~500 μL . Cells were resuspended and plated onto TAP-agar plates containing hygromycin (25 $\mu\text{g mL}^{-1}$) and paromomycin (20 $\mu\text{g mL}^{-1}$). Plates were kept in low light (2-10 $\mu\text{mol photons m}^{-2} \text{s}^{-1}$) for ~2 weeks when colonies appeared. The native copies of Rubisco and STA2 in the dual-tagged line were present.

Screening transformants for STA2-mCherry fluorescence:

A 96-well culture plate was prepared containing 200 μL of liquid TAP in each well with appropriate antibiotics (hygromycin (6.25 $\mu\text{g mL}^{-1}$) for the single-tagged lines and paromomycin (5 $\mu\text{g mL}^{-1}$) and hygromycin for dual tagged lines). Individual colonies were numbered and transferred to each well and were left to grow for 5 days in 50 $\mu\text{mol photons m}^{-2} \text{s}^{-1}$ shaking at 125 rpm. 50 μL of each culture was transferred to 100 μL of liquid Tris-Phosphate (TP) (with appropriate antibiotics) in a new 96-well plate for 24 hours. A

ClarioStar plate reader (Tecan M1000Pro) was used to check for mCherry fluorescence using excitation 585/12 nm and emission 615/12 nm.

Confocal microscopy preparation:

Candidate colonies were grown in liquid TAP (and antibiotics) in a volume of 2 mL in 15 mL screw-cap plastic tubes for 5 days at 125 rpm and 50 $\mu\text{mol photons m}^{-2} \text{s}^{-1}$. Cells were upscaled and grown in 25 mL of liquid TAP (and antibiotics) for 2 days in 100 mL conical flasks with shaking. 24 hours before image acquisition, cells were centrifuged at 1000 g for 4 min, the supernatant removed, and re-suspended in 25 mL of TP in 100 mL conical flasks. Cells were grown as before. 40 μL of each culture was pipetted into individual wells in a poly-L-lysine coated Ibidi plate and allowed to dry for 5 minutes. 160 μL of 1.5% (w/v) TP low-melting-point agarose at $\sim 34^\circ\text{C}$ was pipetted into each well and allowed to dry for a further 5 minutes. 200 μL of anti-evaporation oil (Ibidi) was pipetted on top.

Confocal microscopy image acquisition and analysis

Images were taken using a LSM880 (zeiss) confocal microscope with an Airyscan module and a x63 objective. Excitation lasers and emission filters are as follows: Venus excitation 488 nm, emission 420-480 nm; mCherry excitation 561 nm, emission 570-620 nm; chlorophyll excitation 633 nm, emission 495-550 nm. For the time-lapse, a Z-stack of 20 slices (6.9 μm range, 0.36 μm intervals) was taken every 15 min for 80 cycles. A large field of view (zoom=1) allowed for imaging of many cells simultaneously. For the Rubisco-Venus time-lapse analysis, CZI images were exported to FIJI (Schindelin *et al.*, 2012) as virtual stacks and for each time point, the pixels from the Z-stack were summed. To measure Rubisco-Venus fluorescence over time, Regions of Interest were drawn on the summed Z-stack and RawIntDen values were exported to Excel. The dual-tagged Z-stack CZI images were exported to FIJI as virtual stacks.

Proposed growth conditions and image acquisition for time-lapse microscopy of synchronised cells:

Cells from two colonies (2 biological repeats) should be grown for 5 days in 2 mL of liquid TAP in a 15 mL screw-cap plastic tube (with hygromycin and paromomycin). 1 mL of each liquid culture should be upscaled into 40 mL of liquid TAP (with antibiotics) in a 100 mL duran bottle with magnetic stirrer. The two up-scaled cultures should be stirred at 180 rpm in 50 $\mu\text{mol photons m}^{-2}\text{s}^{-1}$ light under a 12-hour light/ 12-hour dark cycle to synchronise cultures. Chlamydomonas should be imaged 1 hour after the light to dark transition when division occurs (Onishi *et al.*, 2019). Cultures should be subcultured so that cells remain in the exponential phase ($\sim 1\text{-}4 \times 10^6 \text{ mL}^{-1}$) and should be synchronised after 2 weeks.

Alternatively, larger volumes of cultures could be grown in $150 \mu\text{mol photons m}^{-2}\text{s}^{-1}$ and bubbled in 0.04% volume CO_2 , stirred and synchronised as above. Microscopy preparation should be carried out as above and the microscope settings reused.

Starch modifier bioinformatics

Candidates were identified using known starch modifying Arabidopsis genes identified in Streb and Zeeman (2012) which were used to BLAST (Goodstein *et al.*, 2012) for homologues in Chlamydomonas using Phytozome V13; <https://phytozome-next.jgi.doe.gov/>. Further candidates were identified by downloading protein sequences from the Chlamydomonas genome annotated by PFAM to have carbohydrate-binding modules (CBMs), and from literature searches (Ball, 2002; Zhan *et al.*, 2018). Candidates were then screened for mRNA expression that was elevated or peaked during division (~1 hour after lights off) (Strenkert *et al.*, 2019). Only candidates with a mean per kilobase of transcript per million mapped reads (FPKM) value over the time course which equalled >1 were included. Candidates with p-values less than 1×10^{-10} were included ((Zones *et al.*, 2015; Hughes, Hogenesch and Kornacker, 2010) using the algorithm JTK (Jonckheere-Terpstra-Kendall) cycle). Expression data was normalised to between 0 and 1. Disorder and PFAM annotation plots were obtained from IUPred2A (Mészáros *et al.*, 2018; El-Gebali *et al.*, 2019; Erdős and Dosztányi, 2020), coiled-coil probabilities were obtained from The MPI Bioinformatics Toolkit (<https://toolkit.tuebingen.mpg.de>) (Lupas *et al.*, 1991; Zimmermann *et al.*, 2018), and protein structural modelling from Phyre2 (Kelley *et al.*, 2015).

Results

Microscopy to reveal insights into Rubisco dynamics and simultaneous starch movement during pyrenoid division

To simultaneously visualise movement of the pyrenoid matrix and starch sheath during pyrenoid division a Rubisco-Venus, STA2-mCherry dual-tagged line was developed. This dual tagged line was imaged every 15 minutes over 20 hours in air levels of CO₂. The heterogeneity of the tagged population meant some cells appeared to have only single tagged Rubisco-Venus. Fig. 7 shows an example time-lapse of a cell within this Rubisco-Venus subpopulation. The cell divided once, producing 2 cells after 75 min (Fig. 7A), and then divided again to produce a total of 4 cells after 135 min (Fig. 7B). During division, Rubisco-Venus total fluorescence intensity was monitored in the pyrenoid (or coalescing puncta), stroma and chloroplast to gain insights into matrix dynamics. The Rubisco-Venus signal dispersed from the pyrenoid into the stroma (Fig. 7A) as the cell prepared to undergo the first division. Rubisco-Venus fluorescence in the pyrenoid decreased by 83% during this dispersal, whilst the stromal signal increased (Fig. 7D). Recovery of pyrenoid fluorescence occurred towards the end of the first division (Fig. 7D), where puncta formed *de novo* and coalesced into an apparent pyrenoid (Fig. 7A, B). In the second round of division larger puncta grew whilst smaller puncta shrank (Fig. 7B) and puncta in daughter cells coalesced over time to form an apparent pyrenoid (Fig. 7C). Again, dispersal of Rubisco-Venus from the pyrenoids into the stroma occurred (Fig. 7B, D), and the Rubisco-Venus signal in the pyrenoids recovered due to coalescing puncta (Fig. 7C, D).

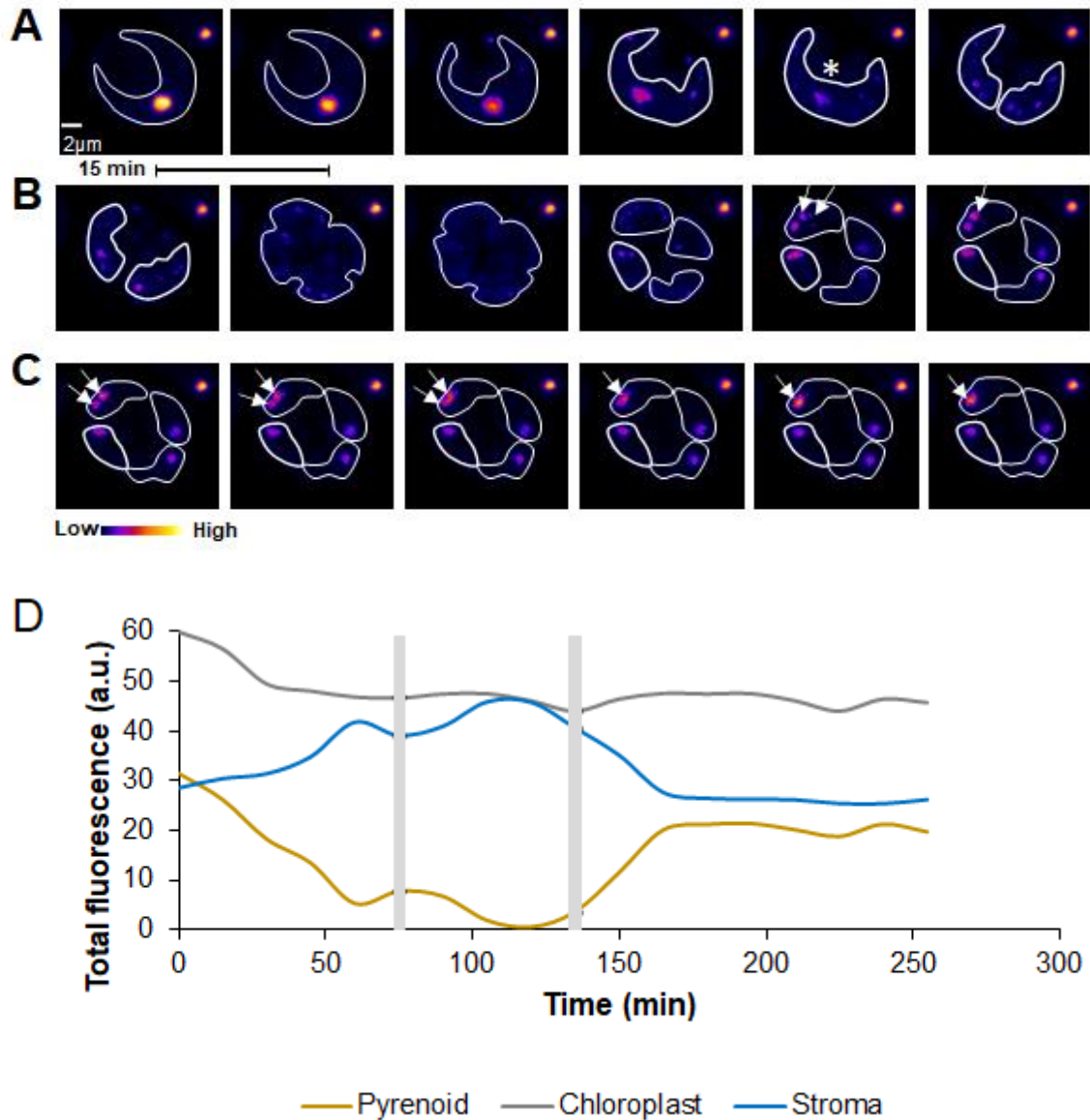


Figure 7. Rubisco-Venus disperses and *de novo*-formed puncta fuse during division. Stills from the time-lapse shown have a time interval of 15 min, and the Rubisco-Venus signal was summed for each Z-stack. The fluorescence intensity is indicated from low to high. The chlorophyll signal is indicated with a white outline. A control (non-dividing) cell pyrenoid is visible at the top right-hand corner of each still image.

A) The first round of division produced two daughter cells. Pyrenoid matrix Rubisco-Venus dispersal at 60 min is indicated with an asterisk.

B) Two daughter cells divided further to produce 4 cells in total. Smaller Rubisco-Venus puncta shrank and growth of larger puncta occurred (white arrows).

C) Puncta fused to form an apparent pyrenoid (white arrows).

D) Raw signal of Rubisco-Venus from A, B and C, in pyrenoids (or puncta which coalesced), stroma and chloroplasts was measured to gain insight into pyrenoid matrix dynamics during division. Vertical grey bars indicate when there were gaps between chlorophyll signals, indicating cells had divided.

To investigate starch sheath dynamics during pyrenoid division, Z-stacks were taken of cells during different stages of the cell cycle (Fig. 8). Cells during interphase had correct localisation of STA2-mCherry signal to the starch sheath, which surrounds the pyrenoid matrix Rubisco-Venus signal (Fig. 8A). There were discernible gaps in the sheath suggesting the STA2-mCherry signal localised to the starch plates as expected (Fig. 8A). A cell with an apparent chloroplast cleavage furrow had a 'stretched' Rubisco signal indicating dispersal (Fig. 8B, Fig. S1). The starch plates appeared to be separate from each other and dissociated from the Rubisco-Venus signal (Fig. 8B, Fig. S1). A cell which had undergone pyrenoid division, but had not yet completed chloroplast division, contained two pyrenoids both with Rubisco aggregates surrounded by starch plates with gaps (Fig. 8C). Traversing thylakoids were also present within these pyrenoids (Fig. 8C). A cell undergoing division which had already produced two separate pyrenoids, appeared to show division in a third pyrenoid (Fig. 8D, Fig. S2). Two lobes of Rubisco-Venus signal joined by a bridge of Rubisco-Venus were observed, whilst the STA2-mCherry signal remained in close association to the periphery of the Rubisco-Venus signal (Fig. 8D, Fig. S2). Future work should aim to capture pyrenoid starch sheath movement during division as in Fig. 8 by using the time-lapse conditions used for data acquisition in Fig. 7.

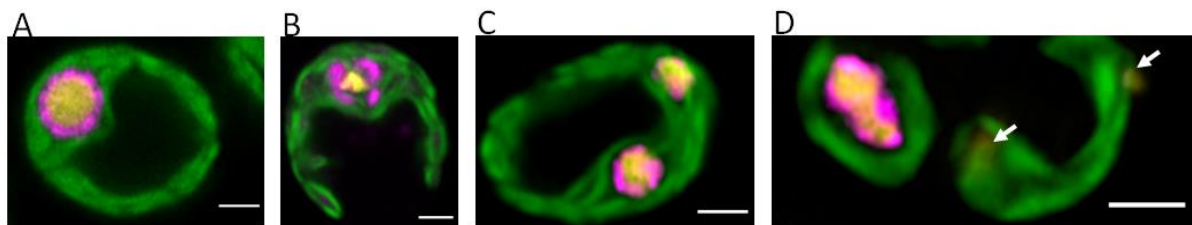


Figure 8. Representative stages of cell division with dual tagged Rubisco-Venus (yellow, pyrenoid matrix) and STA2-mCherry (pink, starch sheath). Each image shows a single section from a Z-stack of each cell. Chlorophyll signal, which aligns with the chloroplast thylakoids and traversing pyrenoid thylakoids, is green. All scale bars are 2 μ m.

- A. Pre-division cell with STA2-mCherry signal (starch sheath) surrounding the Rubisco-Venus (pyrenoid matrix) signal. Gaps between the starch plates were visible.
- B. Cell with apparent dispersal of Rubisco-Venus signal and separation between the plates and Rubisco-Venus signal, and between starch plates.
- C. Cell with two pyrenoids, both with associated starch sheath and traversing thylakoids.
- D. Cell with two pyrenoids (white arrows) and a pyrenoid with apparent lobes and adjoining bridge, and associated STA2-mCherry signal.

Bioinformatics to investigate possible pyrenoid starch degradation and synthesis during pyrenoid division

Starch synthesis

To investigate the hypothesis that starch degradation and synthesis may be involved in starch inheritance during pyrenoid division, a bioinformatics approach was used. To firstly identify potential candidates involved in starch modification in *Chlamydomonas*, proteins involved in *Arabidopsis* starch synthesis and degradation identified in Streb and Zeeman (2012) (Fig. 6B) were used to BLAST for *Chlamydomonas* homologs (Phytozome V13) (Table 1, 2). All proteins reported to be involved in starch synthesis in *Arabidopsis* (Streb and Zeeman, 2012) showed homology to *Chlamydomonas* proteins, and respective homologs had equivalent descriptions of function (Phytozome V13). Interestingly, the four *Arabidopsis* AGPase LSU's (APL1-4) appeared to have greater homology to the *Chlamydomonas* AGPase LSU STA1, than *Chlamydomonas* LSU's AGP2 and AGP3 (Table 1).

Table 1. Proteins involved in starch synthesis in *Arabidopsis thaliana* (Streb and Zeeman, 2012; Abt *et al.*, 2020) showed homology to starch synthesis proteins in *Chlamydomonas reinhardtii*. Only the top hits are presented.

<i>Arabidopsis thaliana</i>			<i>Chlamydomonas reinhardtii</i>				
Gene ID	Alias	Description	Gene ID	Alias	Description	E-value	Identity (%)
AT4G24620.1	PGI	Phosphoglucose isomerase	Cre03.g175400.t2.1	PGI1	Phosphoglucose isomerase	5.82E-38	28
AT5G51820.1	PGM	Phosphoglucosmutase	Cre06.g278210.t1.1	GPM1	Phosphoglucosmutase	<4.70E-176	68
AT5G48300.1	APS1	AGPase small subunit 1	Cre03.g188250.t1.2	STA6	ADP-glucose pyrophosphorylase small subunit	<4.70E-176	65
AT1G05610.1	APS2	AGPase small subunit-like 2	Cre13.g567950.t1.2	STA1	ADP-glucose pyrophosphorylase large subunit	1.25E-110	42
AT5G19220.1	APL1	AGPase large subunit 1	Cre13.g567950.t1.2	STA1	ADP-glucose pyrophosphorylase large subunit	<4.70E-176	64
AT1G27680.1	APL2	AGPase large subunit 2	Cre13.g567950.t1.2	STA1	ADP-glucose pyrophosphorylase large subunit	<4.70E-176	55
AT4G39210.1	APL3	AGPase large subunit 3	Cre13.g567950.t1.2	STA1	ADP-glucose pyrophosphorylase large subunit	<4.70E-176	52
AT2G21590.1	APL4	AGPase large subunit 4	Cre13.g567950.t1.2	STA1	ADP-glucose pyrophosphorylase large subunit	4.70E-176	56
AT1G32900.1	GBSS	Granule-bound starch synthase 1	Cre17.g721500.t1.2	STA2	Granule-bound starch synthase I	2.40E-171	53
AT5G24300.1	SS1	Soluble starch synthase 1	Cre12.g521700.t1.2	SSS6	Soluble starch synthase	6.09E-164	53
AT3G01180.1	SS2	Soluble starch synthase 2	Cre03.g185250.t1.2	SSS2	Soluble starch synthase II	<4.70E-176	64
AT1G11720.2	SS3	Soluble starch synthase 3	Cre06.g282000.t1.1	STA3	Soluble starch synthase III	<4.70E-176	42
AT4G18240.1	SS4	Soluble starch synthase 4	Cre16.g663850.t1.1	SSS5	Putative soluble starch synthase	1.89E-135	41
AT5G65685.1	SS5	Soluble starch synthase 5	Cre16.g663850.t1.1	SSS5	Putative soluble starch synthase	3.20E-40	30
AT3G20440.2	SBE1	Starch branching enzyme 1	Cre06.g270100.t1.1	SBE2	Starch Branching Enzyme	1.27E-149	42
AT5G03650.1	SBE2	Starch branching enzyme 2	Cre10.g444700.t1.1	SBE3	Starch Branching Enzyme	<4.70E-176	61
AT2G36390.1	SBE3	Starch branching enzyme 3	Cre10.g444700.t1.1	SBE3	Starch Branching Enzyme	<4.70E-176	60
AT2G39930.1	ISA1	Isoamylase 1, starch debranching enzyme	Cre03.g155001.t1.1	ISA1	Isoamylase, starch debranching enzyme	<4.70E-176	52
AT1G03310.2	ISA2	Isoamylase 2, starch debranching enzyme	Cre03.g155001.t1.1	ISA1	Isoamylase, starch debranching enzyme	3.18E-99	31

In addition to homologs identified in Table 1, carbohydrate-binding module (CBM) containing proteins identified by PFAM (Phytozome V13), and other putative proteins involved in starch modification in *Chlamydomonas* (Ball, 2002; Zhan *et al.*, 2018) were taken on for further analysis. The expression of normalised mRNA abundance for candidate genes was surveyed and reported if peak or increased expression occurred during the division window (~1 hour after lights-off), or in the case of starch synthases, in contrast to expected diurnal patterns of expression (Strenkert *et al.*, 2019). Known chloroplast division proteins FTSZ1 and 2, MIND1 and MINE1 (Hu *et al.*, 2008) had mRNA abundance profiles which peaked 2-4 hours before division (Fig. 9). Therefore, starch modifying candidates were also included if their mRNA abundance peaked in preparation for division.

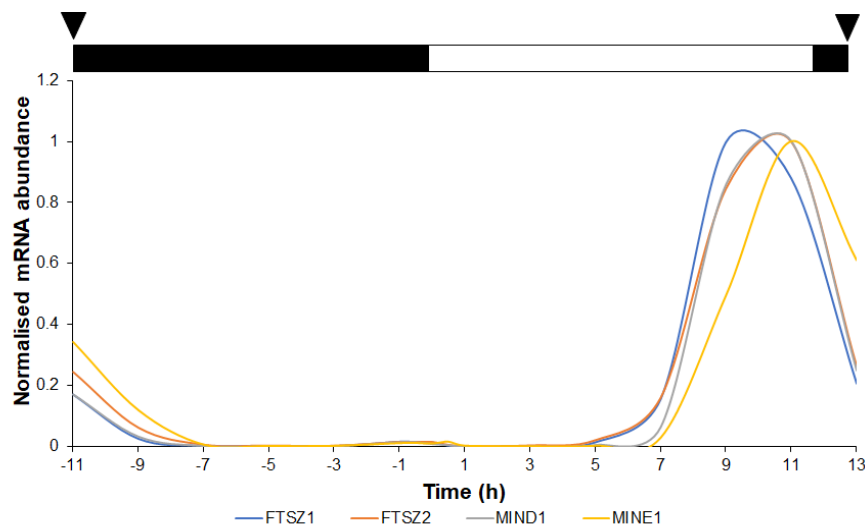


Figure 9. mRNA abundance profiles for proteins known to be involved in chloroplast division (FTSZ1, FTSZ2, MIND1, MINE1). mRNA abundance (Strenkert *et al.*, 2019) was normalised to between 0 and 1. The black and white bars (top) indicate the dark phase and light phase respectively. Black arrows show time of division.

Identification of *Chlamydomonas* proteins which may be involved in starch synthesis (Table 1) allowed investigation of starch synthesis proteins which may be exclusively involved during the time of division, through surveying mRNA abundance. Starch synthases SSS2 and SSS6 identified in Table 1 show increased mRNA abundance during the dark, and reduced abundance during the light phase (Fig. 10). SSS2 had high mRNA abundance from -7h, whilst SSS6 had high mRNA abundance later in the night. Both SSS2 and SSS6 had an additional mRNA abundance peak at dawn.

In addition to starch synthases, *Arabidopsis* starch granule initiation proteins SS4, SS5, and PTST1 and 2 proteins are required for starch synthesis (Roldán *et al.*, 2007; Ragel *et al.*, 2013; Seung *et al.*, 2017, Seung *et al.*, 2018; Abt *et al.*, 2020). *Arabidopsis* SS4 has

41% identity to *Chlamydomonas* SSS5 whilst *Arabidopsis* SS5 has 30% identity with *Chlamydomonas* SSS5 (Phytozome V13, Table 1). Although *Arabidopsis* SS5 is a noncanonical isoform (Abt *et al.*, 2020), homology-based modelling shows *Chlamydomonas* soluble starch synthases closely resemble the family of *Arabidopsis* starch synthases (Table S1).

Whilst the *Arabidopsis* starch granule initiation proteins MRC and MFP1 show no homology to *Chlamydomonas* proteins (Phytozome V13), MRC and MFP1 interact with PTST2 and 3 (Seung *et al.*, 2018) which have 44% and 41% identity to *Chlamydomonas* Cre10.g457500 respectively. Cre10.g457500 is predicted to encode a regulatory β -subunit of a 5'-AMP-activated protein kinase (AMPK1) and contains an AMPK1 CBM (Phytozome V13). Cre10.g457500 interestingly shows peak mRNA abundance at the time of division (Fig. 10). Homology based modelling shows Cre10.g457500 may have some structural resemblance to PTST2 and 3 (Table S2).

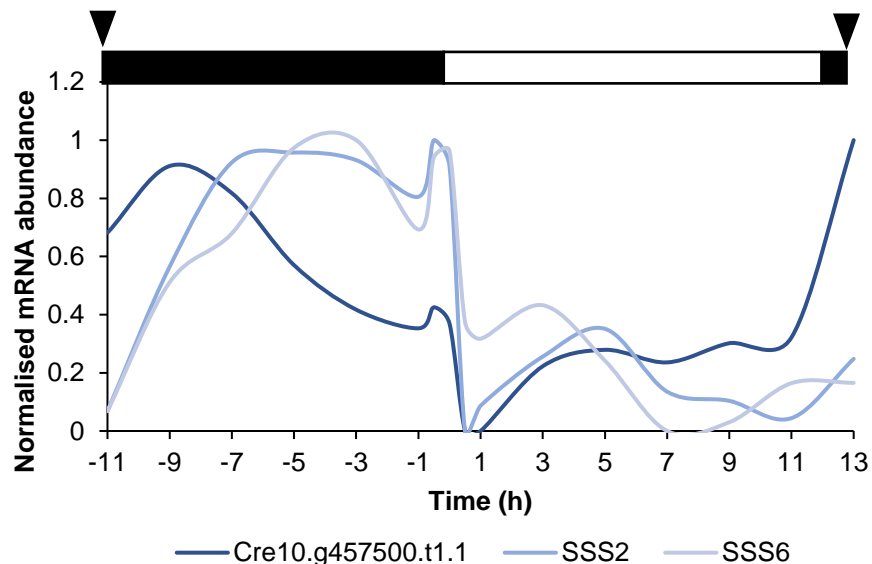
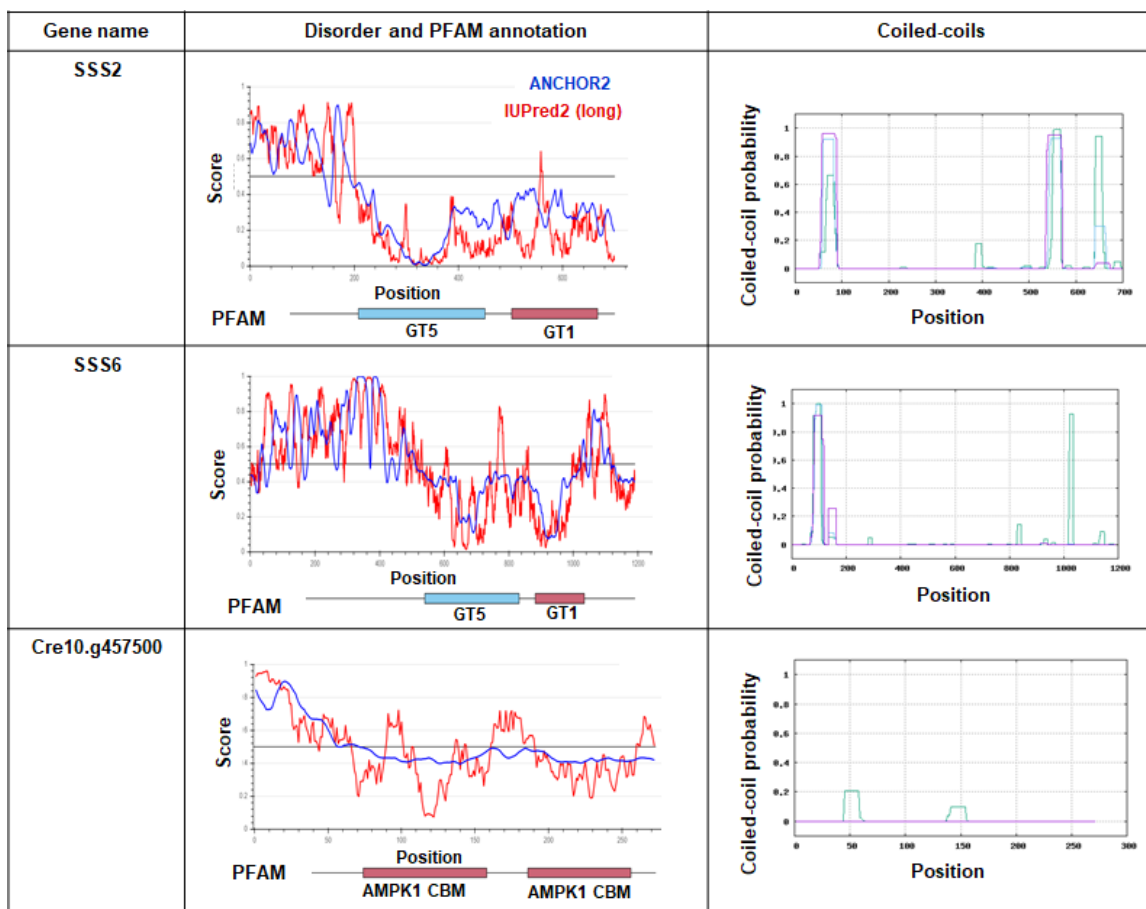


Figure 10. *Chlamydomonas* proteins proposed to be involved in starch synthesis with peak normalised mRNA abundance during the dark phase. mRNA abundance (Strenkert *et al.*, 2019) was normalised to between 0 and 1. The black and white bars (top) indicate the dark phase and light phase respectively. Black arrows show time of division.

Several pyrenoid associated starch binding proteins have been identified, including SAGA1 (Itakura *et al.*, 2019) and LCI9 (Mackinder *et al.*, 2017). Structural analysis of these proteins show that they contain carbohydrate-binding modules, starch-related catalytic domains (Phytozome V13), regions of disorder needed for interactions with proteins in the pyrenoid matrix (Mackinder *et al.*, 2016; Meyer *et al.*, 2020) and coiled-coil domains with unknown function (Itakura *et al.*, 2019). Candidates identified to be homologous to *Arabidopsis* starch

synthesis proteins (Table 1) and to have division-related mRNA abundance profiles (Fig. 10) were then surveyed for characteristics known to be important for proteins which associate with the pyrenoid and pyrenoid starch specifically. Both SSS2 and SSS6 contain glycosyl transferase family domains GT1 and GT5, frequently found in glycosyl transferases (Campbell *et al.*, 1997; Ross *et al.*, 2001), supporting their predicted function (Table 2). SSS2 and SSS6 appear to have a high probability of forming coiled-coils at the N and C-termini, with the C-terminal coiled-coil in SSS2 coinciding with its GT1 domain. This potentially highlights a role for SSS2 interacting with other starch modifying proteins, as a coiled-coil region within the GT1 domain of PTST1 enables interaction with GBSSI, targeting GBSSI to the starch sheath (Seung *et al.*, 2015). SSS2 and SSS6 appear to contain a large region of disorder at the N-terminus, which may suggest they are involved in pyrenoid matrix interactions (Itakura *et al.*, 2019), however they do not contain Rubisco-binding motifs (Meyer *et al.*, 2020). Cre10.g457500 contains two AMPK1 CBM domains and whilst may have regions with disorder, has a low probability of containing coiled-coiled regions (Table 2).

Table 2. Disorder profiles (IUPred2A), PFAM annotations and coiled-coil probabilities (MPI Bioinformatics Toolkit) for *Chlamydomonas* candidates potentially involved in starch synthesis during or after division.



CBM-containing proteins

The presence of CBM-containing proteins which have peak mRNA abundance during the division window may indicate that starch modifying proteins are directly binding to starch during this time. More specifically, CBM20-containing proteins including SAGA1, have been proposed to be important for pyrenoid starch morphology (Itakura *et al.*, 2019). To explore the possibility that CBM-containing proteins (like Cre10.g457500) may be involved in pyrenoid starch sheath remodelling during division, all proteins with annotated CBMs (from PFAM) were surveyed for peak expression during the division window. Two further AMPK1 CBM-containing genes were identified, Cre06.g283400 (CGL101), a predicted sucrose-phosphate phosphatase, and a dual specificity protein phosphatase, DSP8 (Phytozome V13), suggesting they may play a similar role in degrading starch, like other phosphatases (Kötting *et al.*, 2009; Santelia *et al.*, 2011; Streb and Zeeman, 2012). The CBM48-containing protein isoamylase 3 (ISA3) also showed peak mRNA abundance during division and had increased abundance at night (Fig. 11). Similar to Arabidopsis ISA3, peak expression coincides with enzymes which are involved in degrading starch at night (Wattebled *et al.*, 2005). One CBM20-containing protein, Cre06.g269650, also showed peak mRNA abundance during division, with an additional increase in abundance in the middle of the day (Fig. 11). Cre06.g269650 is predicted to be a cyclomaltodextrin glucanotransferase (CGTase) (Phytozome V13). CGTases catalyse the formation of cyclodextrins and have hydrolase activity (Penninga *et al.*, 1995). Therefore, these CBM-containing candidates may be involved in pyrenoid starch binding during division and are predicted to be involved in starch degradation.

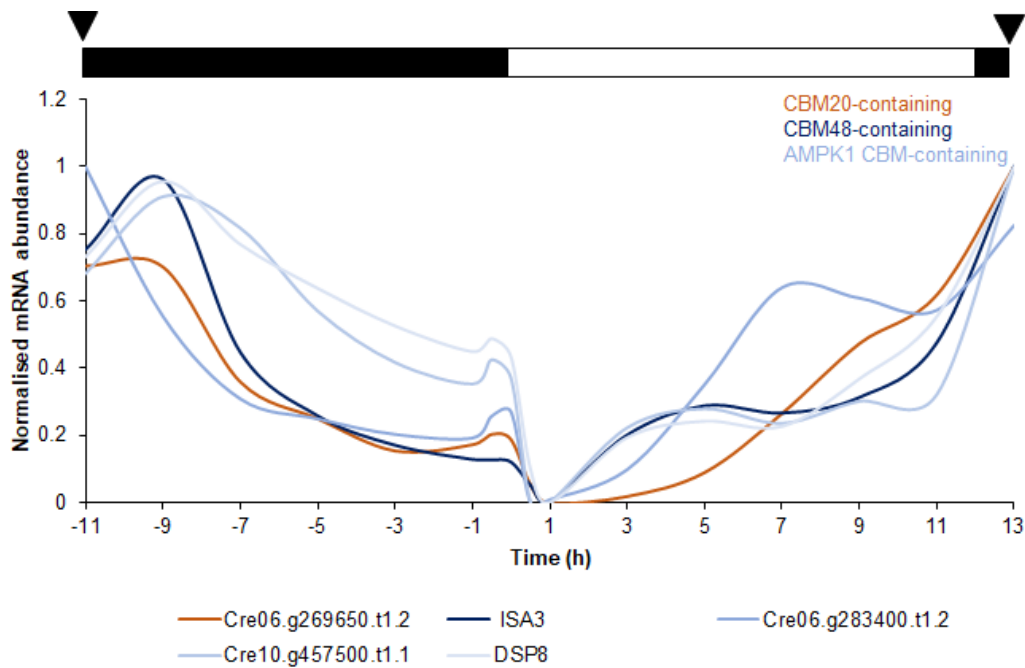


Figure 11. CBM-containing proteins with peak normalised mRNA abundance during the division window (Strenkert *et al.*, 2019). The black and white bars (top) indicate the dark phase and light phase respectively. Black arrows show time of division.

Starch degradation

During division, the pyrenoid matrix has been shown to undergo a phase transition, and form a ‘dumbbell’ shape when two lobes of matrix prepare to separate (Fig. 7, 8D) (Freeman Rosenzweig *et al.*, 2017). This suggests the surrounding starch sheath must undergo a degree of loosening to allow Rubisco escape, which may involve modification by degradation. To investigate this hypothesis, a list of potential *Chlamydomonas* proteins involved in starch degradation were identified using known *Arabidopsis* degradation proteins to BLAST for homologs (Streb and Zeeman, 2012) (Table 3). All nine *Arabidopsis* β -amylases (BAMs) showed the greatest homology to a single β -amylase *Chlamydomonas* AMB1, whilst the three α -amylases (AMs) in *Arabidopsis* showed the greatest homology to *Chlamydomonas* α -amylase AMA2 (Table 3). *Arabidopsis* α -glucan phosphorylases PHS1 and PHS2 showed homology to *Chlamydomonas* STA4 (Table 3).

Table 3. Proteins involved in starch degradation in *Arabidopsis thaliana* (Streb and Zeeman, 2012) showed homology to starch degradation proteins in *Chlamydomonas reinhardtii*. Only the top hits are presented.

<i>Arabidopsis thaliana</i>			<i>Chlamydomonas reinhardtii</i>				
Gene ID	Alias	Description	Gene ID	Alias	Description	E-value	Identity (%)
AT1G10760.1	GWD1 , SEX1	Glucan, water dikinase 1	Cre07.g3193 00.t1.1	GWD1	R1 Protein, α -glucan water dikinase	<9.32E-177	38
AT4G24450.1	GWD2	Glucan, water dikinase 2	Cre07.g3193 00.t1.1	GWD1	R1 Protein, α -glucan water dikinase	<9.32E-177	38
AT5G26570.1	PWD, GWD3	Phosphoglucan, water dikinase	Cre17.g7199 00.t1.2	PWD1	Phosphoglucan water dikinase	2.49E-146	43
AT3G52180.1	SEX4	Starch excess 4, phosphoglucan phosphatase	Cre03.g1510 00.t1.2	DSP8	Dual-specificity protein phosphatase	3.79E-86	49
AT3G10940.1	LSF2	Like Sex Four 2, phosphoglucan phosphatase	Cre09.g4030 50.t1.1	DSP6	Dual-specificity protein phosphatase	1.43E-65	40
AT3G01510.1	LSF1	Like Sex Four 1, phosphoglucan phosphatase	Cre03.g1510 00.t1.2	DSP8	Dual-specificity protein phosphatase	2.60E-26	32
AT3G23920.1	BAM1	Exo-amylase β -amylase	Cre06.g3071 50.t1.1	AMB1	β -amylase	1.63E-155	48
AT4G00490.1	BAM2	Exo-amylase β -amylase	Cre06.g3071 50.t1.1	AMB1	β -amylase	1.93E-126	45
AT4G17090.1	BAM3	Exo-amylase β -amylase	Cre06.g3071 50.t1.1	AMB1	β -amylase	4.54E-161	49
AT5G55700.1	BAM4	Exo-amylase β -amylase	Cre06.g3071 50.t1.1	AMB1	β -amylase	8.94E-127	41
AT4G15210.1	BAM5	Exo-amylase β -amylase	Cre06.g3071 50.t1.1	AMB1	β -amylase	3.46E-122	44
AT2G32290.1	BAM6	Exo-amylase β -amylase	Cre06.g3071 50.t1.1	AMB1	β -amylase	6.39E-139	47
AT2G45880.1	BAM7	Exo-amylase β -amylase	Cre06.g3071 50.t1.1	AMB1	β -amylase	1.36E-108	40
AT5G45300.1	BAM8	Exo-amylase β -amylase	Cre06.g3071 50.t1.1	AMB1	β -amylase	1.51E-92	38
AT5G18670.1	BAM9	Exo-amylase β -amylase	Cre06.g3071 50.t1.1	AMB1	β -amylase	8.10E-78	36
AT4G25000.1	AMY1	Endo-amylase α -amylase	Cre08.g3624 50.t1.2	AMA2	α -amylase	1.66E-116	48
AT1G76130.1	AMY2	Endo-amylase α -amylase	Cre08.g3624 50.t1.2	AMA2	α -amylase	9.65E-156	52
AT1G69830.1	AMY3	Endo-amylase α -amylase	Cre08.g3624 50.t1.2	AMA2	α -amylase	1.26E-149	52
AT4G09020.1	ISA3	Isoamylase 3, starch debranching enzyme	Cre03.g2077 13.t1.1	ISA3	Isoamylase, starch debranching enzyme	<9.32E-177	57

AT5G04360.1	LDA, PU1	Limit dextrinase, starch debranching enzyme	Cre11.g4766 50.t1.1	PUL1	Pullulanase-type starch debranching enzyme	<9.32E-177	42
AT3G29320.1	PHS1	A-glucan phosphorylase	Cre12.g5522 00.t1.2	STA4	Starch phosphorylase	<9.32E-177	50
AT3G46970.1	PHS2	A-glucan phosphorylase	Cre12.g5522 00.t1.2	STA4	Starch phosphorylase	<9.32E-177	54
AT5G64860.1	DPE1	4- α -glucanotransferase disproportionating enzyme	Cre03.g1815 00.t1.2	DPE1; STA11	4- α -glucanotransferase	9.32E-177	49
AT2G40840.1	DPE2	4- α -glucanotransferase disproportionating enzyme	Cre02.g0951 26.t1.1	DPE2	α -1,4-glucanotransferase	<9.32E-177	45

Identified starch degradation candidates were then surveyed for peak mRNA abundance during division. Whilst DSP8 and ISA3 were identified in Fig. 11, a further five candidates showed peak mRNA abundance during the division window, including GWD1 (α -glucan water dikinase), AMA2 (α -amylase), and 4- α -glucanotransferase (DPE1/STA11) (Fig. 12). The role of α -amylases in starch degradation is unclear and may rely on the cooperative action of β -amylases (Yu *et al.*, 2005; Seung *et al.*, 2013). However, similar to Arabidopsis BAMs, no diurnal pattern of expression of Chlamydomonas β -amylases was observed (Smith *et al.*, 2004). Intriguingly, Chlamydomonas AMA2 shows a high probability of having a coiled-coil between position 200-300, which coincides with an area of disorder, and has annotated catalytic domains which confirm its proposed function (Table S3). Arabidopsis DPE1 is an important starch degradation enzyme (Critchley *et al.*, 2001; Yu *et al.*, 2001), and whilst it has been suggested that GWD1 is a regulator of starch degradation (Yu *et al.*, 2001), its role in degradation has more recently been questioned (Skeffington *et al.*, 2014). GWD1 was shown to have a diurnal pattern of mRNA abundance previously (Smith *et al.*, 2004), and also appears to have an additional increase in mRNA abundance during the light period in Chlamydomonas (Fig 12). The plastidial starch phosphorylases PHO2 (PHOA) and STA4 (PHOB) (Phytozome V13) also show peak mRNA abundance during division (Fig. 12). A-glucan phosphorylases were originally thought to be involved in starch degradation (Kruger and ap Rees, 1983), however, this is unclear (Zeeman *et al.*, 2004). Instead, mutants of the STA4 locus in Chlamydomonas suggested phosphorylases contribute to starch synthesis (Dauvillée *et al.*, 2006). Whilst it is not clear that Arabidopsis enzymes previously thought to be involved in starch degradation fulfil this role, mRNA abundance of modifying enzymes in Chlamydomonas peak during the division window, and highlight candidates potentially involved in pyrenoid starch degradation and loosening during division.

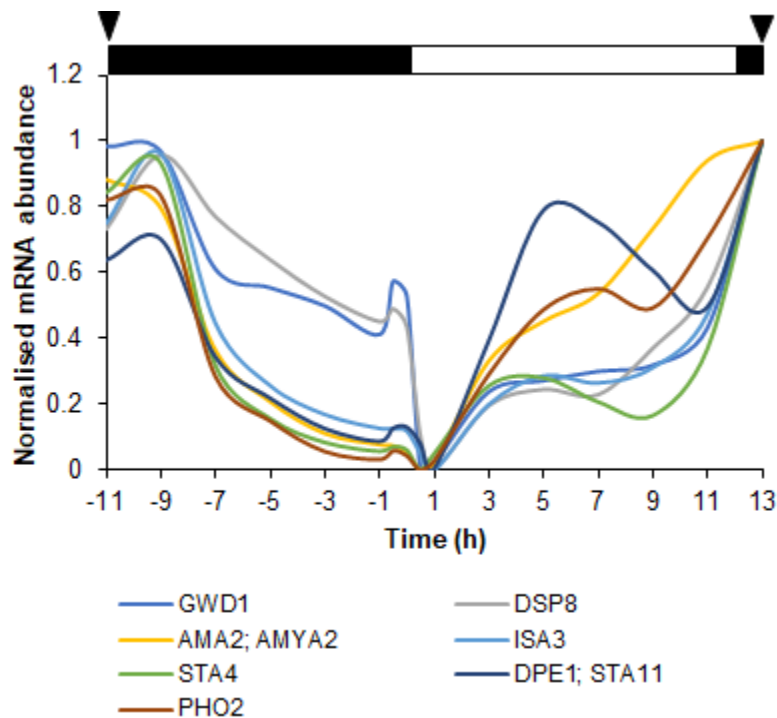


Figure 12. Chlamydomonas proteins potentially involved in starch degradation with peak normalised mRNA abundance during the division window (~1 hour after the light-dark transition) (Strenkert *et al.*, 2019). The black and white bars (top) indicate the dark phase and light phase respectively. Black arrows show time of division.

CCM genes

Previously identified Chlamydomonas proteins proposed to be involved in the formation of pyrenoid starch were surveyed for peak mRNA abundance during division. These candidates were compared to the mRNA abundance of several CCM genes, including the master regulator CCM1 (Fukuzawa *et al.*, 2001), matrix-localised proteins (RBCS1, rbcL, EPYC1, RCA1), puncta-forming proteins involved in CO₂ recapture (LCIB/LCIC) (Spalding *et al.*, 1983a; Mackinder *et al.*, 2017), and inorganic carbon transporters (LCI1, LCIA and HLA3) (Spalding, 2008). CCM genes have peak mRNA abundance either at the dark-light transition or during the light phase (Fig. 13), as seen previously (Zones *et al.*, 2015). LCI9, which is proposed to form a mesh structure between the plates of the starch sheath (Mackinder *et al.*, 2017) shows a similar mRNA abundance profile to other CCM proteins (Fig. 13). However, two phosphofructokinases PFK1 and 2 showed peak mRNA abundance during the division window (Fig. 13). PFK1 and 2 are proposed to form a carbohydrate metabolism module with LCI9 and the Chlamydomonas starch branching enzyme SBE3 (Mackinder *et al.*, 2017), and may regulate glycolysis (Johnson and Alric, 2013). PFK1 and 2 are interesting candidates, in addition to those identified above, as they may be directly involved in modifying pyrenoid starch during the division window.

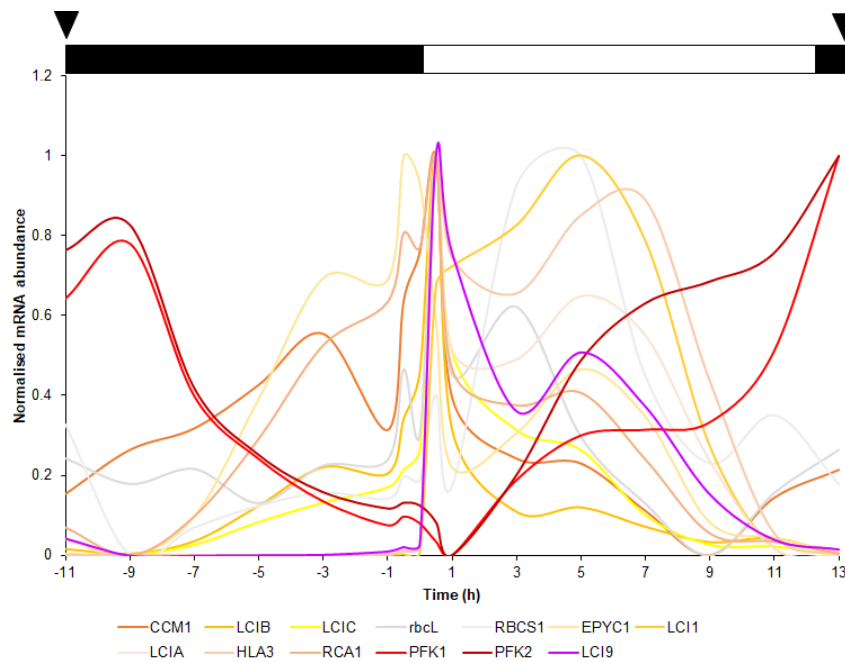


Figure 13. mRNA abundance profiles of CCM genes and previously characterised pyrenoid starch-associated proteins (Strenkert *et al.*, 2019). The black and white bars (top) indicate the dark phase and light phase respectively. Black arrows show time of division.

Discussion

Rubisco dynamics show the pyrenoid is a LLPS organelle

Time-lapse imaging was carried out to observe Rubisco-Venus movement during cell division (Fig. 7). The chlorophyll signal showed that chloroplast division was complete at 75 min (Fig. 7A), which correlated with expected chloroplast division speed (~30-80 min) (Freeman Rosenzweig *et al.*, 2017). In both rounds of division, the reduction of Rubisco-Venus signal in pyrenoids with concurrent increase in stromal signal (dissolution) and then formation of *de novo* puncta (condensation) is indicative of a phase transition (Brangwynne *et al.*, 2009; Freeman Rosenzweig *et al.*, 2017) (Fig 7). The transition from an aggregated to soluble phase is a property of other LLPS compartments (Brangwynne *et al.*, 2009). This phase transition may correspond to a decrease in matrix surface tension, which may be required to allow the passage of the cleavage furrow through the pyrenoid (Freeman Rosenzweig *et al.*, 2017). Dispersal of matrix material may also allow equal partitioning to daughter cells (Freeman Rosenzweig *et al.*, 2017). In the second round of division, coalescence of puncta which appeared *de novo* seemed to form a new daughter pyrenoid (Fig. 7B, C). It is suggested this is the pyrenoid inheritance pattern seen in only 6-7% of all daughter cells (Freeman Rosenzweig *et al.*, 2017). The fusion of droplets (Fig. 7C) suggests material may exchange between puncta. Furthermore, larger puncta grew at the expense of smaller ones (Fig. 7B), a phenomenon known as Ostwald ripening. Therefore, our results

confirm the observation that pyrenoids belong to the class of liquid-liquid phase separated organelles (Hyman *et al.*, 2014; Freeman Rosenzweig *et al.*, 2017). Future work to simultaneously capture starch sheath and Rubisco movement during pyrenoid division is now possible due to the development of a dual-tagged Rubisco-Venus, STA2-mCherry tagged-line.

A possible role for the pyrenoid matrix-starch interface during division

In vitro experiments where the pyrenoid matrix was reconstituted by mixing Rubisco and EPYC1 shows the propensity for matrix material to form large droplets (Wunder *et al.*, 2018). Furthermore, our observations of Ostwald ripening (Fig. 7B), puncta fusion (Fig. 7C) and that ~90% of available Rubisco aggregates into the pyrenoid matrix under LC conditions, show that there is a natural tendency for the matrix to aggregate into a single pyrenoid (Borkhsenius *et al.*, 1998). During division, when one pyrenoid becomes two, this tendency must be counteracted. Recently, a model was proposed which suggested that the enzyme SAGA1 plays a role in constraining the pyrenoid matrix by affecting the surface area of the starch sheath (Itakura *et al.*, 2019). SAGA1 interacts with both large and small subunits of Rubisco, has a CBM20 starch-binding motif and could span the ~30nm gap between matrix and starch (Itakura *et al.*, 2019). The *SAGA1* mutant has ~10 pyrenoids per chloroplast, and the starch sheath plates are elongated and thinner than WT (Itakura *et al.*, 2019). Therefore, the *SAGA1* mutant can counteract the tendency of the matrix to undergo Ostwald ripening to form a single pyrenoid (Itakura *et al.*, 2019).

The proposed mechanism for the role of SAGA1 in controlling pyrenoid number is as follows: the pyrenoid matrix “wets” to one side of each starch plate due to the ability of SAGA1 to simultaneously bind Rubisco and starch, and elongated starch sheath plates in *SAGA1* “pinch off” regions of matrix material to form multiple, smaller droplets. It could be hypothesised that the surface area of the starch sheath plates may influence pyrenoid matrix fission during cell division. Association of the starch sheath with the pyrenoid matrix undergoing fission (two lobes of matrix with an adjoining bridge of matrix) has been previously observed (Goodenough, 1970) and reported in this study (Fig. 8D, Fig. S2). The association of the starch sheath with the matrix during division may be passive, where the cleavage furrow divides the matrix to which the starch stays attached. Division of the single large starch granule in *O. tauri* by the cleavage furrow (Ral *et al.*, 2004) also suggests the pyrenoid starch sheath could be inherited by this mechanism. However, it could be suggested that the morphology and surface area of the starch sheath, under the influence of matrix-starch gap spanning proteins like SAGA1, may be actively involved in the partitioning of matrix material. Fig. 14 provides a visual diagram showing the passive movement or role

of starch association with the matrix during fission (Fig. 14A), along with alternative modes of starch inheritance during division, which will be discussed (Fig. 14B, C, D).

The putative starch synthases SSS2 and SSS6 may be involved in starch synthesis in the dark

Although association of the starch sheath to the matrix during pyrenoid fission seems to be uniform around the matrix periphery (Fig. 8D, Fig. S2), a previous electron micrograph suggests that starch may preferentially bind to one lobe during fission (Goodenough, 1970). This raises the question of how pyrenoid starch may be inherited equally between daughter cells. The phase transition of Rubisco (to the soluble phase) is suggested to be the mechanism for ensuring roughly equal inheritance of matrix material between daughter cells (Freeman Rosenzweig *et al.*, 2017). To ensure there is equal partitioning of pyrenoid starch between daughter cells, one possible mechanism may be the sequential degradation of the starch sheath in the mother cell and synthesis in the daughter cells (Fig. 14B).

Arabidopsis starch synthases SS1 and SS2, which showed homology to *Chlamydomonas* SSS6 and SSS2 respectively (Table 1), are responsible for amylopectin synthesis (Delvallé *et al.*, 2005; Zhang *et al.*, 2008). SSS2 and SSS6 may be implicated in starch synthesis and remodelling after division, as they show increased mRNA abundance in the dark (Fig. 10). This is unexpected given that *Chlamydomonas* starch accumulation is reported to occur during the light period, and be degraded in the dark (Levi and Gibbs, 1984; Klein, 1987; Thyssen *et al.*, 2001; Zones *et al.*, 2015). Conversely, Arabidopsis SS2 (which shows homology to SSS2) shows increased transcript expression after transition to the light (Smith *et al.*, 2004). However, it has been demonstrated that transcript abundance does not coordinate within isoforms or proteins involved in the same pathway, and many important starch modifying proteins do not change in transcript abundance diurnally (Smith *et al.*, 2004). Therefore, there is a caveat with correlating peak mRNA abundance time to function, as post transcriptional and post translational regulation are not taken into account (Smith *et al.*, 2004). Indeed, it has been shown that the α -glucan water dikinase GWD1 does not change in protein abundance diurnally, suggesting changes in transcript abundance do not equate to changes in protein abundance, and regulation may be post translational (Skeffington *et al.*, 2014).

SSS2 and SSS6 contain coiled-coils and Cre10.g457500 may be involved in starch granule initiation during division

Both Arabidopsis SS4 and SS5 show homology to *Chlamydomonas* SSS5 (Table 1). Arabidopsis SS4 is proposed to form primer glucans which evade degradation by α -amylase

AMY3 (Seung *et al.*, 2016) and is proposed to control normal starch granule shape (Seung *et al.*, 2017), whilst the recently reported glucan-binding SS5 has also been implicated in granule initiation (Abt *et al.*, 2020). Arabidopsis SSs contain glucosyl transferase catalytic domains GT1 and GT5 at the C-terminus and SS3, SS4 and SS5 contain N-terminal coiled-coil domains (Pfister and Zeeman, 2016; Raynaud *et al.*, 2016; Abt *et al.*, 2020). Coiled-coils consist of α -helices which wrap around each other to form a supercoil, and facilitate protein-protein interactions or act as scaffolds (Mason and Arndt, 2004; Rose and Meier, 2004; Lohmeier-Vogel *et al.*, 2008; Raynaud *et al.*, 2016). Coiled-coil containing proteins may be enriched in the pyrenoid, and have been shown to be important for promoting LLPS (Fang *et al.*, 2019). *Chlamydomonas* SSS6 and SSS2, which peak in mRNA abundance during the dark (Fig. 10), also have GT1 and GT5 domains, and have areas of disorder and coiled-coil propensity similar to Arabidopsis SSs (Table 2). SSS2 appears to have a coiled-coil at its C-terminus which coincides with its GT1 domain (Table 2). This is intriguing as PTST1 is proposed to interact with GBSSI, targeting it to starch, with a coiled-coil domain on its GT1 domain (Seung *et al.*, 2015). Multimeric complex formation of starch modifying proteins has been reported in Arabidopsis and in *Chlamydomonas* (Tetlow *et al.*, 2004; Mackinder *et al.*, 2017). Specifically regarding coiled-coil containing proteins in *Chlamydomonas*, SAGA1 shows homology to coiled-coil containing proteins (Itakura *et al.*, 2019), and Bimodal Starch Granule (BSG1), which may play a role in switching starch metabolism synthesis from pyrenoid to storage starch, also contains a predicted coiled-coil domain (Findinier *et al.*, 2019). Therefore, SSS6 and SSS2 may interact with other starch modifying enzymes through their coiled-coils, and due to their transcriptional expression, may specifically be involved in pyrenoid starch synthesis after pyrenoid division.

In order to extend α -1,4-linked polysaccharides, it is proposed that SSs require a glucan substrate, and therefore rely on the presence of an already present 'granule initial' (Seung and Smith, 2019). Cre10.g457500, which shows homology to starch granule initiation proteins PTST2 and 3 also has peak mRNA abundance at the time of division (Fig. 10). The already identified *Chlamydomonas* protein BSG1 has been suggested to play a similar role to PTST/MRC/MFP proteins, and therefore may also be involved in initiation (Findinier *et al.*, 2019).

PTST2 and 3 are CBM48 and coiled-coil containing (Seung *et al.*, 2017, Seung *et al.*, 2018) and Cre10.g457500 contains two AMPK1 CBM domains (CBM 48 family (CAZy; <http://www.cazy.org>)) (Lombard *et al.*, 2014) and is annotated to be a β -subunit of 5'-AMP-activated protein kinase (AMPK) (Table 2) (Phytozome V13). SnRK1 is the plant ortholog of AMPK and is a heterotrimer containing an α -catalytic subunit, and two regulatory γ and β (CBM-containing) subunits (Polge and Thomas, 2007; Avila-Castañeda *et al.*, 2014; Broeckx *et al.*, 2016; Ruiz-Gayosso *et al.*, 2018). SnRK1 is involved in the target of rapamycin (TOR)

pathway in plants, having an impact on growth-related processes (John *et al.*, 2011) and global regulation of metabolism in response to stress (Polge and Thomas, 2007). Therefore whilst Cre10.g457500 could be implicated in starch granule initiation, if it is part of the Chlamydomonas SnRK1 complex, it may also be involved in global regulation of many downstream targets (Rolland *et al.*, 2006).

In Arabidopsis, the number of starch granules is correlated to the volume of stroma, and granule initiation is carried out when chloroplasts divide (Crumpton-Taylor *et al.*, 2012). Starch granules in immature leaves were more abundant and smaller than in mature leaves, meaning when mesophyll cells expand and chloroplasts undergo several rounds of division (Marrison *et al.*, 1999) there is a larger surface area for synthesis and degradation of starch (Crumpton-Taylor *et al.*, 2012). This, along with the increased mRNA abundance of Cre10.g457500 during division (Fig. 10), may suggest new starch granules may be initiated after chloroplast division in Chlamydomonas. However, it is not clear whether Chlamydomonas requires starch granule initiation proteins as it has been reported that degrading Chlamydomonas starch completely was not possible (Ral *et al.*, 2004), which is also supported by Fig. 8. Nevertheless, if starch is degraded completely or partially at the beginning of division, SSS2 and SSS6, which appear to have increased expression in the dark (Fig. 10), may enable sequential pyrenoid starch sheath synthesis. This would ensure new daughter pyrenoids are surrounded by a starch sheath, which may be needed to allow LLPS of Rubisco (Itakura *et al.*, 2019), localise peripheral components (Toyokawa *et al.*, 2020) and trap CO₂ for the CCM (Ramazanov *et al.*, 1994).

CBM48-containing proteins may play a role in remodelling starch during division

Further investigation of CBM-containing proteins which have peak mRNA expression during the division window revealed more candidates which may be involved in remodelling the pyrenoid starch sheath during this time (Fig. 11). A further two proteins identified contained AMPK1 CBM domains (CBM48 family (CAZy; <http://www.cazy.org>)) (Lombard *et al.*, 2014) (Fig. 11), and like Cre10.g457500, Cre06.g283400 and DSP8 are annotated to be β -subunits of 5'-AMP-activated protein kinase (AMPK) (Phytozome V13.) The CBM48 family is closely related to the CBM20 family, however there are differences in binding-site residues (Christiansen *et al.*, 2009). CBM20-containing proteins are suggested to be important for pyrenoid starch (Itakura *et al.*, 2019), however only one CBM20-containing protein, Cre06.g269650, showed peak mRNA abundance during division (Fig. 11). It could be hypothesised that CBM20-containing proteins are involved in pyrenoid structural organisation, and CBM48-containing proteins are involved in pyrenoid starch remodelling. Cre06.g269650 is a predicted cyclomaltodextrin glucanotransferase (CGTase). It is intriguing that this putative CGTase peaks in mRNA abundance during division, as CGTases are

industrially relevant enzymes involved in the modification and hydrolysis of starch (Benavent-Gil *et al.*, 2020).

Starch degradation of the pyrenoid starch may take place during division

In comparison to the number of starch synthesis candidates with peak mRNA abundance during division (Fig. 10), Fig. 12 shows evidence that starch degradation may be more prominent during this time. Whilst these candidates lack disorder and have different domains, AMYA2, DSP8, STA4 and PHO2 may all contain coiled-coils (Table S3). ISA3 has been reported to function in starch degradation during the night (Delatte *et al.*, 2006) which illustrates that it is difficult to predict which proteins may be exclusively involved in the potential process of starch degradation at the pyrenoid periphery during the division window (~1 hour after the light-dark transition) and the diurnal pattern of starch degradation (Levi and Gibbs, 1984; Klein, 1987; Thyssen *et al.*, 2001; Zones *et al.*, 2015). However, the number of potential candidates involved in degradation with peak expression at 1 hour after the light-dark transition suggests it is possible that the pyrenoid starch sheath is degraded during division (Fig. 12). This prediction must be made with some caution however, as it is not clear whether the Arabidopsis homologs of Chlamydomonas degradation candidates are involved in degradation (Zeeman *et al.*, 2004; Skeffington *et al.*, 2014) or whether they are functionally redundant (Seung *et al.*, 2013). Whilst the starch sheath may not be completely degraded (Fig. 8), a degree of loosening of the starch sheath plates may be needed for Rubisco to escape and undergo a phase transition.

CCM genes show expected diurnal rhythms of expression, however PFK1 and 2 may be involved during division

CCM genes show changes in mRNA abundance with peak levels coinciding with the transition to light, as expected for genes involved in photosynthesis (Strenkert *et al.*, 2019). CCM genes were compared to the mRNA abundance profiles of previously identified proteins proposed to be associated with Chlamydomonas starch (Mackinder *et al.*, 2017). PFK1 and 2 show similar mRNA abundance profiles to candidates in Fig. 12, with peak abundance coinciding with the transition into dark and division (Fig. 13). PFK is regulated by ATP and converts Fru6P into fructose 1,6-bisphosphate (Johnson and Alric, 2013). PFK1 and 2 are proposed to form a carbohydrate-metabolism module in Chlamydomonas with the predicted glucan 1,4- α -glucosidase LC19 (pyrenoid mesh-layer), and starch branching enzyme SBE3, which interacts with starch synthase STA3 and disproportionating enzyme DPE2 (Mackinder *et al.*, 2017). Therefore whilst PFK1 and 2 may play a role in regulating glycolysis (Johnson and Alric, 2013), their interaction with other pyrenoid-starch associated proteins and peak mRNA abundance during division suggests they may be specifically involved in pyrenoid starch modification during division.

Pyrenoid starch dissociation and the involvement of thylakoids

An alternative explanation for starch sheath movement and inheritance during division is that starch plates dissociate from the matrix allowing the matrix to ‘escape’ the starch sheath to undergo the phase transition (Fig. 8B, Fig. S1, Fig. 14C). Observations also suggest there may be involvement of the traversing pyrenoid thylakoids during division, as traversing thylakoids are present in both daughter pyrenoids in the mother cell before cytokinesis (Fig. 8C). The pyrenoid thylakoids are proposed to anchor the pyrenoid to the base of the cell. Interestingly, a mutant lacking the pyrenoid matrix is still able to retain the correct thylakoid network localisation, suggesting matrix and thylakoid biogenesis are separate processes (Caspari *et al.*, 2017). However, in this mutant, starch granules still localise to the region where the pyrenoid would normally reside. If Rubisco escapes out of the starch sheath during the phase transition (Fig. 8B, Fig. S1, Fig. 14C) it could be suggested that starch granules stay localised to this region by the thylakoids (Fig. 14D). However, direct interaction was not observed between the knotted thylakoids and starch in the matrix-less mutant (Caspari *et al.*, 2017). Therefore, further work is needed to understand whether starch dissociation and/or movement of thylakoids may be involved during division.

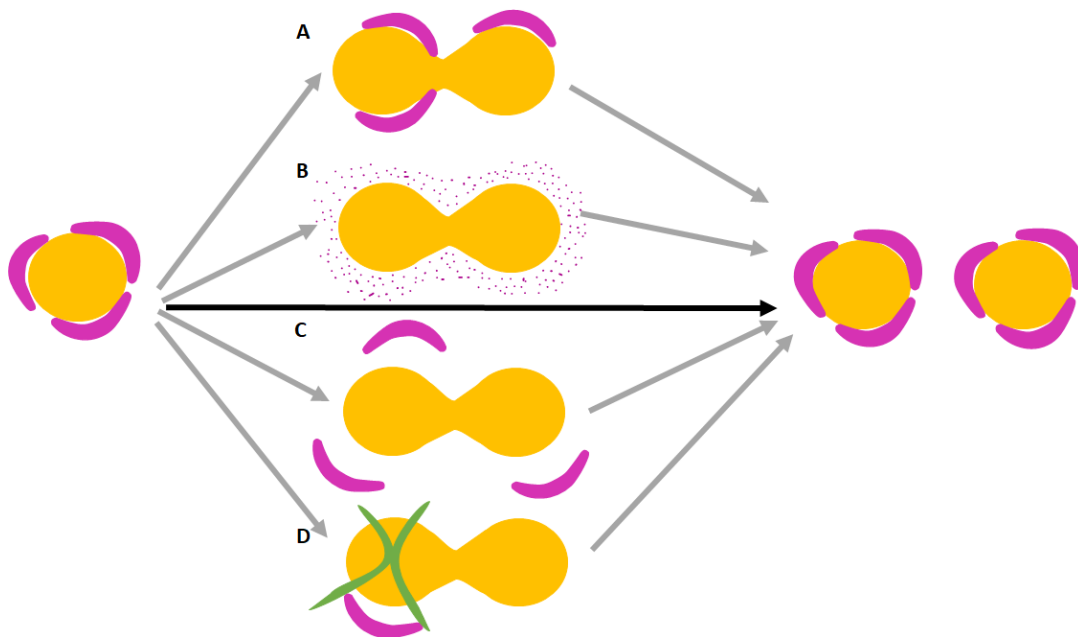


Figure 14. Hypothetical models of pyrenoid starch dynamics during pyrenoid fission.

- A) The starch sheath stays associated or is involved in “pinching” matrix off during fission.
- B) Sequential degradation and synthesis of starch may occur.
- C) The starch sheath may dissociate from the matrix, allowing the matrix to “escape” between starch plates.
- D) The role of the traversing pyrenoid thylakoids should be considered during pyrenoid fission.

The role of the starch sheath in the CCM as a trap for CO₂

There has been some contention over the importance of the starch sheath for the CCM (Villarejo *et al.*, 1996). However, the recent elucidation of the requirement of starch to localise LCIB puncta to the pyrenoid periphery (Toyokawa *et al.*, 2020) suggests the starch sheath plays a key role in the CCM. The combined effect of starch as a suggested CO₂ barrier (Ramazanov *et al.*, 1994) in physical association to the proposed β -carbonic anhydrase activity of LCIB (Jin *et al.*, 2016) may contribute to an efficient CO₂-trapping function for the CCM. This is particularly intriguing when considering LCIB to be part of a C_i recycling mechanism (Chapter 4), which may be aided by enrichment of LCIB in the gaps of the starch sheath (Yamano *et al.*, 2010; Mukherjee *et al.*, 2019). However further work is needed to find a linker protein enabling this interaction between the starch sheath and LCIB, as the LCIB/C complex does not contain starch-binding domains (Toyokawa *et al.*, 2020). Starch branching enzyme SBE3, LCI9 and ISA1 contain carbohydrate-binding domains and therefore could act as starch-LCIB linkers, much like SAGA1 acts as a Rubisco-starch linker (Mackinder *et al.*, 2017; Zhan *et al.*, 2018; Itakura *et al.*, 2019; Toyokawa *et al.*, 2020). Alternatively, this interaction may be mediated by LCIB/C binding to BST1-3 (Mackinder *et al.*, 2017).

Chapter 4: LCIB/C and BST1-3 may interact to aid inorganic carbon recycling

Chapter summary

The CCM of *Chlamydomonas* relies on C_i transport to the pyrenoid and mechanisms which prevent CO_2 escape. Transport of HCO_3^- into the pyrenoid thylakoid tubules and hydration of CO_2 to HCO_3^- to maintain intracellular C_i are functions proposed to be carried out by BST1-3 and LCIB/C respectively. It has been suggested that BST1-3 and LCIB/C work together to form a C_i recycling mechanism, which would maximise their contribution to the CCM. To investigate previously reported protein-protein interactions between these complexes, recombineering was carried out to fuse key proteins to the fluorophore mScarlet-i. The development of LCIB-mScarlet-i and BST1-mScarlet-i constructs means transformation of single Venus-tagged *Chlamydomonas* lines can now be carried out, for further analysis of interactions using Förster Resonance Energy Transfer (FRET). Appropriate controls for future FRET experiments have been suggested, along with direction for further investigation of potential LCIB binding to the C-termini of BST1-3. Interrogation of the proposed C_i recycling mechanism in *Chlamydomonas* may reveal key components for consideration when engineering pyrenoids into higher plants.

Introduction

The *Chlamydomonas* CCM requires several HCO_3^- and CO_2 transporters to increase intracellular concentrations of C_i (Moroney and Ynalvez, 2007). CCM induction occurs simultaneously with the formation of structures, such as the starch sheath and LCIB/C puncta, which are suggested to prevent CO_2 escape (Ramazanov *et al.*, 1994; Duanmu *et al.*, 2009; Yamano *et al.*, 2010; Wang and Spalding 2014). In VLC conditions, HCO_3^- must be actively transported from the extracellular environment (Reinfelder, 2011) and converted by a carbonic anhydrase (CAH3) to CO_2 in proximity to Rubisco (Sinetova *et al.*, 2012). The channels responsible for HCO_3^- transport across the plasma and chloroplast membranes are well-known (Im and Grossman, 2002; Wang and Spalding, 2014; Yamano *et al.*, 2015; Kono *et al.*, 2020), however the proteins proposed to transport HCO_3^- across the thylakoid membranes have only recently been elucidated. Three thylakoid membrane localised proteins were identified and named Bestrophin-like proteins (BST1-3) (Mukherjee *et al.*, 2019). Bestrophin proteins have been found in diverse species, including the bestrophin-like

protein, AtVCCN1, found in Arabidopsis (Herdean *et al.*, 2016), the Human Bestrophin-1 (Best1) and its bacterial homolog, KpBest (Yang *et al.* 2014). Bestrophins are typically anion channels which transport Chloride (Cl⁻) ions, but Best1 is also HCO₃⁻ permeable (Qu and Hartzell, 2008). In Chlamydomonas, BST1-3 were found to localise to the chloroplast thylakoids and pyrenoid thylakoid tubules (Mukherjee *et al.*, 2019). RNA interference of BST1-3 caused reduced growth in LC, poor C_i affinity and the inability to accumulate HCO₃⁻ (Mukherjee *et al.*, 2019). Therefore BST1-3 are proposed to be involved in the final step of HCO₃⁻ transport across the thylakoid membrane, for conversion to CO₂ by CAH3.

BST1 may play a greater role in HCO₃⁻ transport and C_i recycling than BST2 and BST3. Modelling of BST1 shows it contains an entry pore with a neutral/negative electrostatic potential and its selection pore is positively charged, increasing its likelihood to transport negatively charged ions such as HCO₃⁻ (Mukherjee *et al.*, 2019). This is further supported by preliminary *Xenopus laevis* electrophysiology data which shows BST1 is HCO₃⁻ permeable (unpublished data from the Mackinder laboratory). Therefore, BST1 should be given priority for further analysis.

Whilst we now have more insight into the delivery of HCO₃⁻ to Rubisco, how CO₂ is prevented from escaping the pyrenoid is still largely unknown. The starch sheath surrounding the pyrenoid matrix has been proposed to be a barrier to escaping CO₂ (Ramazanov *et al.*, 1994), whilst the protein complex LCIB/C is also thought to act as a CO₂ trap (Duanmu *et al.*, 2009). Recently, the interconnectedness of these structures has been elucidated, as the starch sheath is required for localising LCIB puncta to the periphery of the pyrenoid (Toyokawa *et al.*, 2020). LCIB plays a key role in the CCM to acclimate to LC conditions (Spalding *et al.*, 1983a; Wang and Spalding, 2006) and is proposed to act by hydrating CO₂ to HCO₃⁻ (Wang *et al.*, 2015). Structural analysis of LCIB has confirmed it belongs to a family of β-carbonic anhydrases due to similar zinc-binding motifs, active sites and overall folding compared to other β-carbonic anhydrases. Whilst carbonic anhydrase activity for LCIB has yet to be demonstrated, homologs from other species have carbonic anhydrase activity (Jin *et al.*, 2016). It has been suggested that LCIB works downstream of CAH3, and therefore LCIB is proposed to trap the CO₂ released by CAH3 which does not react with Rubisco (Duanmu *et al.*, 2009). In the stroma, LCIB interacts with LCIC to form a 350kDa complex (Yamano *et al.*, 2010), in a 1:1 stoichiometry (Jin *et al.*, 2016). LCIB/C changes localisation under different conditions; in the light and in limiting-CO₂ conditions LCIB/C localises to the pyrenoid periphery whilst in the dark and in HC conditions LCIB/C localises in a diffuse pattern in the stroma (Yamano *et al.*, 2010). The function of LCIC has not yet been shown, but it could be hypothesised that it is needed for correct LCIB localisation.

Therefore, it is proposed that LCIB is both a CO₂ trap and concurrently a contributor to the stromal HCO₃⁻ pool (Wang *et al.*, 2015). This stromal HCO₃⁻ is proposed to enter the thylakoid lumen through BST1-3 for dehydration in proximity to Rubisco by CAH3. Therefore a C_i recycling mechanism has been proposed involving LCIB/C, BST1-3 and CAH3 (Fig. 15) (Mukherjee *et al.*, 2019). To avoid a futile cycle whereby HCO₃⁻ enters the thylakoid lumen, is converted to CO₂ and escapes again, CAH3 has been shown to localise to the pyrenoid tubules under LC conditions (Blanco-Rivero *et al.*, 2012; Mukherjee *et al.*, 2019).

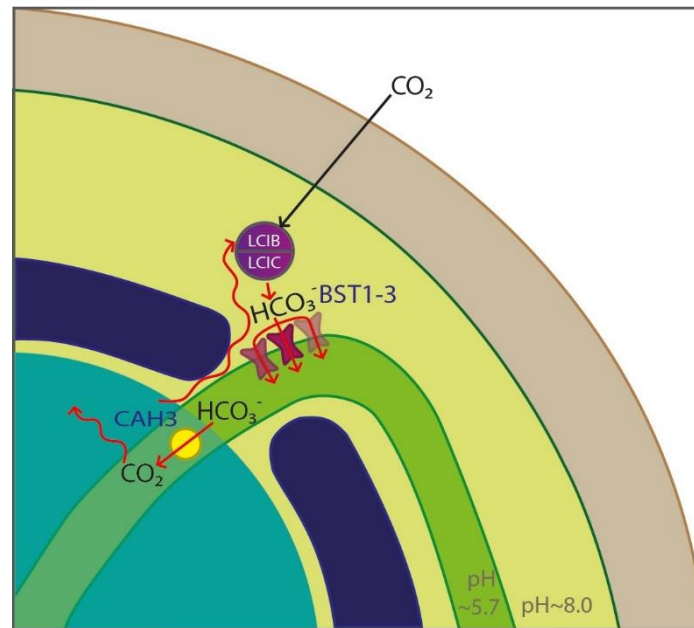


Figure 15. C_i recycling by LCIB/C, BST1-3 and CAH3 allows CO₂ to be released in close proximity to Rubisco whilst preventing CO₂ escape from the pyrenoid matrix.

This proposed C_i recycling mechanism has led to the hypothesis that the key CCM components involved may interact. In order to identify interactions between CCM components, affinity purification mass spectrometry (AP-MS) has previously been used, whereby bait proteins were interrogated using prey proteins containing a 3xFLAG tag (Mackinder *et al.*, 2017). It was shown that BST1-3 interact with each other, LCIB and LCIC interact with BST3, and LCIC also interacts with BST1 (Mackinder *et al.*, 2017). However, this technique is limited; AP-MS cannot distinguish between interactions that are direct and indirect. Therefore proteins which form large complexes may appear to interact with the bait when this interaction may be limited to specific complex members (Mackinder *et al.*, 2017).

Whilst BST1-3 proteins show low sequence identity to human Best1 and Arabidopsis AtVCCN1, BST1-3 proteins are >80% identical to each other (Mukherjee *et al.*, 2019). However, BST1-3 proteins have differences in their C-termini and therefore may play different roles in the CCM (Mukherjee *et al.*, 2019). Whilst BST1-3 may have redundant

functions, the individual BST proteins may contribute to varying degrees to the recycling of C_i in association with LCIB/C. Therefore, further interrogation of the interactions between BST1-3 and the LCIB/C complex is needed.

To investigate specific interactions between CCM components an alternative method, Förster Resonance Energy Transfer (FRET), can be used. FRET is a process where energy is transferred non-radiatively from an excited donor fluorophore to an acceptor molecule (Ishikawa-Ankerhold *et al.*, 2012). FRET can only occur within the range of less than 10 nm and therefore indicates fluorophores are in close proximity (Ishikawa-Ankerhold *et al.*, 2012). By fusing fluorophores to proteins hypothesised to interact, FRET is able to indicate the formation of a long-lived, specific complex between the donor- and acceptor-labelled proteins (Gu *et al.*, 2004). There are several FRET detection techniques, including acceptor-sensitized emission FRET (seFRET) which allows measurement of the change of the donor emission in the presence of the acceptor. If FRET occurs, the donor emission decreases whilst the acceptor emission increases (Gu *et al.*, 2004). An additional intensity-based FRET technique called acceptor depletion FRET (adFRET) measures donor fluorescence after photobleaching the acceptor. This will result in de-quenching of the donor, causing an increase in donor fluorescence (Gu *et al.*, 2004).

FRET requires the excitation spectrum of the acceptor molecule to overlap with the emission spectrum of the donor molecule (Stryer, 1978). Whilst there are many appropriate fluorophores which can act as FRET pairs (Ishikawa-Ankerhold *et al.*, 2012), the fluorophores most easily available for this study include Venus, a yellow fluorescent protein (YFP), and mScarlet-i, a red fluorescent protein (RFP). Venus has an absorption maximum of 514nm (Rekas *et al.*, 2002) whilst mScarlet-i has an absorption maximum of 569nm (Bindels *et al.*, 2017) therefore Venus can be used as a donor, and mScarlet-i as an acceptor. Using mScarlet-i as the FRET acceptor is advantageous because it has been shown to outperform other RFPs for FRET (Bindels *et al.*, 2017). Already available *Chlamydomonas* lines with single Venus-tagged proteins can be transformed with mScarlet-i-tagged proteins to investigate interactions. Until now, the mScarlet-i-tagged CCM proteins needed to investigate the C_i recycling hypothesis have not been available. Therefore, FRET can now be used to study these key CCM protein interactions, by using appropriate FRET-pair fluorophores fused to BST1-3 and LCIB/C.

Tagging *Chlamydomonas* proteins with fluorophores has previously been carried out by constructing plasmids using Gibson Assembly (Mackinder *et al.*, 2017). Genomic DNA was PCR-amplified and cloned in frame with a C-terminal Venus tag and a strong PsaD promoter. A short linker was constructed between the target protein and fluorescent protein (GDLGGSGGR) (Mackinder *et al.*, 2017). However for this cloning method, cloning success was reduced for long genes and for genes with a low expression level (Mackinder *et al.*,

2017). This becomes challenging for cloning *Chlamydomonas* genes, which have an average length of 4312 bp (Merchant *et al.*, 2007). The gene length of LCIB is 3036 bp, whilst BST1 is 2843 bp long (Goodstein *et al.*, 2012). The *Chlamydomonas* nuclear genome also poses problems for PCR-based cloning because it is GC-rich (68%) and genes are intron-rich, which are long (98.5% are >100bp) and have repeating sequences (Merchant *et al.*, 2007). It has been recently shown that introns from native highly expressed genes in *Chlamydomonas* are able to enhance nuclear gene expression through intron-mediated enhancement, especially when introns are in close proximity to the transcription start site (Baier *et al.*, 2020).

An alternative method, recombineering, is independent of gene size and allows introns and native regulatory structures, including promoters, to be maintained. Maintenance of these parts has been shown to be important for transgene expression in *Chlamydomonas* (Schroda, 2019). Recombineering has recently been used in *Arabidopsis* where >250 genes were tagged (Brumos *et al.*, 2020) and the method for recombineering in *Chlamydomonas* has recently been made available (Emrich-Mills *et al.*, 2020). To undergo recombination, Bacterial Artificial Chromosomes (BACs) in *Escherichia coli* (*E. coli*) are made competent for recombination by introducing the proteins from the bacteriophage lambda virus, Red α , β and γ (Fig. 16A) (Yu *et al.*, 2000; Copeland *et al.*, 2001). 50 bp homology arms needed to retrieve the gene of interest from the BAC are PCR-amplified at both ends of the fluorophore (which is contained within a linearised plasmid) (Fig. 16B). Tagging target genes with fluorophores via recombineering allows visualisation of endogenous expression and localisation of the gene in interest (Sarov *et al.*, 2006). In this study, recombineering was used to fuse a mScarlet-i tag to LCIB and BST1 which can then be transformed into a combination of lines containing different Venus-tagged proteins. Transformations for the creation of appropriate control lines would allow investigation of specific protein-protein interactions using FRET. Interrogation of the interactions between BST1-3 and LCIB/C via FRET may elucidate the key proteins within these complexes which are responsible for C_i recycling in the CCM.

Methods

Recombineering:

Bacterial strains:

DH10B *Escherichia coli* cells containing LCIB and BST1 within bacterial artificial chromosomes (BACs) are available from the Chlamydomonas Resource Centre, University of Minnesota, USA.

pLM162, which contains the mScarlet-i fluorophore and hygromycin resistance gene (*AphVII*) was maintained in DB3.1 *E. coli* cells. DB3.1 cells were obtained from ThermoFisher Scientific, and contain *ccdA*, the *ccdB* antidote gene for recombineering vector maintenance.

For recombination competence, DH5a *E. coli* cells containing a pRed vector were used. The pRed vector expresses viral proteins (Red $\alpha\beta\gamma$) and *recA* controlled by an arabinose inducible promoter, which when transformed into the BAC strain, gives the potential for recombination (Sarov *et al.*, 2006).

Day 0-Preparation for transformation:

One colony of pRed containing cells was grown at 37°C overnight, shaking at 200 rpm, with lysogeny broth (LB) and tetracycline (5 $\mu\text{g mL}^{-1}$) in a 3 mL volume. One colony of pLM162 containing cells were grown at 37°C overnight, shaking at 200 rpm, with lysogeny broth (LB) and kanamycin (25 $\mu\text{g mL}^{-1}$) in a 3 mL volume. The following day, pRed and pLM162 plasmids were extracted (Plasmid Mini Kit, QIAGEN) and concentrations were ascertained by a nanodrop spectrophotometer and stored at 4°C (pRed) and -70°C (pLM162). One colony of each BAC strain containing LCIB and BST1 genes were grown overnight at 37°C, with shaking at 200 rpm, in yeast extract nutrient broth (YENB) containing Chloramphenicol (12.5 $\mu\text{g mL}^{-1}$). All of the growth steps were carried out in a 3 mL volume in a 15 mL screw-cap plastic tube.

Day 1-pRed transformation preparation:

The pRed plasmid was diluted to 0.1 ng μL^{-1} in H₂O, making a volume of 100 μL for each reaction. Before transformation, the microcentrifuge was pre-cooled to 4°C, and the 10% (v/v) glycerol, 2 mm gap electroporation cuvettes (1 per reaction), 2 mL micro-centrifuge tubes (1 per reaction) and diluted pRed plasmid were cooled on ice. At room temperature, 2 mL micro-centrifuge tubes (1 per reaction) containing 800 μL super optimal broth with catabolite repression (SOC) were prepared.

Day 1-pRed transformation:

After ~16h of growth, 40 μL of the BAC strains from the previous day were inoculated into 900 μL of YENB with Chloramphenicol ($12.5 \mu\text{g mL}^{-1}$) in a 2 mL micro-centrifuge tube and grown for 3 hours at 37°C . The saturated BAC strain growth was transferred to a pre-cooled 2 mL micro-centrifuge tube for 2 min (on ice), and then centrifuged for 10 min at 4°C and 5000 g . The supernatant was removed, and the tube was put back on ice. 1 mL 10% (v/v) glycerol was used to resuspend the pellet gently, followed by centrifugation and the supernatant removal as before, then put back on ice. The pellet was resuspended in 100 μL $0.1 \text{ ng } \mu\text{L}^{-1}$ pRed plasmid and transferred to a pre-chilled cuvette, which was electroporated using a Gene Pulser II (Bio-Rad) at 2500 V, 400 Ω and 25 μF (Fig. 16A). For recovery, immediate transfer of the cells to the pre-prepared SOC followed by 90 min of recovery growth at 30°C with shaking at 200 rpm was carried out. After recovery 400 μL of the outgrowth was inoculated into 1 mL YENB with chloramphenicol ($12.5 \mu\text{g mL}^{-1}$) and tetracycline ($5 \mu\text{g mL}^{-1}$), and grown overnight at 30°C with shaking at 200 rpm.

Day 1-Preparation of the PCR product:

The recombineering cassette from pLM162 was amplified by PCR (Phusion Hotstart II polymerase, ThermoFisher Scientific) in a 50 μL reaction using primers which contain 50 bp homology arms which flank the target gene (Fig. 16B, supplementary method 1). 1 μL of the PCR product was analysed on an agarose gel and the product was kept at 4°C overnight.

Day 2-PCR product transformation preparation:

The PCR product was purified using a MinElute Gel Extraction Kit, QIAGEN and the concentration was measured using a nanodrop spectrophotometer. The PCR product was diluted to $5 \text{ ng } \mu\text{L}^{-1}$ in H_2O , for a volume of 100 μL for each reaction. After ~16h of growth, 120 μL of saturated outgrowth from the previous day were inoculated into 950 μL of YENB with Chloramphenicol ($12.5 \mu\text{g mL}^{-1}$) and tetracycline ($5 \mu\text{g mL}^{-1}$) in a 2 mL micro-centrifuge tube and grown for 3 hours at 30°C with shaking as before. 20 μL of 10% (w/v) L-arabinose was added to each tube and grown at 37°C for 1 hour with shaking as before. The following pre-cooling and transformation steps were performed as outlined previously, with the only change being the addition of 100 μL of $5 \text{ ng } \mu\text{L}^{-1}$ of the PCR product, instead of the diluted pRed plasmid (Fig. 16C). 90 min of recovery growth was carried out at 37°C . 900 μL of outgrowth was plated on 2 LB agar plates with kanamycin ($25 \mu\text{g mL}^{-1}$), therefore 450 μL on each plate, allowed to dry and incubated at 37°C overnight. The following day, 8 colonies from each reaction were picked with a sterile loop and seeded onto an LB agar plate with $25 \mu\text{g mL}^{-1}$ kanamycin and grown at 37°C overnight whilst the same loop was used to inoculate LB liquid media with kanamycin ($25 \mu\text{g mL}^{-1}$) in a 3 mL volume and grown at 37°C overnight

with shaking as before. The following day, plasmids were extracted from the liquid growth (Plasmid Mini Kit, QIAGEN) and the concentration was measured using a nanodrop spectrophotometer. The plasmids underwent a *SacI* restriction enzyme digest which was analysed on an agarose gel. Geneious software (Geneious 11.1.5) was used to carry out in silico plasmid assembly and to visualise sequencing data (GATC Bioscience). Sequencing was carried out on the recombineered constructs LCIB-mScarlet-i (forward primer: 5'-GAGCAAACGTACGGCAAAGC-3', reverse primer: 5'-CTGCCGTGGGACTAGATGTT-3') and BST1-mScarlet-i (forward primer: 5'-ATGCAAGCAAACCGTTCGTA-3', reverse primer: 5'-CTGCCGTGGGACTAGATGTT-3').

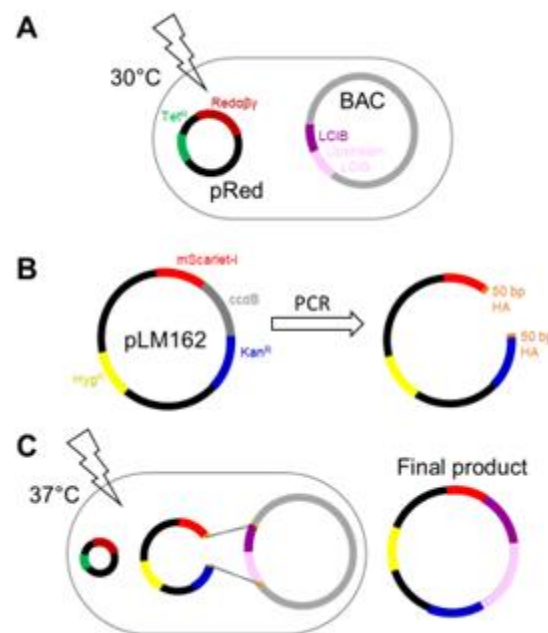


Figure 16. Visual representation of recombineering method for LCIB-mScarlet-i. A) The pRed plasmid was transformed into a BAC strain containing the gene of interest (LCIB) to give the potential for recombineering. B) The mScarlet-i containing plasmid was PCR amplified using primers containing 50 bp homology arms. C) To undergo homologous recombination the pRed plasmid was activated at 37°C with addition of L-arabinose, producing a final product containing the gene of interest and fluorophore (LCIB-mScarlet-i). The same method was carried out to produce BST1-mScarlet-i. The plasmid maps of the final products of LCIB-mScarlet-i and BST1-mScarlet-i are shown in Fig. S3.

Results

To investigate the interactions of key CCM components for confirmation of the C_i recycling hypothesis, *Chlamydomonas* lines containing appropriate FRET-pair fluorophores needed to be generated. Recombineering was used to fluorescently tag the genes of interest, LCIB and BST1, with the monomeric fluorescent protein mScarlet-i (Fig. 16). A restriction enzyme digestion was then carried out to verify that recombination had been successful (Fig.

17). For LCIB-mScarlet-i, colony 2 (C2) represents an example colony showing the expected banding pattern, whilst colony 1 (C1) represents an example colony showing the expected banding pattern with addition larger bands, suggesting partial digestion of the plasmid occurred (Fig. 17A).

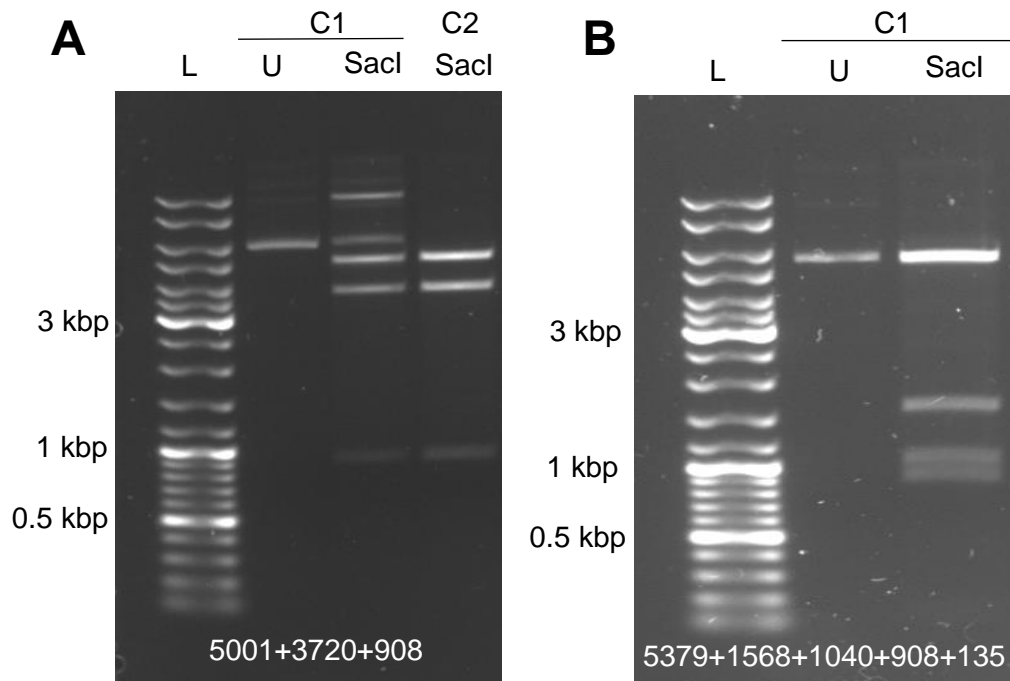


Figure 17. DNA gel electrophoresis of A) LCIB-mScarlet-i and B) BST1-mScarlet-i after restriction enzyme digest using *SacI*, to ascertain if recombination had been successful. Expected band sizes after digestion by *SacI* are presented at the bottom of the gel in white. L: ladder, U: undigested DNA, *SacI*: DNA digested with *SacI* restriction enzyme, C1: colony 1, C2: colony 2.

For LCIB-mScarlet-i, two out of eight colonies (colony 2 and 3) showed correct band patterns when compared to a virtual gel created by in-silico recombineering (Fig. S4A, B). The other six out of eight colonies showed correct bands with additional larger bands, suggesting partial digestion of the plasmid occurred (Fig. S4A, B). For BST1-mScarlet-i, only colony 1 appeared to have the correct banding pattern (Fig. 17B, Fig. S4C, D). However, four other colonies (colony 3, 6, 7, 8) showed similar banding patterns with either less clarity or additional partial digestion bands, but may serve as additional candidates (Fig. S4C, D). Due to partial digestions it was difficult to determine success rates, but examples that showed correct complete digestions gave success rates of 25% for LCIB-mScarlet-i and 12.5% for BST1-mScarlet-i. To verify that the recombineered plasmids were correct, candidate colonies from Fig. 17 were selected and confirmed by sequencing (Fig. S5). Plasmid maps for BST1-mScarlet-i and LCIB-mScarlet-i are presented in Fig. S3.

Discussion

FRET may now be possible due to recombineered mScarlet-i containing plasmids

The successful recombination of LCIB-mScarlet-i and BST1-mScarlet-i (Fig. 17) means it is now possible to create dual-tagged *Chlamydomonas* lines by transformation for FRET. Confirmation that plasmids are correct by sequencing (Fig. S5) means a combination of *Chlamydomonas* transformations can now be carried out, to create appropriate controls and results using FRET (Table 4 and Chapter 3, Methods). Screening for fluorescence would require a plate reader assay, and correct localisation of fluorescence would require confocal imaging (Chapter 3, Methods). However, the caveats of recombineering should be considered, including the effect of random insertion and the presence of the native copy of the gene.

For FRET, further controls will be needed to account for spectral bleed-through, which occurs due to the spectral overlap between the fluorophores. This may be from the donor emission into the acceptor emission (emission cross-talk), and by direct excitation of the acceptor through excitation of the donor (excitation cross-talk) (Ishikawa-Ankerhold *et al.*, 2012; Broussard *et al.*, 2013). Cells containing single Venus-tagged proteins need to be imaged to calculate a correction for emission cross-talk, whilst cells containing single mScarlet-i-tagged proteins are needed for the excitation cross-talk correction. Also, additional background fluorescence may be present in the acceptor channel. Therefore, control unlabelled cells should be imaged to measure autofluorescence (Broussard *et al.*, 2013). Additionally, spectral unmixing may be necessary to remove unwanted signals (Gu *et al.*, 2004). By taking control measurements into account, seFRET image processing and analysis can be carried out (Broussard *et al.*, 2013).

Table 4. Proposed combinations of *Chlamydomonas* transformations using already available *Chlamydomonas* lines and recombineered plasmids from this study. The resulting dual-tagged lines will allow for testing of LCIB/C and BST1 proximity using FRET. Single-tagged Venus and mScarlet-i lines will be needed as additional controls, to correct for emission and excitation cross-talk.

Purpose	Previous work (<i>Chlamydomonas</i> line)	Work from this study (recombineered plasmid)
Proximity test	LCIB-Venus	BST1-mScarlet-i
Proximity test	LCIC-Venus	BST1-mScarlet-i
Positive control	LCIC-Venus	LCIB-mScarlet-i
Negative control	STA2-Venus	LCIB-mScarlet-i

FRET offers a suitable method to study protein-protein proximity within the CCM but has caveats

To define the proximity of fluorophores, the Förster distance (the distance where FRET is at 50% maximum efficiency) can be calculated. The Förster distance between donor Venus and acceptor RFPs such as mCherry is between 5-6 nm, and the Förster distance between mVenus and mScarlet is 6.16 nm (Ishikawa-Ankerhold *et al.*, 2012; Lambert, 2019). Therefore, if FRET was achieved between tagged combinations of LCIB/C and BST1-3, we can assume that the proteins being tested are forming a long-lived, specific complex.

FRET-pair choices are important because FRET efficiency relies on: the quantum yield (brightness) and fluorescence lifetime of the donor, and the spectral overlap, orientation, and distance between fluorophores (Gu *et al.*, 2004). FRET using a YFP-mScarlet-i fusion showed that mScarlet-i has the largest sensitized emission compared to other RFP's (3.3-fold of mCherry and >2.5-fold greater than mRuby2). Therefore mScarlet-i is the most suitable RFP for FRET (Bindels *et al.*, 2017). Another important consideration when choosing fluorophores for FRET is that if the fluorophores themselves dimerise, then false positive interactions may occur or localisation may be perturbed (Kremers *et al.*, 2006). Whilst mScarlet-i is monomeric (Bindels *et al.*, 2017), Venus can form dimers (Rekas *et al.*, 2002) therefore the use of monomeric Venus (mVenus) may be advantageous (Kremers *et al.*, 2006). Monomerization of Venus can be carried out by introducing the mutation A206K (Kremers *et al.*, 2006). However, by using a previously generated single-tagged Venus-containing *Chlamydomonas* line for transformation of mScarlet-i-tagged proteins, cost and time for generating strains can be reduced.

However, there are caveats to FRET which should be taken into account. The small distance in which FRET is possible is a disadvantage when studying protein-protein interactions between multiprotein complexes (Ishikawa-Ankerhold *et al.*, 2012). This may pose a problem when studying the interactions of the 350kDa hexamer complex LCIB/C (Yamano *et al.*, 2010) and BST1-3 which are also proposed to interact with each other (Mackinder *et al.*, 2017). Therefore, a false negative result may be given if the proteins being tested interact, but the fluorophores are not close enough to undergo FRET (Broussard *et al.*, 2013). False negatives may also arise because even highly efficient FRET-pairs only produce FRET efficiencies of 10-40% (Broussard *et al.*, 2013). However, despite these caveats, FRET offers an advantage over AP-MS to test the proximity of proteins on the nanometer scale.

The C-termini of BST1-3 may be the location of LCIB/C binding

It is now possible through development of LCIB-mScarlet-i and BST1-mScarlet-i constructs to investigate the proximity of key CCM components proposed to carry out C_i recycling. Due to limited information on *Chlamydomonas* BST1-3, it is not yet clear how BST1-3 interact with each other, how they interact with LCIB/C and the extent to which each Bestrophin-like protein contributes to C_i recycling. Human Best1 proteins are proposed to form homodimers (Stanton *et al.*, 2006), tetramers and pentamers (Sun *et al.*, 2002). The bacterial homolog of Best1 in *Klebsiella pneumoniae*, KpBest, is proposed to form a pentameric assembly (Yang *et al.*, 2014). Modelling of *Chlamydomonas* BST1 shows that a pentameric assembly is likely for BST1-3 (Mukherjee *et al.*, 2019) but requires further verification. However whilst it has been shown that BST1-3 interact with each other (Mackinder *et al.*, 2017), analyses of the stoichiometry of hBest1, 2, 3, and 4 shows that they form homotetrameric channels despite having considerable conservation (Bharill *et al.*, 2014). Self-assembly of hBest1 requires a coiled-coiled domain at the C-terminus (Bharill *et al.*, 2014).

BST1-3 have differences in their C-termini and therefore may play different roles in C_i recycling (Mukherjee *et al.*, 2019). The identification of a protein kinase C phosphorylation site on the C-terminus of hBest1 (Xiao *et al.*, 2009) suggests BST1-3 regulation by phosphorylation at the C-terminus should be considered. Whilst having a modulatory role, the C-terminus is suggested to be important for protein-protein interactions (Tsunenari *et al.*, 2003). Therefore, if FRET shows interactions exist between proteins in the LCIB/C and BST1-3 complexes, it would be interesting to investigate the C-terminus of BST1-3 as a possible location of LCIB/C binding. However it should be noted that whilst there has been much research on the Bestrophin family, BST1-3 show less than 30% protein sequence similarity to other Bestrophins (Mukherjee *et al.*, 2019) and therefore only tentative predictions can be made when comparing function and regulation between homologs.

In summary, investigation of the proximity between BST1-3 and LCIB/C by FRET is now possible due to the development of LCIB-mScarlet-i and BST1-mScarlet-i constructs by recombineering. The involvement of BST1-3 and LCIB/C in a C_i recycling mechanism is not only important to consider for the algal CCM, but also when engineering a pyrenoid into higher plants.

Chapter 5: Final conclusions and future perspectives

Insights revealed into the dynamic nature of the pyrenoid and progress made in this study

Many questions remain unanswered regarding the dynamic nature of the pyrenoid. The first aim of this study was to use FRAP to study the mobility of Rubisco under different growth conditions, and to test if other CCM components are mobile (Chapter 2). Whilst differences in Rubisco mobility were not observed under different growth conditions (Fig. 4), very preliminary data showed that LCI9, forming the proposed mesh-layer between starch plates, may re-homogenise on longer time scales than Rubisco (Fig. 5). The microscope settings and optimisation of sample preparation developed in this study will enable further data to be collected on Rubisco, LCI9, and LCIB/C mobility. The progress made in this study enables FRAP to be used to investigate the mobility of CCM components in the Mackinder laboratory.

The second aim of this study was to gain insight into the movement of the pyrenoid starch sheath during pyrenoid division (Chapter 3). The development of a dual-tagged Rubisco-starch line, and optimisation of time-lapse microscopy settings and sample preparation, meant preliminary data could be collected. Time-lapse microscopy revealed pyrenoid matrix dynamics during division, including formation of puncta *de novo* (Fig. 7), which was previously reported to be a rare event (Freeman Rosenzweig *et al.*, 2017). The additional observations of a phase transition and coalescence of puncta (Fig. 7), means this study confirms the characterisation of the pyrenoid as a LLPS organelle. The dual-tagged line also enabled visualisation of fluorescently-tagged Rubisco and starch during pyrenoid division for the first time (Fig. 8). This led to the formulation of several hypotheses in the involvement of the starch sheath during division (Fig. 14), including an active “pinching” mechanism, whereby starch may facilitate Rubisco partitioning, possibly through the action of starch-Rubisco linker proteins. Alternatively, starch may play a passive role whilst staying associated with the matrix, move away from the matrix to allow Rubisco “escape”, or the thylakoids may play a role. The hypothesis that sequential starch sheath degradation and synthesis may take place during division was further investigated using bioinformatics. This revealed candidates with peak mRNA abundance during division which had suggested roles in starch modification, either by the presence of functional annotated, CBM, or coiled-coil domains potentially facilitating protein-protein interactions. This study reveals the first

insights into the movement of pyrenoid starch during division and provides materials and candidates for further investigation.

The third aim of this study was to elucidate the potential interaction between the thylakoid HCO_3^- transporter complex BST1-3 and the suggested carbonic anhydrase complex LCIB/C (Chapter 4). Recombineering was carried out to create BST1 and LCIB tagged with mScarlet-i, and transformation controls were suggested so that investigation of BST1 and LCIB/C proximity could be tested using FRET (Table 4). Along with starch, LCIB/C is proposed to act as a CO_2 trap, recycling C_i which escaped from the matrix after being transported into the thylakoids by BST1-3 and converted to CO_2 by CAH3. Understanding if these proteins are in close proximity by using these constructs for FRET will help to elucidate the role of this inorganic carbon recycling mechanism (Mukherjee *et al.*, 2019) (Fig. 15) for the CCM.

The work in this study enables future investigation into the dynamic nature of the pyrenoid

The results presented in Chapter 2 are preliminary where the aim was to set up appropriate microscope settings and analysis methods for FRAP. Future work should focus on using growth conditions which have greater biological relevance. The provision of acetate as the sole carbon source (TAP media) requires the glyoxylate pathway which returns glucose (Kunze *et al.*, 2006), and therefore *Chlamydomonas* growth is independent from photosynthesis. This provided the opportunity to collect preliminary results on Rubisco dynamics with dark-grown *Chlamydomonas*. However, this growth method prevents direct comparison between the light and dark conditions due to the induction of different metabolic pathways, including differences in CCM induction, in TP and TAP media. Therefore, *Chlamydomonas* should be grown at high (3% volume) and low (0.04% volume) CO_2 , in the light and dark, prior to collection of further FRAP data. It has been shown that in HC conditions, ~40% of Rubisco was localised to the pyrenoid with an increased stromal localisation, compared to LC conditions where ~90% of Rubisco localised to the pyrenoid (Borkhsenius *et al.*, 1998). Therefore, HC and LC conditions provide the opportunity to study Rubisco mobility under larger differences in Rubisco localisation compared to growth in TP and TAP media and FRAP curve recoveries may vary between conditions. In conclusion, optimisation of FRAP in this study enables further investigation of Rubisco-Venus mobility under different growth conditions and other CCM components such as LCIB/C. FRAP of LCI9-Venus allowed observation of re-homogenisation on longer time scales than Rubisco-Venus (Fig. 4, 5) which means the settings in this study could also be applied to other starch-associated proteins which may recover slowly.

The development of a dual-tagged line for Rubisco-Venus and STA2-mCherry in this study (Chapter 3) means it is now possible to simultaneously capture the movement of Rubisco and starch during pyrenoid division. The starch inheritance hypotheses put forward can now be investigated using the time-lapse imaging microscopy settings in this study. If the starch sheath is required to “pinch off” the matrix during division, and counteracts the natural tendency of matrix material to form one large pyrenoid (Itakura *et al.*, 2019) it would be interesting to observe how pyrenoid division occurs in a starchless mutant. To investigate the starch degradation and synthesis hypothesis, mutations in the candidates highlighted in Chapter 3 could be introduced, and the effect on pyrenoid starch inheritance could be investigated using the dual-tagged line developed and time-lapse microscopy settings. The Rubisco-starch dual-tagged line could reveal further insights into the role of the thylakoids during pyrenoid division by using it to develop a triple-tagged line, with a fluorescently-tagged thylakoid-associated protein. Further testing of the “pinching”, degradation and synthesis, and “escaping” hypotheses is needed to understand how *Chlamydomonas* organises its starch sheath during the process of division. A recent study has highlighted a role for the starch sheath in localising LCIB to the pyrenoid periphery (Toyokawa *et al.*, 2020). This suggests the starch sheath and LCIB may act synergistically for the function of the CCM, with starch acting as a physical barrier to escaping CO₂ (Ramazanov *et al.*, 1994) and LCIB converting escaping CO₂ back to HCO₃⁻ (Jin *et al.*, 2016). The interaction of starch with LCIB may require a linker protein, or could be enabled by interactions with the thylakoid HCO₃⁻ transporters BST1-3, enabling a C_i recycling mechanism (Mukherjee *et al.*, 2019).

Due to the development of LCIB-mScarlet-i and BST1-mScarlet-i constructs and suggested controls for FRET in this study, it is now possible to investigate BST1-3 and LCIB/C proximity. Further examination of the role of these proteins in C_i recycling could involve growing cells at varying levels of CO₂. In HC conditions, LCIB localisation is diffuse in the stroma (Yamano *et al.*, 2010) and therefore the likelihood of interaction with BST1-3 may be reduced. Conversely, the interaction between LCIB/C and BST1-3 may change under VLC conditions, where LCIB plays a lesser role for the CCM than in air levels of CO₂ (Wang and Spalding, 2006). However, in VLC LCIB is localised around the pyrenoid periphery (Yamano *et al.*, 2010) suggesting interaction with BST1-3 may be possible. More specifically, the C-termini of BST1-3 should be considered as the location of LCIB/C binding if FRET reveals protein proximity. This could be tested by carrying out a series of yeast two-hybrid assays with LCIB/C (bait) and BST1-3 with C-terminal truncations (prey).

The work in this study may aid engineering of the pyrenoid into higher plants

The highly efficient biophysical CCM of eukaryotic algae provides an intriguing avenue for engineering and improving photosynthesis in higher plants (Mackinder 2017). The similarity of Rubisco concentrations in algal and plant chloroplasts (Harris and Königer 1997; Freeman Rosenzweig *et al.* 2017) may indicate that Rubisco could be assembled into a pyrenoid in plant chloroplasts. Recent efforts to form Rubisco-EPYC1 condensates in higher plants were limited as EPYC1 was a target for proteolytic degradation (Atkinson *et al.*, 2019), suggesting further work is needed to understand the underlying biophysical and biochemical principles governing LLPS in algal pyrenoids. This includes understanding how different growth conditions affect Rubisco mixing (Chapter 2), especially as plants growing in a terrestrial environment are subject to fluctuating environmental conditions which differ greatly to the aquatic environment of algae. To prevent EPYC1 proteolytic degradation, a starch sheath surrounding the pyrenoid matrix may need to be engineered into higher plants, as a protective role for the starch sheath in preventing incoming O₂ reacting with Rubisco and causing photorespiration has already been suggested (Colman, 1989). Thought must also be given to how pyrenoids might be inherited during mitosis of dividing plant cells, and how the starch sheath plays a role in Rubisco inheritance (Chapter 3). The starch degradation and synthesis candidates revealed by bioinformatics undertaken in this study (Chapter 3) offer an avenue to explore how a pyrenoid starch sheath can be modified and engineered into higher plants. The role for starch as a CO₂ leakage barrier requires further investigation (Ramazanov *et al.*, 1994), either as a physical barrier or in localising components such as the putative carbonic anhydrase LCIB to the pyrenoid periphery for CO₂ recapture (Toyokawa *et al.*, 2020). Whilst the HCO₃⁻ transporters HLA3 and LCIA have been targeted to appropriate locations in *Arabidopsis* and *N.benthamiana* (Atkinson *et al.* 2016), the localisation of the recently identified thylakoid HCO₃⁻ transporters BST1-3 (Mukherjee *et al.* 2019) should also be studied in higher plants. As in *Chlamydomonas*, the BST1-3 and LCIB/C complexes may be required for inorganic carbon recycling in higher plants (Chapter 4).

Final conclusion

This study shows that the pyrenoid is a dynamic organelle, and enables further investigation into CCM components, through development of fluorescently-tagged constructs and *Chlamydomonas* lines, optimisation of microscope settings and sample preparation. Future FRAP, time-lapse and FRET experiments will hopefully reveal the mobilities of CCM components both internally within structures (Chapter 2), and in relation to associated structures (Chapter 3). Further investigation into candidates potentially involved in remodelling of the starch sheath has been enabled by a bioinformatics approach (Chapter 3). Whilst these candidates may be directly involved in starch sheath modification, they may also play an indirect role in the inheritance of the pyrenoid matrix during division. The study of the mixing and movement of large structures within the pyrenoid must be accompanied by experiments which probe individual CCM component interactions (Chapter 4), bearing in mind the role of these proteins for the function of the CCM. The progress made in this study, and the ensuing work which has now been enabled, means we are closer to understanding the components required for engineering a CCM into higher plants.

Supplementary materials

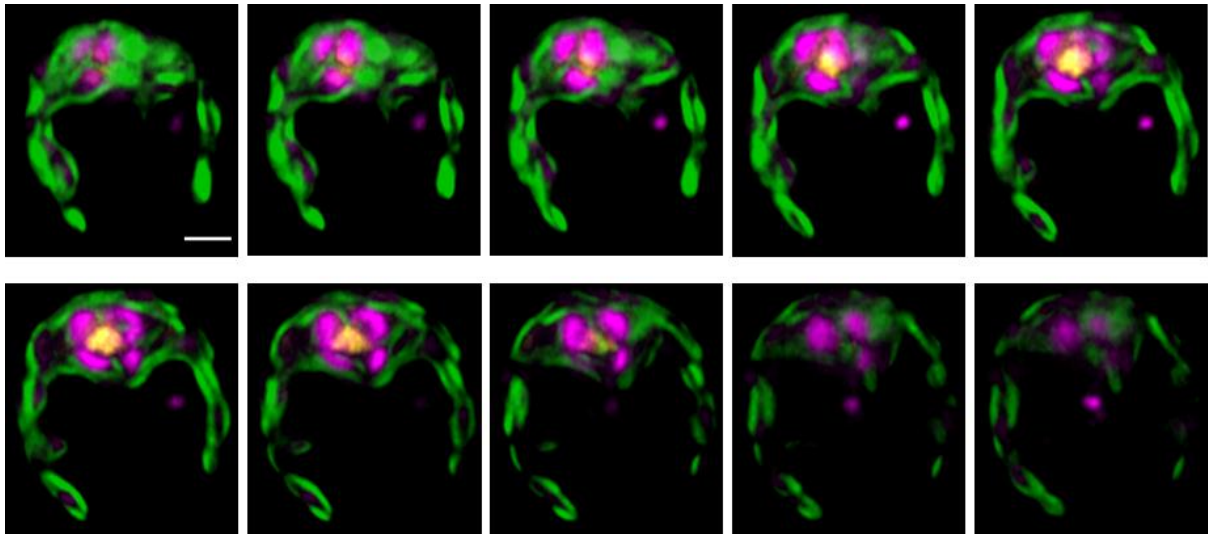


Figure S1. Dispersal of Rubisco during the phase-transition may require dissociation from the starch sheath plates. Z-stack images (0.39 μm apart) show movement of Rubisco-Venus signal (yellow) with traversing thylakoids (green). The STA2-mCherry signal (pink) appears separated from the Rubisco signal. Scale bar = 2 μm .

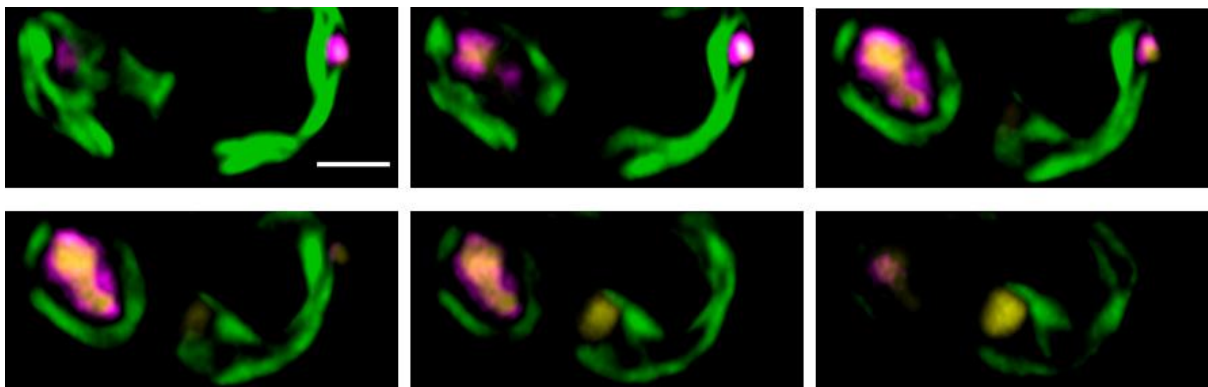


Figure S2. Pyrenoid matrix fission may require association with the starch sheath. Z-stack images (0.44 μm apart) show two lobes of Rubisco-Venus signal (yellow) with an adjoining bridge of Rubisco signal. The STA2-mCherry signal (pink) appears to be associated at the periphery of the Rubisco signal. Scale bar = 2 μm .

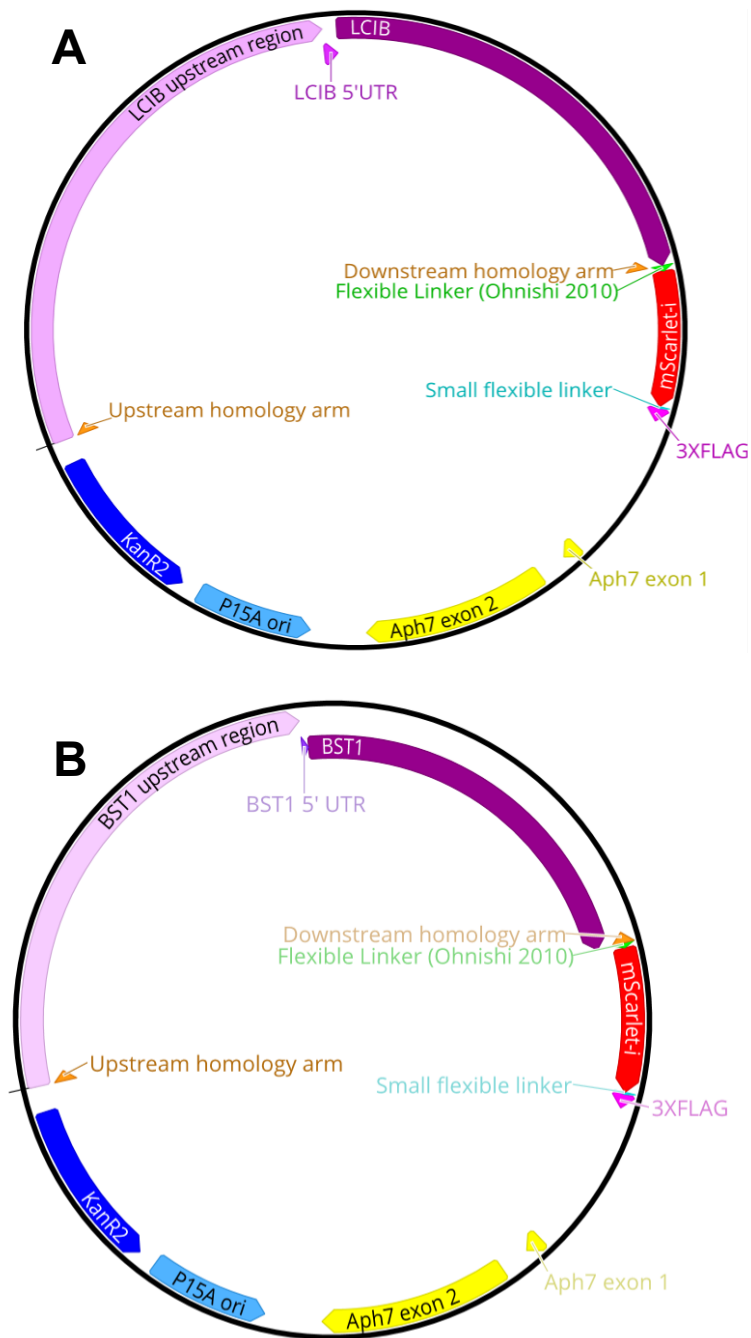


Figure S3. Plasmid maps of A) LCIB-mScarlet-i and B) BST1-mScarlet-i showing the upstream regions (light pink), 5'UTRs (medium purple), and LCIB and BST1 genes (dark purple), homology arms (orange), mScarlet-i tag (red), origin of replication (medium blue), hygromycin resistance gene (yellow), kanamycin resistance gene (dark blue) and 3XFLAG tag (pink.) There is a short, flexible linker (green) preceding the fluorescent protein sequence (GGLGGS₃GGR) and a tri-glycine linker (cyan) preceding the 3XFLAG tag.

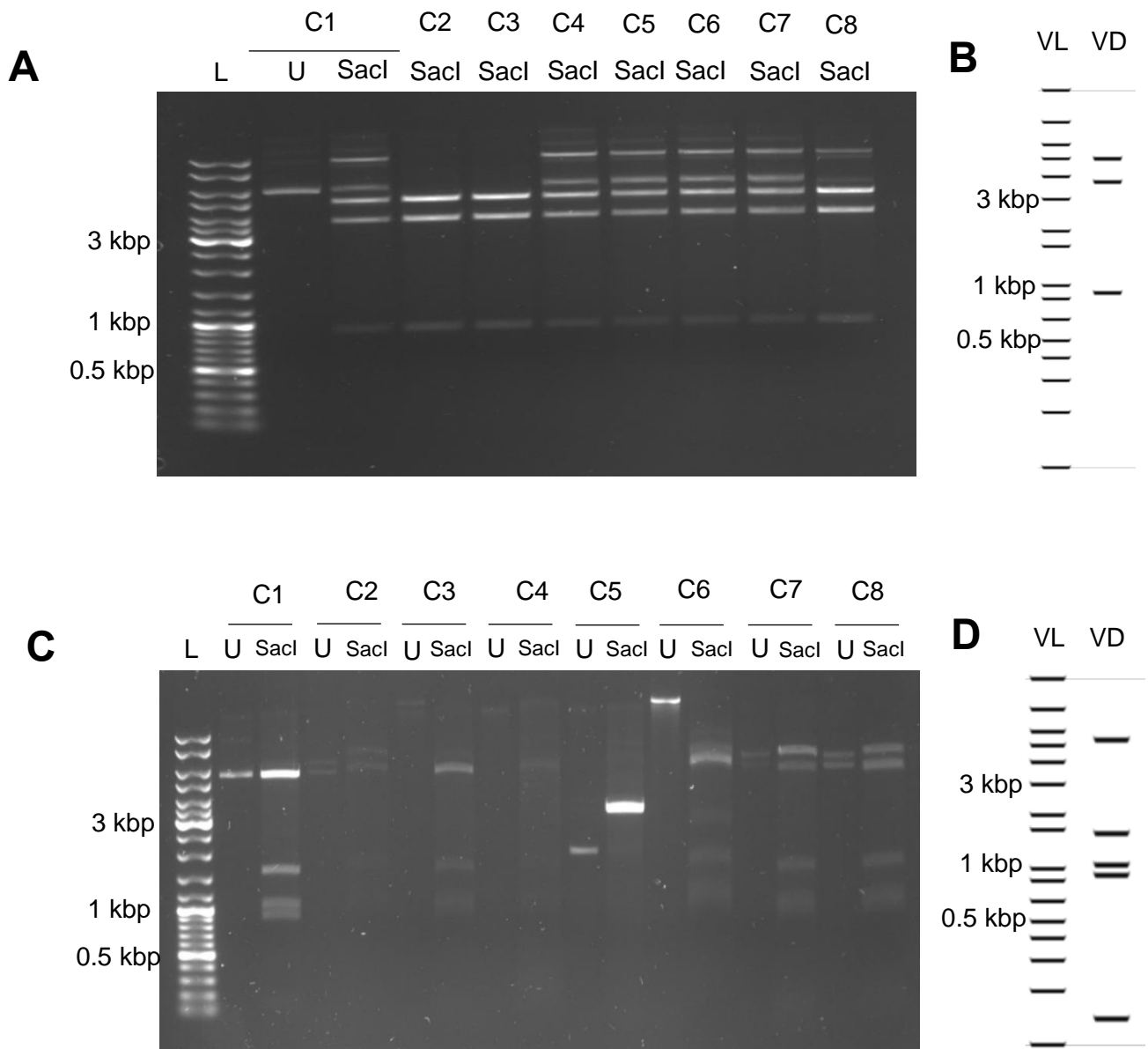


Figure S4. Restriction enzyme digestion by *SacI* tentatively shows recombination success using DNA gel electrophoresis for A) LCIB-mScarlet-i with B) accompanying virtual gel and A) BST1-mScarlet-i with B) accompanying virtual gel. Gel electrophoresis was carried out using a 0.7% (w/v) agarose gel in 1XTAE buffer (40 mM Tris, 20mM acetic acid, 1 mM EDTA). Eight colonies were screened for each. For A) undigested DNA for colony 1 was loaded only, whereas for C) the undigested DNA for each colony was loaded. L: ladder, U: undigested DNA, *SacI*: DNA digested with *SacI* restriction endonuclease, C1: colony 1, C2: colony 2 etc., VL: virtual ladder, VD: virtual digest.

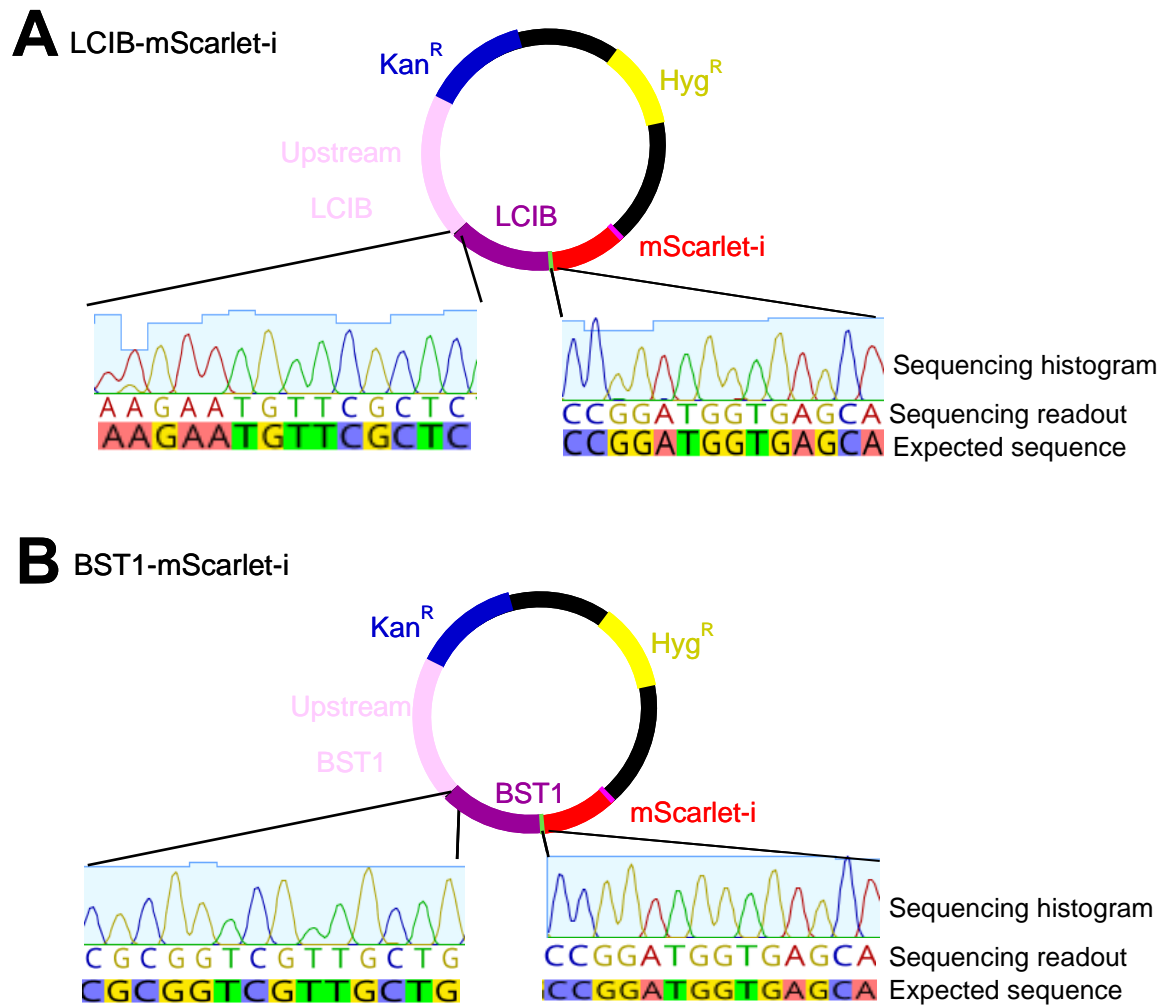


Figure S5. Sequencing confirmed recombineering constructs A) LCIB-mScarlet-i and B) BST1-mScarlet-i were correct. Primers were selected to show that both the 5' ends of the CDS regions of the LCIB and BST1 genes, and the junction from the flexible linker into the 5' end of mScarlet-i were correct. Green and pink bands just upstream and downstream of mScarlet-i depict flexible linkers.

Table S1. Chlamydomonas soluble starch synthases appear to closely resemble the family of Arabidopsis starch synthases. Homology-based modelling and images were acquired from Phyre2.

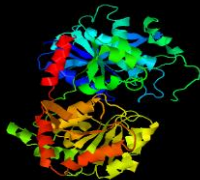
Arabidopsis thaliana protein name	Phyre2 model	Confidence score (%)	Coverage (%)	Top template information	Chlamydomonas reinhardtii protein name (homolog)	Phyre2 model	Confidence score (%)	Coverage (%)	Top template information
SS1		100.0	69	Glycogen synthase basal state UDP complex	SSS6		100.0	41	Glycogen synthase basal state UDP complex
SS2		100.0	56	Glycogen synthase basal state UDP complex	SSS2		100.0	68	Granule bound starch synthase I from <i>Cyanophora paradoxa</i> bound to Acarbose and ADP
SS3		100.0	39	Granule bound starch synthase I from <i>Cyanophora paradoxa</i> bound to Acarbose and ADP	STA3		100.0	33	Glycogen synthase basal state UDP complex
SS4		100.0	48	Catalytic domain of starch synthase IV from <i>A.thaliana</i> bound to ADP and Acarbose	SSS5		100.0	59	Glycogen synthase basal state UDP complex
SS5		100.0	50	Glycogen synthase basal state UDP complex	SSS5		100.0	59	Glycogen synthase basal state UDP complex

Table S2. Cre10.g457500 may show some structural resemblance to PTST2 and 3. Homology-based modelling and images were acquired from Phyre2.

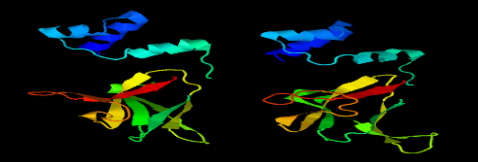
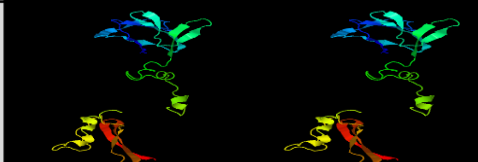
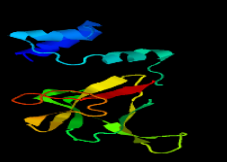
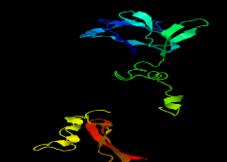
<i>Arabidopsis thaliana</i> protein name	PTST2	PTST3	Phyre2 model	Confidence score (%)	Coverage (%)	Top template information	<i>Chlamydomonas reinhardtii</i> protein name (homolog)	Phyre2 model	Confidence score (%)	Coverage (%)	Top template information
				99.8	23	Structure of a plant phosphatase	Cre10.g457500		100.0	62	Full length human AMPK in complex with a small molecule activator, a thienopyridone derivative
				99.8	20	Structure of a plant phosphatase	Cre10.g457500		100.0	62	Full length human AMPK in complex with a small molecule activator, a thienopyridone derivative

Table S3. AMYA2, DSP8, STA4 and PHO2 potentially contain coiled-coils. Disorder and PFAM annotations were obtained from IUPred2A and coiled-coil probabilities were obtained from the MPI Bioinformatics Toolkit.

Gene name	Disorder and PFAM annotation	Coiled-coils
AMYA2	<p>ANCHOR2 IUPred2 (long)</p> <p>Score</p> <p>Position</p> <p>PFAM</p> <p>Alpha-amylase Alpha-amylase C2</p>	<p>Coiled-coil probability</p> <p>Position</p>
DSP8	<p>DSPc AMPK1-CBM</p> <p>Score</p> <p>Position</p> <p>PFAM</p> <p>DSPc AMPK1-CBM</p>	<p>Coiled-coil probability</p> <p>Position</p>
STA4	<p>Phosphorylase</p> <p>Score</p> <p>Position</p> <p>PFAM</p> <p>Phosphorylase</p>	<p>Coiled-coil probability</p> <p>Position</p>
PHO2	<p>Phosphorylase</p> <p>Score</p> <p>Position</p> <p>PFAM</p> <p>Phosphorylase</p>	<p>Coiled-coil probability</p> <p>Position</p>

Supplementary method 1: PCR protocol for amplifying recombineering cassette from pLM162.

Reagents:		Thermocycler conditions:	
Nuclease-free water	28.1 µl	<u>98°C</u>	<u>1 min</u>
NEB GC buffer (5X)	10 µl		
(New England Biolabs)		98°C	30 s
DMSO (100%)	4.5 µl	63°C	30 s x 30
pLM099 (10 ng/µl)	1 µl	<u>72°C</u>	<u>100 s</u>
dNTPs (10 mM)	1 µl		
Phusion HS II (2U/µl)	0.4 µl	72°C	10 min
(ThermoFisher Scientific)		10°C	hold
Primers (10 µM)	2.5 µl each		

Primers with homology arms:

The primer which binds 2000bp upstream of the start codon at the 5' end of the gene encompasses the native promoter and untranslated region (UTR). The primer at the 3' end of the gene is designed to bind just upstream of the stop codon. The reagents, thermocycler conditions (above) and primers (below) with underlined homology arms were used.

Primers with homology arms:

LCIB forward primer:

5'-

ATCCTTGTTAATAAGGTCATCATGGTGAGTTTGTCCATCTTTCAAGGTGTGAAGATCCTT
TGATCTTTTCTACGGG-3'

LCIB reverse primer:

5'-

GCCTCGGTGGGTCTAGAGGCAAGAACCCCGGAGCTTCCTCCCCACGTGCCCGAGCC
CGCTGAGGTACC-3'

BST1 forward primer:

5'-

AAAGGGAGCAACAAAGCGCAAAGGCTTTGTCACAAAACATGAGGAAGGGAGAAGATCC
TTTGATCTTTTCTACGGG-3'

BST1 reverse primer:

5'-

GCCTCGGTGGGTCTAGAGGGAACGCGAGGGGTGGGTACCGGTGGGCGTGAACCTCC
GGCAACAACCTC-3'

References

- Abt, M., Pfister, B., Sharma, M., Eicke, S., Bürgy, L., Neale, I., Seung, D., and Zeeman, S.C. (2020). STARCH SYNTHASE5, a Noncanonical Starch Synthase-Like Protein, Promotes Starch Granule Initiation in Arabidopsis. *The Plant cell*, 32(8), 2543–2565.
- Atkinson, N., Feike, D., Mackinder, L.C.M., Meyer, M.T., Griffiths, H., Jonikas, M.C., Smith, A.M., and McCormick, A.J. (2016). Introducing an algal carbon-concentrating mechanism into higher plants: location and incorporation of key components. *Plant biotechnology journal*, 14(5), 1302–1315.
- Atkinson, N., Velanis, C.N., Wunder, T., Clarke, D.J., Mueller-Cajar, O., and McCormick, A.J. (2019). The pyrenoidal linker protein EPYC1 phase separates with hybrid Arabidopsis–Chlamydomonas Rubisco through interactions with the algal Rubisco small subunit. *Journal of Experimental Botany*, 70(19), 5271–5285.
- Avila-Castañeda, A., Gutiérrez-Granados, N., Ruiz-Gayosso, A., Sosa-Peinado, A., Martínez-Barajas, E., and Coello, P. (2014). Structural and functional basis for starch binding in the SnRK1 subunits AKIN β 2 and AKIN β y. *Frontiers in plant science*, 5, doi: 10.2289/fpls.2014.00199.
- Badger, M.R., Kaplan, A., and Berry, J.A. (1980). Internal Inorganic Carbon Pool of *Chlamydomonas reinhardtii*: evidence for a carbon dioxide-concentrating mechanism. *Plant physiology*, 66(3), 407–413.
- Baier, T., Jacobebbinghaus, N., Einhaus, A., Lauersen, K.J., and Kruse, O. (2020). Introns mediate post-transcriptional enhancement of nuclear gene expression in the green microalga *Chlamydomonas reinhardtii*. *PLoS genetics*, 16(7), e1008944.
- Ball, S., Marianne, T., Dirick, L., Fresnoy, M., Delrue, B., and Decq, A. (1991). A *Chlamydomonas reinhardtii* low-starch mutant is defective for 3-phosphoglycerate activation and orthophosphate inhibition of ADP-glucose pyrophosphorylase. *Planta*, 185(1), 17–26.
- Ball, S.G. (2002). The Intricate Pathway of Starch Biosynthesis and Degradation in the Monocellular Alga *Chlamydomonas reinhardtii*. *Australian journal of chemistry*, 55(2), 49–59.

- Ball, S.G. and Morell, M.K. (2003). From bacterial glycogen to starch: understanding the biogenesis of the plant starch granule. *Annual review of plant biology*, 54, 207–233.
- Bassham, J.A. and Calvin, M. (1962). The way of CO₂ in plant photosynthesis. *Comparative biochemistry and physiology*, 4, 187–204.
- Bauwe, H., Hagemann, M., and Fernie, A.R. (2010). Photorespiration: players, partners and origin. *Trends in plant science*, 15(6), 330–336.
- Benavent-Gil, Y., Rosell, C.M., and Gilbert, E.P. (2020). Understanding CGTase action through the relationship between starch structure and cyclodextrin formation. *Food hydrocolloids*, 112, 106316.
- Bharill, S., Fu, Z., Palty, R., Isacoff, E.Y. (2014). Stoichiometry and specific assembly of Best ion channels. *Proceedings of the National Academy of Sciences of the United States of America*, 111(17), 6491–6496.
- Bindels, D.S., Haarbosch, L., van Weeren, L., Postma, M., Wiese, K.E., Mastop, M., Aumonier, S., Gotthard, G., Royant, A., Hink, M.A., and Gadella, T.W.J., Jr (2017). mScarlet: a bright monomeric red fluorescent protein for cellular imaging. *Nature methods*, 14(1), 53–56.
- Blanco-Rivero, A., Shutova, T., Román, M.J., Villarejo, A., and Martinez, F. (2012). Phosphorylation controls the localization and activation of the lumenal carbonic anhydrase in *Chlamydomonas reinhardtii*. *PloS one*, 7(11), e49063.
- Borkhsenius, O.N., Mason, C.B., and Moroney, J.V. (1998). The intracellular localization of ribulose-1,5-bisphosphate Carboxylase/Oxygenase in *chlamydomonas reinhardtii*. *Plant physiology*, 116(4), 1585–1591.
- Brangwynne, C.P., Eckmann, C.R., Courson, D.S., Rybarska, A., Hoege, C., Gharakhani, J., Julicher, F., and Hyman, A.A. (2009). Germline P Granules Are Liquid Droplets That Localize by Controlled Dissolution/Condensation. *Science*, 324(5935), 1729–1732.
- Brangwynne, C.P., Mitchison, T.J., and Hyman, A.A. (2011). Active liquid-like behavior of nucleoli determines their size and shape in *Xenopus laevis* oocytes. *Proceedings of the National Academy of Sciences of the United States of America*, 108(11), 4334–4339.
- Brangwynne, C.P., Tompa, P., and Pappu, R.V. (2015). Polymer physics of intracellular phase transitions. *Nature physics*, 11, 899–904.

- Broeckx, T., Hulsmans, S., and Rolland, F. (2016). The plant energy sensor: evolutionary conservation and divergence of SnRK1 structure, regulation, and function. *Journal of experimental botany*, 67(22), 6215–6252.
- Broussard, J.A., Rappaz, B., Webb, D.J., and Brown, C.M. (2013). Fluorescence resonance energy transfer microscopy as demonstrated by measuring the activation of the serine/threonine kinase Akt. *Nature protocols*, 8(2), 265–281.
- Brueggeman, A.J., Gangadharaiah, D.S., Cserhati, M.F., Casero, D., Weeks, D.P., and Ladunga, I. (2012). Activation of the carbon concentrating mechanism by CO₂ deprivation coincides with massive transcriptional restructuring in *Chlamydomonas reinhardtii*. *The Plant cell*, 24(5), 1860–1875.
- Brumos, J., Zhao, C., Gong, Y., Soriano, D., Patel, A.P., Perez-Amador, M.A., Stepanova, A.N., and Alonso, J.M. (2020). An Improved Recombineering Toolset for Plants. *The Plant cell*, 32(1), 100–122.
- Caemmerer, S. von. and Farquhar, G.D. (1981). Some relationships between the biochemistry of photosynthesis and the gas exchange of leaves. *Planta*, 153, 376–387.
- Campbell, J.A., Davies, G.J., Bulone, V., and Henrissat, B. (1997). A classification of nucleotide-diphospho-sugar glycosyltransferases based on amino acid sequence similarities. *Biochemical Journal*, 326(3), 929–939.
- Caspari, O.D., Meyer, M.T., Tolleter, D., Wittkopp, T.M., Cunniffe, N.J., Lawson, T., Grossman, A.R., and Griffiths, H. (2017). Pyrenoid loss in *Chlamydomonas reinhardtii* causes limitations in CO₂ supply, but not thylakoid operating efficiency. *Journal of experimental botany*, 68(14), 3903–3913.
- Caspar, T., Huber, S.C., and Somerville, C. (1985). Alterations in Growth, Photosynthesis, and Respiration in a Starchless Mutant of *Arabidopsis thaliana* (L.) Deficient in Chloroplast Phosphoglucomutase Activity. *Plant physiology*, 79(1), 11–17.
- Cegelski, L. and Schaefer, J. (2006). NMR determination of photorespiration in intact leaves using in vivo ¹³CO₂ labeling. *Journal of magnetic resonance*, 178(1), 1–10.
- Chevalier, D., Morris, E.R., and Walker, J.C. (2009). 14-3-3 and FHA domains mediate phosphoprotein interactions. *Annual review of plant biology*, 60, 67–91.

- Choi, J.-M., Holehouse, A.S., and Pappu, R.V. (2020). Physical Principles Underlying the Complex Biology of Intracellular Phase Transitions. *Annual review of biophysics*, 49, 107–133.
- Christiansen, C., Abou Hachem, M., Janecek, S., Viksø-Nielsen, A., Blennow, A., and Svensson, B. (2009). The carbohydrate-binding module family 20 - diversity, structure, and function. *The FEBS journal*, 276(18), 5006–5029.
- Colletti, K.S., Tattersall, E.A., Pyke, K.A., Froelich, J.E., Stokes, K.D., and Osteryoung, K.W. (2000). A homologue of the bacterial cell division site-determining factor MinD mediates placement of the chloroplast division apparatus. *Current biology*, 10(9), 507–516.
- Colman, B. (1989). Photosynthetic carbon assimilation and the suppression of photorespiration in the cyanobacteria. *Aquatic botany*, 34(1), 211–231.
- Colombo, S.L., Pollock, S.V., Eger, K.A., Godfrey, A.C., Adams, J.E., Mason, C.B., and Moroney, J.V. (2002). Use of the bleomycin resistance gene to generate tagged insertional mutants of *Chlamydomonas reinhardtii* that require elevated CO₂ for optimal growth. *Functional plant biology*, 29(3), 231–241.
- Copeland, N.G., Jenkins, N.A., and Court, D.L. (2001). Recombineering: a powerful new tool for mouse functional genomics. *Nature reviews genetics*, 2(10), 769–779.
- Craigie, R.A. and Cavalier-Smith, T. (1982). Cell Volume and the Control of the *Chlamydomonas* Cell Cycle. *Journal of cell science*, 54(1), 173–191.
- Critchley, J.H., Zeeman, S.C., Takaha, T., Smith, A.M., and Smith, S.M. (2001). A critical role for disproportionating enzyme in starch breakdown is revealed by a knock-out mutation in *Arabidopsis*. *The Plant Journal*, 26(1), 89–100.
- Cross, F.R. and Umen, J.G. (2015). The *Chlamydomonas* cell cycle. *The Plant Journal*, 82(3), 370–392.
- Crumpton-Taylor, M., Grandison, S., Png, K.M.Y., Bushby, A.J., and Smith, A.M. (2012). Control of starch granule numbers in *Arabidopsis* chloroplasts. *Plant physiology*, 158(2), 905–916.
- Cuevas-Velazquez, C.L. and Dinneny, J.R. (2018). Organization out of disorder: liquid-liquid phase separation in plants. *Current opinion in plant biology*, 45, 68–74.

- Dauvillee, D., Colleoni, C., Shaw, E., Mouille, G., D'Hulst, C., Morell, M., Samuel, M.S., Bouchet, B., Gallant, D.J., Sinskey, A., and Ball, S. (1999). Novel, Starch-Like Polysaccharides Are Synthesized by an Unbound Form of Granule-Bound Starch Synthase in Glycogen-Accumulating Mutants of *Chlamydomonas*. *Plant physiology*, 119(1), 321–330.
- Dauvillée, D., Chochois, V., Steup, M., Haebel, S., Eckermann, N., Ritte, G., Ral, J.-P., Colleoni, C., Hicks, G., Wattebled, F., Deschamps, P., d'Hulst, C., Liénard, L., Cournac, L., Putaux, J.-L., Dupeyre, D., and Ball, S.G. (2006). Plastidial phosphorylase is required for normal starch synthesis in *Chlamydomonas reinhardtii*. *The Plant Journal*, 48(2), 274–285.
- Delatte, T., Trevisan, M., Parker, M.L., and Zeeman, S.C. (2005). Arabidopsis mutants Atisa1 and Atisa2 have identical phenotypes and lack the same multimeric isoamylase, which influences the branch point distribution of amylopectin during starch synthesis: Isoamylase function in Arabidopsis. *The Plant Journal*, 41(6), 815–830.
- Delatte, T., Umhang, M., Trevisan, M., Eicke, S., Thorneycroft, D., Smith, S.M., and Zeeman, S.C. (2006). Evidence for distinct mechanisms of starch granule breakdown in plants. *The Journal of biological chemistry*, 281(17), 12050–12059.
- Delrue, B., Fontaine, T., Routier, F., and Decq, A. (1992). Waxy *Chlamydomonas reinhardtii*: monocellular algal mutants defective in amylose biosynthesis and granule-bound starch synthase activity accumulate a structurally modified amylopectin. *Journal of bacteriology*, 174(11), 3612-3620.
- Delvallé, D., Dumez, S., Wattebled, F., Roldán, I., Planchot, V., Berbezy, P., Colonna, P., Vyas, D., Chatterjee, M., Ball, S., Mérida, Á., and D'Hulst, C. (2005). Soluble starch synthase I: a major determinant for the synthesis of amylopectin in *Arabidopsis thaliana* leaves: SSI mutant of Arabidopsis. *The Plant Journal*, 43(3), 398–412.
- De Marais, D.J. (2000). Evolution. When did photosynthesis emerge on Earth? *Science*, 289(5485), 1703–1705.
- DiMario, R.J., Quebedeaux, J.C., Longstreth, D.J., Dassanayake, M., Hartman, M.M., and Moroney, J.V. (2016). The Cytoplasmic Carbonic Anhydrases β CA2 and β CA4 Are Required for Optimal Plant Growth at Low CO₂. *Plant physiology*, 171(1), 280–293.
- Dismukes, G.C., Klimov, V.V., Baranov, S.V., Kozlov, Y.N., DasGupta, J., and Tyryshkin, A. (2001). The origin of atmospheric oxygen on Earth: the innovation of oxygenic

- photosynthesis. *Proceedings of the National Academy of Sciences of the United States of America*, 98(5), 2170–2175.
- Dou, Z., Heinhorst, S., Williams, E.B., Murin, C.D., Shively, J.M., and Cannon, G.C. (2008). CO₂ fixation kinetics of *Halothiobacillus neapolitanus* mutant carboxysomes lacking carbonic anhydrase suggest the shell acts as a diffusional barrier for CO₂. *The Journal of biological chemistry*, 283(16), 10377–10384.
- Duanmu, D., Wang, Y., and Spalding, M.H. (2009). Thylakoid Lumen Carbonic Anhydrase (CAH3) Mutation Suppresses Air-Dier Phenotype of LCIB Mutant in *Chlamydomonas reinhardtii*. *Plant physiology*, 149(2), 929–937.
- Dumez, S., Wattedled, F., Dauvillee, D., Delvalle, D., Planchot, V., Ball, S.G., and D’Hulst, C. (2006). Mutants of *Arabidopsis* lacking starch branching enzyme II substitute plastidial starch synthesis by cytoplasmic maltose accumulation. *The Plant cell*, 18(10), 2694–2709.
- Elbaum-Garfinkle, S., Kim, Y., Szczepaniak, K., Chen, C.C.-H., Eckmann, C.R., Myong, S., and Brangwynne, C.P. (2015). The disordered P granule protein LAF-1 drives phase separation into droplets with tunable viscosity and dynamics. *Proceedings of the National Academy of Sciences of the United States of America*, 112(23), 7189–7194.
- El-Gebali, S., Mistry, J., Bateman, A., Eddy, S.R., Luciani, A., Potter, S.C., Qureshi, M., Richardson, L.J., Salazar, G.A., Smart, A., Sonnhammer, E.L.L., Hirsh, L., Paladin, L., Piovesan, D., Tosatto, S.C.E., and Finn, R.D. (2019). The Pfam protein families database in 2019. *Nucleic acids research*, 47(D1), D427–D432.
- Ellis, R.J. and John Ellis, R. (1979). The most abundant protein in the world. *Trends in Biochemical Sciences*, 4(11), 241–244.
- Emrich-Mills, T., Yates, G., Barrett, J., Grouneva, I., Lau, C.S., Walker, C.E., Kwok, T.K., Davey, J.W., Johnson, M.P., and Mackinder, L.C.M. (2020). A recombineering pipeline to clone large and complex genes in *Chlamydomonas*. *bioRxiv*, doi: 10.1101/2020.05.06.080416.
- Engel, B.D., Schaffer, M., Kuhn Cuellar, L., Villa, E., Plitzko, J.M., and Baumeister, W. (2015). Native architecture of the *Chlamydomonas* chloroplast revealed by in situ cryo-electron tomography. *eLife*, 4, e04889.

- Erdős, G. and Dosztányi, Z. (2020). Analyzing Protein Disorder with IUPred2A. *Current protocols in bioinformatics*, 70(1), e99.
- Espada, J. (1962). Enzymic Synthesis of Adenosine Diphosphate Glucose from Glucose 1-Phosphate and Adenosine Triphosphate. *The Journal of biological chemistry*, 237(12), 3577–3581.
- Fang, W., Si, Y., Douglass, S., Casero, D., Merchant, S.S., Pellegrini, M., Ladunga, I., Liu, P., and Spalding, M.H. (2012). Transcriptome-wide changes in *Chlamydomonas reinhardtii* gene expression regulated by carbon dioxide and the CO₂-concentrating mechanism regulator CIA5/CCM1. *The Plant cell*, 24(5), 1876–1893.
- Fang, X., Wang, L., Ishikawa, R., Li, Y., Fiedler, M., Liu, F., Calder, G., Rowan, B., Weigel, D., Li, P., and Dean, C. (2019). Arabidopsis FLL2 promotes liquid-liquid phase separation of polyadenylation complexes. *Nature*, 569(7755), 265–269.
- FAO (2009). Global agriculture towards 2050. Rome, FAO.
- Field, C.B., Behrenfeld, M.J., Randerson, J.T., and Falkowski, P. (1998). Primary production of the biosphere: integrating terrestrial and oceanic components. *Science*, 281(5374), 237–240.
- Findinier, J., Laurent, S., Duchêne, T., Roussel, X., Lancelon-Pin, C., Cuié, S., Putaux, J.-L., Li-Beisson, Y., D’Hulst, C., Wattebled, F., and Dauvillée, D. (2019). Deletion of BSG1 in *Chlamydomonas reinhardtii* leads to abnormal starch granule size and morphology. *Scientific reports*, 9(1), 1990.
- Freeman Rosenzweig, E.S., Xu, B., Kuhn Cuellar, L., Martinez-Sanchez, A., Schaffer, M., Strauss, M., Cartwright, H.N., Ronceray, P., Pnitzko, J.M., Förster, F., Wingreen, N.S., Engel, B.D., Mackinder, L.C.M., and Jonikas, M.C. (2017). The Eukaryotic CO₂-Concentrating Organelle Is Liquid-like and Exhibits Dynamic Reorganization. *Cell*, 171(1), 148–162.
- Fukuzawa, H., Miura, K., Ishizaki, K., Kucho, K.I., Saito, T., Kohinata, T., and Ohyama, K. (2001). Ccm1, a regulatory gene controlling the induction of a carbon-concentrating mechanism in *Chlamydomonas reinhardtii* by sensing CO₂ availability. *Proceedings of the National Academy of Sciences of the United States of America*, 98(9), 5347–5352.

- Fulton, D.C., Stettler, M., Mettler, T., Vaughan, C.K., and Li, J. (2008). β -AMYLASE4, a noncatalytic protein required for starch breakdown, acts upstream of three active β -amylases in Arabidopsis chloroplasts. *The Plant cell*, 20(4), 1040-1058.
- Goodenough, U.W. (1970). CHLOROPLAST DIVISION AND PYRENOID FORMATION IN CHLAMYDOMONAS REINHARDI 1. *Journal of phycology*, 6(1), 1–6.
- Goodstein, D.M., Shu, S., Howson, R., Neupane, R., Hayes, R.D., Fazo, J., Mitros, T., Dirks, W., Hellsten, U., Putnam, N., and Rokhsar, D.S. (2012). Phytozome: a comparative platform for green plant genomics. *Nucleic acids research*, 40, D1178–86.
- Gorman, D.S. and Levine, R.P. (1965). Cytochrome f and plastocyanin: their sequence in the photosynthetic electron transport chain of Chlamydomonas reinhardi. *Proceedings of the National Academy of Sciences of the United States of America*, 54(6), 1665–1669.
- Gowik, U., Bräutigam, A., Weber, K.L., Weber, A.P.M., and Westhoff, P. (2011). Evolution of C4 photosynthesis in the genus Flaveria: how many and which genes does it take to make C4? *The Plant cell*, 23(6), 2087–2105.
- Graf, A., Schlereth, A., Stitt, M., and Smith, A.M. (2010). Circadian control of carbohydrate availability for growth in Arabidopsis plants at night. *Proceedings of the National Academy of Sciences of the United States of America*, 107(20), 9458–9463.
- Gu, Y., Di, W.L., Kellsell, D.P., and Zicha, D. (2004). Quantitative fluorescence resonance energy transfer (FRET) measurement with acceptor photobleaching and spectral unmixing. *Journal of microscopy*, 215(2), 162–173.
- Hansen, P.I., Spraul, M., and Dvortsak, P. (2009). Starch phosphorylation—Maltosidic restrains upon 3'-and 6'-phosphorylation investigated by chemical synthesis, molecular dynamics and NMR spectroscopy. *Biopolymers*, 91(3), 179-193.
- Harris, G.C. and Königer, M. (1997). The “high” concentrations of enzymes within the chloroplast. *Photosynthesis research*, 54(1), 5–23.
- Hejazi, M., Fettke, J., Haebel, S., Edner, C., Paris, O., Froberg, C., Steup, M., and Ritte, G. (2008). Glucan, water dikinase phosphorylates crystalline maltodextrins and thereby initiates solubilization. *The Plant Journal*, 55(2), 323–334.
- Hejazi, M., Fettke, J., Kötting, O., Zeeman, S.C., and Steup, M. (2010). The Laforin-like dual-specificity phosphatase SEX4 from Arabidopsis hydrolyzes both C6- and C3-phosphate

- esters introduced by starch-related dikinases and thereby affects phase transition of alpha-glucans. *Plant physiology*, 152(2), 711–722.
- Heldt, F.S., Tyson, J.J., Cross, F.R., and Novák, B. (2020). A Single Light-Responsive Sizer Can Control Multiple-Fission Cycles in *Chlamydomonas*. *Current biology*, 30(4), 634–644.
- Herdean, A., Teardo, E., Nilsson, A.K., Pfeil, B.E., Johansson, O.N., Ünneper, R., Nagy, G., Zsiros, O., Dana, S., Solymosi, K., Garab, G., Szabó, I., Spetea, C., and Lundin, B. (2016). A voltage-dependent chloride channel fine-tunes photosynthesis in plants. *Nature communications*, 7, 11654.
- Holdsworth, R.H. (1968). The presence of a crystalline matrix in pyrenoids of the diatom, *Achnanthes brevipes*. *The Journal of cell biology*, 37(3), 831–837.
- Hughes, M.E., Hogenesch, J.B., and Kornacker, K. (2010). JTK_CYCLE: an efficient nonparametric algorithm for detecting rhythmic components in genome-scale data sets. *Journal of biological rhythms*, 25(5), 372–380.
- Hughes, R.M. and Waters, M.L. (2006). Arginine Methylation in a β -Hairpin Peptide: Implications for Arg- π Interactions, ΔC_p° , and the Cold Denatured State. *Journal of the American Chemical Society*, 128(39), 12735–12742.
- Hu, Y., Chen, Z.-W., Liu, W.-Z., Liu, X.-L., and He, Y.-K. (2008). Chloroplast division is regulated by the circadian expression of FTSZ and MIN genes in *Chlamydomonas reinhardtii*. *European Journal of Phycology*, 43(2), 207–215.
- Hyman, A.A., Weber, C.A., and Jülicher, F. (2014). Liquid-liquid phase separation in biology. *Annual review of cell and developmental biology*, 30, 39–58.
- Im, C.S. and Grossman, A.R. (2002). Identification and regulation of high light-induced genes in *Chlamydomonas reinhardtii*. *The Plant Journal*, 30(3), 301–313.
- Ishikawa-Ankerhold, H.C., Ankerhold, R., and Drummen, G.P.C. (2012). Advanced Fluorescence Microscopy Techniques—FRAP, FLIP, FLAP, FRET and FLIM. *Molecules*, 17(4), 4047–4132.
- Itakura, A.K., Chan, K.X., Atkinson, N., Pallesen, L., Wang, L., Reeves, G., Patena, W., Caspari, O., Roth, R., Goodenough, U., McCormick, A.J., Griffiths, H., and Jonikas, M.C. (2019). A Rubisco-binding protein is required for normal pyrenoid number and starch

- sheath morphology in *Chlamydomonas reinhardtii*. *Proceedings of the National Academy of Sciences of the United States of America*, 116(37), 18445-18454.
- Izumo, A., Fujiwara, S., Sakurai, T., Ball, S.G., Ishii, Y., Ono, H., Yoshida, M., Fujita, N., Nakamura, Y., Buléon, A., and Tsuzuki, M. (2011). Effects of granule-bound starch synthase I-defective mutation on the morphology and structure of pyrenoidal starch in *Chlamydomonas*. *Plant Science*, 180(2), 238–245.
- Jin, S., Sun, J., Wunder, T., Tang, D., Cousins, A.B., Sze, S.K., Mueller-Cajar, O., and Gao, Y.G (2016). Structural insights into the LCIB protein family reveals a new group of beta-carbonic anhydrases. *Proceedings of the National Academy of Sciences of the United States of America*, 113(51), 14716–14721.
- John, F., Roffler, S., Wicker, T., and Ringli, C. (2011). Plant TOR signaling components. *Plant signaling & behavior*, 6(11), 1700–1705.
- Johnson, U.G. and Porter, K.R. (1968). Fine structure of cell division in *Chlamydomonas reinhardtii*. Basal bodies and microtubules. *The Journal of cell biology*, 38(2), 403–425.
- Johnson, X. and Alric, J. (2013). Central carbon metabolism and electron transport in *Chlamydomonas reinhardtii*: metabolic constraints for carbon partitioning between oil and starch. *Eukaryotic cell*, 12(6), 776–793.
- Karlsson, J., Clarke, A.K., Chen, Z.Y., Huggins, S.Y., Park, Y.I., Husic, H.D., Moroney, J.V., and Samuelsson, G. (1998). A novel alpha-type carbonic anhydrase associated with the thylakoid membrane in *Chlamydomonas reinhardtii* is required for growth at ambient CO₂. *The EMBO journal*, 17(5), 1208–1216.
- Kedersha, N., Cho, M.R., Li, W., Yacono, P.W., Chen, S., Gilks, N., Golan, D.E., and Anderson, P. (2000). Dynamic shuttling of TIA-1 accompanies the recruitment of mRNA to mammalian stress granules. *The Journal of cell biology*, 151(6), 1257–1268.
- Kedersha, N., Panas, M.D., Achorn, C.A., Lyons, S., Tisdale, S., Hickman, T., Thomas, M., Lieberman, J., McInerney, G.M., Ivanov, P., and Anderson, P. (2016). G3BP–Caprin1–USP10 complexes mediate stress granule condensation and associate with 40S subunits. *Journal of Cell Biology*, 212(7), 845-860.
- Kelley, L.A., Mezulis, S., Yates, C.M., Wass, M.N., and Sternberg, M.J.E. (2015). The Phyre2 web portal for protein modeling, prediction and analysis. *Nature protocols*, 10(6), 845–858.

- Keys, A.J., Ellis, R.J. and Gray, J.C. (1986). Rubisco: its role in photorespiration. *Philosophical transactions of the Royal Society of London*, 313(1162), 325–336.
- Klein, U. (1987). Intracellular Carbon Partitioning in *Chlamydomonas reinhardtii*. *Plant physiology*, 85(4), 892–897.
- Kombrink, E. and Wöber, G. (1980). Identification and subcellular localization of starch-metabolizing enzymes in the green alga *Dunaliella marina*. *Planta*, 149(2), 130–137.
- Kono, A., Chou, T.-H., Radhakrishnan, A., Bolla, J.R., Sankar, K., Shome, S., Su, C.-C., Jernigan, R.L., Robinson, C.V., Yu, E.W., and Spalding, M.H. (2020). Structure and Function of LC11: A plasma membrane CO₂ channel in the *Chlamydomonas* CO₂ concentrating mechanism. *The Plant Journal*, 102(6), 1107-1126.
- Kötting, O., Santelia, D., Edner, C., Eicke, S., Marthaler, T., Gentry, M.S., Comparot-Moss, S., Chen, J., Smith, A.M., Steup, M., Ritte, G., and Zeeman, S.C. (2009). STARCH-EXCESS4 is a laforin-like phosphoglucan phosphatase required for starch degradation in *Arabidopsis thaliana*. *The Plant Cell*, 21(1), 334-346.
- Kremers, G.-J., Goedhart, J., van Munster, E.B., and Gadella, T.W.J., Jr. (2006). Cyan and yellow super fluorescent proteins with improved brightness, protein folding, and FRET Förster radius. *Biochemistry*, 45(21), 6570–6580.
- Kropat, J., Hong-Hermesdorf, A., Casero, D., Ent, P., Castruita, M., Pellegrini, M., Merchant, S.S., and Malasarn, D. (2011). A revised mineral nutrient supplement increases biomass and growth rate in *Chlamydomonas reinhardtii*. *The Plant Journal*, 66(5), 770–780.
- Kroschwald, S., Maharana, S., Mateju, D., Malinowska, L., Nüske, E., Poser, I., Richter, D., and Alberti, S. (2015). Promiscuous interactions and protein disaggregases determine the material state of stress-inducible RNP granules. *eLife*, 4, e06807.
- Kruger, N.J. and ap Rees, T. (1983). Properties of α -glucan phosphorylase from pea chloroplasts. *Phytochemistry*, 22(9), 1891–1898.
- Kuchitsu, K., Tsuzuki, M., and Miyachi, S. (1988). Changes of starch localization within the chloroplast induced by changes in CO₂ concentration during growth of *Chlamydomonas reinhardtii*: independent regulation of pyrenoid starch and stroma starch. *Plant & cell physiology*, 29(8), 1269–1278.

- Kunze, M., Pracharoenwattana, I., Smith, S.M., and Hartig, A. (2006). A central role for the peroxisomal membrane in glyoxylate cycle function. *Biochimica et biophysica acta*, 1763(12), 1441–1452.
- Kwon, I., Kato, M., Xiang, S., Wu, L., Theodoropoulos, P., Mirzaei, H., Han, T., Xie, S., Corden, J.L., and McKnight, S.L. (2013). Phosphorylation-regulated binding of RNA polymerase II to fibrous polymers of low-complexity domains. *Cell*, 155(5), 1049–1060.
- Lambert, T.J. (2019). FPbase: a community-editable fluorescent protein database. *Nature methods*, 16(4), 277–278.
- Lao, N.T., Schoneveld, O., Mould, R.M., Hibberd, J.M., Gray, J.C., and Kavanagh, T.A. (1999). An Arabidopsis gene encoding a chloroplast-targeted β -amylase. *The Plant Journal*, 20(5), 519–527.
- Levi, C. and Gibbs, M. (1984). Starch Degradation in Synchronously Grown *Chlamydomonas reinhardtii* and Characterization of the Amylase. *Plant physiology*, 74(3), 459–463.
- Lien, T. and Knutsen, G. (1979). Synchronous growth of *Chlamydomonas reinhardtii* (chlorophyceae): a review of optimal conditions 1. *Journal of phycology*, 15(2), 191–200.
- Li, P., Banjade, S., Cheng, H.-C., Kim, S., Chen, B., Guo, L., Llaguno, M., Hollingsworth, J.V., King, D.S., Banani, S.F., Russo, P.S., Jiang, Q.-X., Nixon, B.T., and Rosen, M.K. (2012). Phase transitions in the assembly of multivalent signalling proteins. *Nature*, 483(7389), 336–340.
- Lloyd, J.R., Kossmann, J., and Ritte, G. (2005). Leaf starch degradation comes out of the shadows. *Trends in plant science*, 10(3), 130–137.
- Lohmeier-Vogel, E.M., Kerk, D., Nimick, M., Wrobel, S., Vickerman, L., Muench, D.G., and Moorhead, G.B.G. (2008). Arabidopsis At5g39790 encodes a chloroplast-localized, carbohydrate-binding, coiled-coil domain-containing putative scaffold protein. *BMC plant biology*, 8, 120.
- Lombard, V., Golaconda Ramulu, H., Drula, E., Coutinho, P.M., and Henrissat, B. (2014). The carbohydrate-active enzymes database (CAZy) in 2013. *Nucleic acids research*, 42, D490–5.
- Long, S.P., Marshall-Colon, A., and Zhu, X.-G. (2015). Meeting the global food demand of the future by engineering crop photosynthesis and yield potential. *Cell*, 161(1), 56–66.

- Lupas, A., Van Dyke, M., and Stock, J. (1991). Predicting coiled coils from protein sequences. *Science*, 252(5009), 1162–1164.
- Lu, Y., Gehan, J.P., and Sharkey, T.D. (2005). Daylength and circadian effects on starch degradation and maltose metabolism. *Plant physiology*, 138(4), 2280–2291.
- Mackinder, L.C.M., Meyer, M.T., Mettler-Altmann, T., Chen, V.K., Mitchell, M.C., Caspari, O., Freeman Rosenzweig, E.S., Pallesen, L., Reeves, G., Itakura, A., Roth, R., Sommer, F., Geimer, S., Mühlhaus, T., Schroda, M., Goodenough, U., Stitt, M., Griffiths, H., and Jonikas, M.C. (2016). A repeat protein links Rubisco to form the eukaryotic carbon-concentrating organelle. *Proceedings of the National Academy of Sciences*, 113(21), pp. 5958–5963.
- Mackinder, L.C.M., Chen, C., Leib, R.D., Patena, W., Blum, S.R., Rodman, M., Ramundo, S., Adams, C.M., and Jonikas, M.C. (2017). A Spatial Interactome Reveals the Protein Organization of the Algal CO₂-Concentrating Mechanism. *Cell*, 171(1), 133–147.
- Mackinder, L.C.M. (2017). The Chlamydomonas CO₂-concentrating mechanism and its potential for engineering photosynthesis in plants. *The New phytologist*, 217(1), 54-61.
- Maddelein, M.L., Libessart, N., Bellanger, F., Delrue, B., D'Hulst, C., Van den Koornhuysse, N., Fontaine, T., Wieruszkeski, J.M., Decq, A., and Ball, S. (1994). Toward an understanding of the biogenesis of the starch granule. Determination of granule-bound and soluble starch synthase functions in amylopectin synthesis. *The Journal of biological chemistry*, 269(40), 25150–25157.
- Marrison, J.L., Rutherford, S.M., Robertson, E.J., Lister, C., Dean, C., and Leech, R.M. (1999). The distinctive roles of five different ARC genes in the chloroplast division process in Arabidopsis. *The Plant Journal*, 18(6), 651–662.
- Mason, J. M. and Arndt, K. M. (2004). Coiled Coil Domains: Stability, Specificity, and Biological Implications. *ChemBioChem*, 5(2), 170-176.
- Ma, Y., Pollock, S.V., Xiao, Y., Cunnusamy, K., and Moroney, J.V. (2011). Identification of a Novel Gene, CIA6, Required for Normal Pyrenoid Formation in *Chlamydomonas reinhardtii*. *Plant Physiology*, 156(2), 884–896.
- Merchant, S.S., Prochnik, S.E., Vallon, O., Harris, E.H., Karpowicz, S.J., Witman, G.B., Terry, A., Salamov, A., Fritz-Laylin, L.K., Maréchal-Drouard, L., Marshall, W.F., Qu, L.-H., Nelson, D.R., Sanderfoot, A.A., Spalding, M.H., Kapitonov, V.V., Ren, Q., Ferris, P.,

- Lindquist, E., Shapiro, H., *et al.*, (2007). The Chlamydomonas genome reveals the evolution of key animal and plant functions. *Science*, 318(5848), 245–250.
- Mészáros, B., Erdos, G., and Dosztányi, Z. (2018). IUPred2A: context-dependent prediction of protein disorder as a function of redox state and protein binding. *Nucleic acids research*, 46(W1), W329–W337.
- Meyer, M.T., Genkov, T., Skepper, J.N., Jouhet, J., Mitchell, M.C., Spreitzer, R.J., and Griffiths, H. (2012). Rubisco small-subunit α -helices control pyrenoid formation in Chlamydomonas. *Proceedings of the National Academy of Sciences of the United States of America*, 109(47), 19474–19479.
- Meyer, M.T., Itakura, A.K., Patena, W., Wang, L., He, S., Emrich-Mills, T., Lau, C.S., Yates, G., Mackinder, L.C.M., and Jonikas, M.C. (2020). Assembly of the algal CO₂-fixing organelle, the pyrenoid, is guided by a Rubisco-binding motif. *Science advances*, 6(46), eabd2408.
- Meyer, M.T., McCormick, A.J., and Griffiths, H. (2016). Will an algal CO₂-concentrating mechanism work in higher plants? *Current opinion in plant biology*, 31, 181–188.
- Meyer, M.T., Whittaker, C., and Griffiths, H. (2017). The algal pyrenoid: key unanswered questions. *Journal of experimental botany*, 68(14), 3739–3749.
- Mitchell, M.C., Meyer, M.T., and Griffiths, H. (2014). Dynamics of carbon-concentrating mechanism induction and protein relocalization during the dark-to-light transition in synchronized Chlamydomonas reinhardtii. *Plant physiology*, 166(2), 1073–1082.
- Mitrea, D.M. and Kriwacki, R.W. (2016). Phase separation in biology; functional organization of a higher order. *Cell communication and signaling*, 14, 1.
- Miura, K., Yamano, T., Yoshioka, S., Kohinata, T., Inoue, Y., Taniguchi, F., Asamizu, E., Nakamura, Y., Tabata, S., Yamato, K.T., Ohyama, K., and Fukuzawa, H. (2004). Expression profiling-based identification of CO₂-responsive genes regulated by CCM1 controlling a carbon-concentrating mechanism in Chlamydomonas reinhardtii. *Plant physiology*, 135(3), 1595–1607.
- Momayyezi, M., McKown, A.D., Bell, S.C.S., and Guy, R.D. (2020). Emerging roles for carbonic anhydrase in mesophyll conductance and photosynthesis. *The Plant Journal*, 101(4), 831–844.

- Moroney, J.V. and Ynalvez, R.A. (2007). Proposed carbon dioxide concentrating mechanism in *Chlamydomonas reinhardtii*. *Eukaryotic cell*, 6(8), 1251–1259.
- Mukherjee, A., Lau, C.S., Walker, C.E., Rai, A.K., Prejean, C.I., Yates, G., Emrich-Mills, T., Lemoine, S.G., Vinyard, D.J., Mackinder, L.C.M., and Moroney, J.V. (2019). Thylakoid localized bestrophin-like proteins are essential for the CO₂ concentrating mechanism of *Chlamydomonas reinhardtii*. *Proceedings of the National Academy of Sciences of the United States of America*, 116(34), 16915–16920.
- Narayanaswamy, R., Levy, M., Tsechansky, M., Stovall, G.M., O’Connell, J.D., Mirrielees, J., Ellington, A.D., and Marcotte, E.M. (2009). Widespread reorganization of metabolic enzymes into reversible assemblies upon nutrient starvation. *Proceedings of the National Academy of Sciences of the United States of America*, 106(25), 10147–10152.
- Nishimura, K., Kato, Y., and Sakamoto, W. (2017). Essentials of Proteolytic Machineries in Chloroplasts. *Molecular plant*, 10(1), 4–19.
- Ohnishi, N., Mukherjee, B., Tsujikawa, T., Yanase, M., Nakano, H., Moroney, J.V, and Fukuzawa, H. (2010). Expression of a Low CO₂-Inducible Protein, LCI1, Increases Inorganic Carbon Uptake in the Green Alga *Chlamydomonas reinhardtii*. *The Plant cell*, 22(9), 3105-3117.
- O’Neill, E.C., Stevenson, C.E.M., Tantanarat, K., Latousakis, D., Donaldson, M.I., Rejzek, M., Nepogodiev, S.A., Limpaseni, T., Field, R.A., and Lawson, D.M. (2015). Structural Dissection of the Maltodextrin Disproportionation Cycle of the Arabidopsis Plastidial Disproportionating Enzyme 1 (DPE1). *The Journal of biological chemistry*, 290(50), 29834–29853.
- Onishi, M., Umen, J.G., Cross, F.R., and Pringle, J.R. (2020). Cleavage-furrow formation without F-actin in *Chlamydomonas*. *Proceedings of the National Academy of Sciences of the United States of America*, 117(31), 18511–18520.
- Owen, I. and Shewmaker, F. (2019). The Role of Post-Translational Modifications in the Phase Transitions of Intrinsically Disordered Proteins. *International journal of molecular sciences*, 20(21), 5501, doi: 10.3390/ijms20215501.
- Patel, A., Malinowska, L., Saha, S., Wang, J., Alberti, S., Krishnan, Y., and Hyman, A.A. (2017). ATP as a biological hydrotrope. *Science*, 356(6339), 753–756.

- Penninga, D., Strokopytov, B., Rozeboom, H.J., Lawson, C.L., Dijkstra, B.W., Bergsma, J., and Dijkhuizen, L. (1995). Site-directed mutations in tyrosine 195 of cyclodextrin glycosyltransferase from *Bacillus circulans* strain 251 affect activity and product specificity. *Biochemistry*, 34(10), 3368–3376.
- Peterhansel, C., Horst, I., Niessen, M., Blume, C., Kebeish, R., Kürkcüoğlu, S., and Kreuzaler, F. (2010). Photorespiration. *The Arabidopsis book*, 8, e0130.
- Pfister, B. and Zeeman, S.C. (2016). Formation of starch in plant cells. *Cellular and molecular life sciences*, 73(14), 2781–2807.
- Phair, R.D., Gorski, S.A., and Misteli, T. (2004). Measurement of dynamic protein binding to chromatin in vivo, using photobleaching microscopy. *Methods in enzymology*, 375, 393–414.
- Polge, C. and Thomas, M. (2007). SNF1/AMPK/SnRK1 kinases, global regulators at the heart of energy control? *Trends in plant science*, 12(1), 20–28.
- Portis, A.R., Jr (2003). Rubisco activase - Rubisco's catalytic chaperone. *Photosynthesis research*, 75(1), 11–27.
- Qu, Z. and Hartzell, H.C. (2008). Bestrophin Cl⁻ channels are highly permeable to HCO₃⁻. *American Journal of Physiology-Cell Physiology*, 294(6), C1371–C1377.
- Ragel, P., Streb, S., Feil, R., Sahrawy, M., Annunziata, M.G., Lunn, J.E., Zeeman, S., and Mérida, Á. (2013). Loss of starch granule initiation has a deleterious effect on the growth of arabidopsis plants due to an accumulation of ADP-glucose. *Plant physiology*, 163(1), 75–85.
- Ral, J.-P., Derelle, E., Ferraz, C., Wattebled, F., Farinas, B., Corellou, F., Buléon, A., Slomianny, M.-C., Delvalle, D., d'Hulst, C., Rombauts, S., Moreau, H., and Ball, S. (2004). Starch division and partitioning. A mechanism for granule propagation and maintenance in the picophytoplanktonic green alga *Ostreococcus tauri*. *Plant physiology*, 136(2), 3333–3340.
- Ramazanov, Z., Rawat, M., Henk, M.C., Mason, C.B., Matthews, S.W., and Moroney, J.V. (1994). The induction of the CO₂-concentrating mechanism is correlated with the formation of the starch sheath around the pyrenoid of *Chlamydomonas reinhardtii*. *Planta*, 195(2), 210–216.

- Ray, D.K., Mueller, N.D., West, P.C., and Foley, J.A. (2013). Yield Trends Are Insufficient to Double Global Crop Production by 2050. *PLoS one*, 8(6), e66428.
- Raynaud, S., Ragel, P., Rojas, T., and Mérida, Á. (2016). The N-terminal Part of Arabidopsis thaliana Starch Synthase 4 Determines the Localization and Activity of the Enzyme. *The Journal of biological chemistry*, 291(20), 10759–10771.
- Recuenco-Muñoz, L., Offre, P., Valledor, L., Lyon, D., Weckwerth, W., and Wienkoop, S. (2015). Targeted quantitative analysis of a diurnal RuBisCO subunit expression and translation profile in Chlamydomonas reinhardtii introducing a novel Mass Western approach. *Journal of proteomics*, 113, 143–153.
- Reinfelder, J.R. (2011). Carbon concentrating mechanisms in eukaryotic marine phytoplankton. *Annual review of marine science*, 3, 291–315.
- Reits, E.A. and Neefjes, J.J. (2001). From fixed to FRAP: measuring protein mobility and activity in living cells. *Nature cell biology*, 3(6), E145–7.
- Rekas, A., Alattia, J.-R., Nagai, T., Miyawaki, A., and Ikura, M. (2002). Crystal structure of venus, a yellow fluorescent protein with improved maturation and reduced environmental sensitivity. *The Journal of biological chemistry*, 277(52), 50573–50578.
- Ritte, G., Heydenreich, M., Mahlow, S., Haebel, S., Kötting, O., and Steup, M. (2006). Phosphorylation of C6- and C3-positions of glucosyl residues in starch is catalysed by distinct dikinases. *FEBS letters*, 580(20), 4872–4876.
- Roldán, I., Wattedled, F., Mercedes Lucas, M., Delvallé, D., Planchot, V., Jiménez, S., Pérez, R., Ball, S., d’Hulst, C., and Mérida, Á. (2007). The phenotype of soluble starch synthase IV defective mutants of Arabidopsis thaliana suggests a novel function of elongation enzymes in the control of starch granule formation. *The Plant Journal*, 49(3), 492–504.
- Rolland, F., Baena-Gonzalez, E., and Sheen, J. (2006). Sugar sensing and signaling in plants: conserved and novel mechanisms. *Annual review of plant biology*, 57, 675–709.
- Rose, A. and Meier, I. (2004). Scaffolds, levers, rods and springs: diverse cellular functions of long coiled-coil proteins. *Cellular and molecular life sciences*, 61(16), 1996–2009.
- Ross, J., Li, Y., Lim, E., and Bowles, D.J. (2001). Higher plant glycosyltransferases. *Genome biology*, 2(2), 3004.

- Ruiz-Gayosso, A., Rodríguez-Sotres, R., Martínez-Barajas, E., and Coello, P. (2018). A role for the carbohydrate-binding module (CBM) in regulatory SnRK1 subunits: the effect of maltose on SnRK1 activity. *The Plant Journal*, 96(1), 163–175.
- Sage, R.F., Pearcy, R.W., and Seemann, J.R. (1987). The nitrogen use efficiency of C3 and C4 plants: III. Leaf nitrogen effects on the activity of carboxylating enzymes in *Chenopodium album* (L.) and *Amaranthus retroflexus*. *Plant physiology*, 85, 355-359.
- Santelia, D., Kötting, O., Seung, D., Schubert, M., Thalmann, M., Bischof, S., Meekins, D.A., Lutz, A., Patron, N., Gentry, M.S., Allain, F.H.-T., and Zeeman, S.C. (2011). The phosphoglucan phosphatase like sex Four2 dephosphorylates starch at the C3-position in *Arabidopsis*. *The Plant cell*, 23(11), 4096–4111.
- Sarov, M., Schneider, S., Pozniakovski, A., Roguev, A., Ernst, S., Zhang, Y., Hyman, A.A., and Stewart, A.F. (2006). A recombineering pipeline for functional genomics applied to *Caenorhabditis elegans*. *Nature methods*, 3(10), 839–844.
- Schindelin, J., Arganda-Carreras, I., Frise, E., Kaynig, V., Longair, M., Pietzsch, T., Preibisch, S., Rueden, C., Saalfeld, S., Schmid, B., Tinevez, J.-Y., White, D.J., Hartenstein, V., Eliceiri, K., Tomancak, P., and Cardona, A. (2012). Fiji: an open-source platform for biological-image analysis. *Nature methods*, 9(7), 676-682.
- Schroda, M. (2019). Good News for Nuclear Transgene Expression in *Chlamydomonas*. *Cells*, 8(12), 1534.
- Seung, D., Thalmann, M., Sparla, F., Abou Hachem, M., Lee, S.K., Issakidis-Bourguet, E., Svensson, B., Zeeman, S.C., and Santelia, D. (2013). *Arabidopsis thaliana* AMY3 is a unique redox-regulated chloroplastic α -amylase. *The Journal of biological chemistry*, 288(47), 33620–33633.
- Seung, D., Soyk, S., Coiro, M., Maier, B.A., Eicke, S., and Zeeman, S.C. (2015). PROTEIN TARGETING TO STARCH is required for localising GRANULE-BOUND STARCH SYNTHASE to starch granules and for normal amylose synthesis in *Arabidopsis*. *PLoS biology*, 13(2), e1002080.
- Seung, D., Lu, K.-J., Stettler, M., Streb, S., and Zeeman, S.C. (2016). Degradation of Glucan Primers in the Absence of Starch Synthase 4 Disrupts Starch Granule Initiation in *Arabidopsis*. *The Journal of biological chemistry*, 291(39), 20718–20728.

- Seung, D., Boudet, J., Monroe, J., Schreier, T.B., David, L.C., Abt, M., Lu, K.-J., Zanella, M., and Zeeman, S.C. (2017). Homologs of PROTEIN TARGETING TO STARCH Control Starch Granule Initiation in Arabidopsis Leaves. *The Plant cell*, 29(7), 1657–1677.
- Seung, D., Schreier, T.B., Bürgy, L., Eicke, S., and Zeeman, S.C. (2018). Two Plastidial Coiled-Coil Proteins Are Essential for Normal Starch Granule Initiation in Arabidopsis. *The Plant cell*, 30(7), 1523–1542.
- Seung, D. and Smith, A.M. (2019). Starch granule initiation and morphogenesis-progress in Arabidopsis and cereals. *Journal of experimental botany*, 70(3), 771–784.
- Sheahan, M.B., Rose, R.J., and McCurdy, D.W. (2004). Organelle inheritance in plant cell division: the actin cytoskeleton is required for unbiased inheritance of chloroplasts, mitochondria and endoplasmic reticulum in dividing protoplasts. *The Plant Journal*, 37(3), 379–390.
- Sinetova, M.A., Kupriyanova, E.V., Markelova, A.G., Allakhverdiev, S.I., and Pronina, N.A. (2012). Identification and functional role of the carbonic anhydrase Cah3 in thylakoid membranes of pyrenoid of *Chlamydomonas reinhardtii*. *Biochimica et biophysica acta*, 1817(8), 1248–1255.
- Skeffington, A.W., Graf, A., Duxbury, Z., Gruissem, W., and Smith, A.M. (2014). Glucan, Water Dikinase Exerts Little Control over Starch Degradation in Arabidopsis Leaves at Night. *Plant Physiology*, 165(2), 866–879.
- Smith, A.M., Denyer, K., and Martin, C. (1997). THE SYNTHESIS OF THE STARCH GRANULE. *Annual review of plant physiology and plant molecular biology*, 48, 67–87.
- Smith, A.M. and Zeeman, S.C. (2020). Starch: A Flexible, Adaptable Carbon Store Coupled to Plant Growth. *Annual review of plant biology*, 71, 217-245.
- Smith, M.W. and Doolittle, R.F. (1992). Anomalous phylogeny involving the enzyme glucose-6-phosphate isomerase. *Journal of molecular evolution*, 34(6), 544–545.
- Smith, S.M., Fulton, D.C., Chia, T., Thorneycroft, D., Chapple, A., Dunstan, H., Hylton, C., Zeeman, S.C., and Smith, A.M. (2004). Diurnal changes in the transcriptome encoding enzymes of starch metabolism provide evidence for both transcriptional and posttranscriptional regulation of starch metabolism in Arabidopsis leaves. *Plant physiology*, 136(1), 2687–2699.

- Spalding, M. H. (2008). Microalgal carbon-dioxide-concentrating mechanisms: Chlamydomonas inorganic carbon transporters. *Journal of experimental botany*, 59(7), 1463–1473.
- Spalding, M.H., Spreitzer, R.J., and Ogren, W.L. (1983a). Carbonic Anhydrase-Deficient Mutant of Chlamydomonas reinhardtii Requires Elevated Carbon Dioxide Concentration for Photoautotrophic Growth. *Plant physiology*, 73(2), 268–272.
- Spalding, M.H., Spreitzer, R.J., and Ogren, W.L. (1983b). Reduced Inorganic Carbon Transport in CO₂-Requiring Mutant of Chlamydomonas reinhardtii. *Plant physiology*, 73, 273–276.
- Stanley, D., Fitzgerald, A.M., Farnden, K.J.F., and MacRae, E.A. (2002). Characterisation of putative alpha-amylases from apple (*Malus domestica*) and *Arabidopsis thaliana*. *Biologia, Bratislava*, 57(11), 137–148.
- Stanton, J.B., Goldberg, A.F.X., Hoppe, G., Marmorstein, L.Y., and Marmorstein, A.D. (2006). Hydrodynamic properties of porcine bestrophin-1 in Triton X-100. *Biochimica et biophysica acta*, 1758(2), 241–247.
- Stein, O. and Granot, D. (2019). An Overview of Sucrose Synthases in Plants. *Frontiers in plant science*, 10, 95.
- Streb, S., Delatte, T., Umhang, M., Eicke, S., Schorderet, M., Reinhardt, D., and Zeeman, S.C. (2008). Starch granule biosynthesis in Arabidopsis is abolished by removal of all debranching enzymes but restored by the subsequent removal of an endoamylase. *The Plant cell*, 20(12), 3448–3466.
- Streb, S., Egli, B., Eicke, S., and Zeeman, S.C. (2009). The debate on the pathway of starch synthesis: a closer look at low-starch mutants lacking plastidial phosphoglucomutase supports the chloroplast-localized pathway. *Plant physiology*, 151(4), 1769–1772.
- Streb, S. and Zeeman, S.C. (2012). Starch metabolism in Arabidopsis. *The Arabidopsis book*, 10, e0160.
- Strenkert, D., Schmollinger, S., Gallaher, S.D., Salomé, P.A., Purvine, S.O., Nicora, C.D., Mettler-Altmann, T., Soubeyrand, E., Weber, A.P.M., Lipton, M.S., Basset, G.J., and Merchant, S.S. (2019). Multiomics resolution of molecular events during a day in the life of Chlamydomonas. *Proceedings of the National Academy of Sciences of the United States of America*, 116(6), 2374–2383.

- Stryer, L. (1978). Fluorescence energy transfer as a spectroscopic ruler. *Annual review of biochemistry*, 47, 819–846.
- Sueoka, N. (1960). MITOTIC REPLICATION OF DEOXYRIBONUCLEIC ACID IN CHLAMYDOMONAS REINHARDI. *Proceedings of the National Academy of Sciences of the United States of America*, 46(1), 83–91.
- Sun, H., Tsunenari, T., Yau, K.-W., and Nathans, J. (2002). The vitelliform macular dystrophy protein defines a new family of chloride channels. *Proceedings of the National Academy of Sciences of the United States of America*, 99(6), 4008–4013.
- Tabata, S., Hizukuri, S., and Nagata, K. (1978). Action of sweet-potato beta-amylase on phosphodextrin of potato starch. *Carbohydrate Research*, 67(1), 189–195.
- Tabita, F.R., Satagopan, S., Hanson, T.E., Kreef, N.E., and Scott, S.S. (2008). Distinct form I, II, III, and IV Rubisco proteins from the three kingdoms of life provide clues about Rubisco evolution and structure/function relationships. *Journal of experimental botany*, 59(7), 1515–1524.
- Takizawa, K., Cruz, J.A., Kanazawa, A., and Kramer, D.M. (2007). The thylakoid proton motive force in vivo. Quantitative, non-invasive probes, energetics, and regulatory consequences of light-induced pmf. *Biochimica et biophysica acta*, 1767(10), 1233–1244.
- Taylor, T.C., Backlund, A., Bjorhall, K., Spreitzer, R.J., and Andersson, I. (2001). First crystal structure of Rubisco from a green alga, *Chlamydomonas reinhardtii*. *The Journal of biological chemistry*, 276(51), 48159–48164.
- Tetlow, I.J., Morell, M.K., and Emes, M.J. (2004). Recent developments in understanding the regulation of starch metabolism in higher plants. *Journal of experimental botany*, 55(406), 2131–2145.
- Thyssen, C., Hermes, M., and Sültemeyer, D. (2003). Isolation and characterisation of *Chlamydomonas reinhardtii* mutants with an impaired CO₂-concentrating mechanism. *Planta*, 217(1), 102–112.
- Thyssen, C., Schlichting, R., and Giersch, C. (2001). The CO₂-concentrating mechanism in the physiological context: lowering the CO₂ supply diminishes culture growth and economises starch utilisation in *Chlamydomonas reinhardtii*. *Planta*, 213(4), 629–639.

- Tilman, D., Balzer, C., Hill, J., and Befort, B.L. (2011). Global food demand and the sustainable intensification of agriculture. *Proceedings of the National Academy of Sciences of the United States of America*, 108(50), 20260–20264.
- Toyokawa, C., Yamano, T., and Fukuzawa, H. (2020). Pyrenoid Starch Sheath Is Required for LCIB Localization and the CO₂-Concentrating Mechanism in Green Algae. *Plant physiology*, 182(4), 1883–1893.
- Tsunenari, T., Sun, H., Williams, J., Cahill, H., Smallwood, P., Yau, K.-W., and Nathans, J. (2003). Structure-function analysis of the bestrophin family of anion channels. *The Journal of biological chemistry*, 278(42), 41114–41125.
- Turkina, M.V., Blanco-Rivero, A., Vainonen, J.P., Vener, A.V., and Villarejo, A. (2006). CO₂ limitation induces specific redox-dependent protein phosphorylation in *Chlamydomonas reinhardtii*. *Proteomics*, 6, 2693–2704.
- Villarejo, A., Martinez, F., Pino Plumed, M., and Ramazanov, Z. (1996). The induction of the CO₂ concentrating mechanism in a starch-less mutant of *Chlamydomonas reinhardtii*. *Physiologia plantarum*, 98(4), 798–802.
- Vitha, S., McAndrew, R.S., and Osteryoung, K.W. (2001). FtsZ ring formation at the chloroplast division site in plants. *The Journal of cell biology*, 153(1), 111–120.
- Vítová, M., Bišová, K., Umysová, D., Hlavová, M., Kawano, S., Zachleder, V., and Čížková, M. (2011). *Chlamydomonas reinhardtii*: duration of its cell cycle and phases at growth rates affected by light intensity. *Planta*, 234, 599-608.
- Wal, van. de. M. (2000). Amylose biosynthesis in potato: interaction between substrate availability and GBSSI activity, regulated at the allelic level. *Wageningen University & Research Centre*, Doctoral Thesis, 33-45.
- Wang, H., Gau, B., Slade, W.O., Juergens, M., Li, P., and Hicks, L.M. (2014a). The global phosphoproteome of *Chlamydomonas reinhardtii* reveals complex organellar phosphorylation in the flagella and thylakoid membrane. *Molecular & cellular proteomics*, 13(9), 2337–2353.
- Wang, J.T., Smith, J., Chen, B.-C., Schmidt, H., Rasoloson, D., Paix, A., Lambrus, B.G., Calidas, D., Betzig, E., and Seydoux, G. (2014b). Regulation of RNA granule dynamics by phosphorylation of serine-rich, intrinsically disordered proteins in *C. elegans*. *eLife*, 3, e04591.

- Wang, L., Yamano, T., Takane, S., Niikawa, Y., Toyokawa, C., Ozawa, S.-I., Tokutsu, R., Takahashi, Y., Minagawa, J., Kanesaki, Y., Yoshikawa, H., and Fukuzawa, H. (2016). Chloroplast-mediated regulation of CO₂-concentrating mechanism by Ca²⁺-binding protein CAS in the green alga *Chlamydomonas reinhardtii*. *Proceedings of the National Academy of Sciences of the United States of America*, 113(44), 12586–12591.
- Wang, Y. and Spalding, M.H. (2006). An inorganic carbon transport system responsible for acclimation specific to air levels of CO₂ in *Chlamydomonas reinhardtii*. *Proceedings of the National Academy of Sciences*, 103(26), 10110–10115.
- Wang, Y. and Spalding, M.H. (2014). Acclimation to very low CO₂: contribution of limiting CO₂ inducible proteins, LCIB and LCIA, to inorganic carbon uptake in *Chlamydomonas reinhardtii*. *Plant physiology*, 166(4), 2040–2050.
- Wang, Y., Stessman, D.J., and Spalding, M.H. (2015). The CO₂ concentrating mechanism and photosynthetic carbon assimilation in limiting CO₂: how *Chlamydomonas* works against the gradient. *The Plant journal: for cell and molecular biology*, 82(3), 429–448.
- Wattebled, F., Buléon, A., Bouchet, B., Ral, J.-P., Liénard, L., Delvallé, D., Binderup, K., Dauvillée, D., Ball, S., and d'Hulst, C. (2002). Granule-bound starch synthase I: A major enzyme involved in the biogenesis of B-crystallites in starch granules. *European journal of biochemistry*, 269(15), 3810–3820.
- Wattebled, F., Dong, Y., Dumez, S., Delvallé, D., Planchot, V., Berbezy, P., Vyas, D., Colonna, P., Chatterjee, M., Ball, S., and D'Hulst, C. (2005). Mutants of *Arabidopsis* lacking a chloroplastic isoamylase accumulate phytyloglycogen and an abnormal form of amylopectin. *Plant physiology*, 138(1), 184–195.
- Wheeler, R.J. and Hyman, A.A. (2018). Controlling compartmentalization by non-membrane-bound organelles. *Philosophical transactions of the Royal Society of London. Series B, Biological sciences*, 373(1747), 20170193.
- Whitney, S.M., Houtz, R.L., and Alonso, H. (2011). Advancing our understanding and capacity to engineer nature's CO₂-sequestering enzyme, Rubisco. *Plant physiology*, 155(1), 27–35.
- Wunder, T., Cheng, S.L.H., Lai, S.-K., Li, H.-Y., and Mueller-Cajar, O. (2018). The phase separation underlying the pyrenoid-based microalgal Rubisco supercharger. *Nature communications*, 9(1), 5076.

- Wunder, T., Oh, Z.G., and Mueller-Cajar, O. (2019). CO₂ -fixing liquid droplets: towards a dissection of the microalgal pyrenoid. *Traffic*, 20, 380-389.
- Xiao, Q., Yu, K., Cui, Y.-Y., and Hartzell, H.C. (2009). Dysregulation of human bestrophin-1 by ceramide-induced dephosphorylation. *The Journal of physiology*, 587, 4379–4391.
- Yamano, T., Tsujikawa, T., Hatano, K., Ozawa, S.-I., Takahashi, Y., and Fukuzawa, H. (2010). Light and Low-CO₂-Dependent LCIB–LCIC Complex Localization in the Chloroplast Supports the Carbon-Concentrating Mechanism in *Chlamydomonas reinhardtii*. *Plant & cell physiology*, 51(9), 1453–1468.
- Yamano, T., Sato, E., Iguchi, H., Fukuda, Y., and Fukuzawa, H. (2015). Characterization of cooperative bicarbonate uptake into chloroplast stroma in the green alga *Chlamydomonas reinhardtii*. *Proceedings of the National Academy of Sciences of the United States of America*, 112(23), 7315–7320.
- Yamano, T., Miura, K., and Fukuzawa, H. (2008). Expression analysis of genes associated with the induction of the carbon-concentrating mechanism in *Chlamydomonas reinhardtii*. *Plant physiology*, 147(1), 340–354.
- Yang, C., Hua, Q., and Shimizu, K. (2000). Energetics and carbon metabolism during growth of microalgal cells under photoautotrophic, mixotrophic and cyclic light-autotrophic/dark-heterotrophic conditions. *Biochemical engineering journal*, 6(2), 87–102.
- Yang, T., Liu, Q., Kloss, B., Bruni, R., Kalathur, R.C., Guo, Y., Kloppmann, E., Rost, B., Colecraft, H.M., and Hendrickson, W.A. (2014). Structure and selectivity in bestrophin ion channels. *Science*, 346(6207), 355–359.
- Yu, D., Ellis, H.M., Lee, E.C., Jenkins, N.A., Copeland, N.G., and Court, D.L. (2000). An efficient recombination system for chromosome engineering in *Escherichia coli*. *Proceedings of the National Academy of Sciences of the United States of America*, 97(11), 5978–5983.
- Yu, T.-S., Kofler, H., Häusler, R.E., Hille, D., Flügge, U.I., Zeeman, S.C., Smith, A.M., Kossmann, J., Lloyd, J., Ritte, G., Steup, M., Lue, W.L., Chen, J., and Weber, A. (2001). The *Arabidopsis* *sex1* mutant is defective in the R1 protein, a general regulator of starch degradation in plants, and not in the chloroplast hexose transporter. *The Plant cell*, 13(8), 1907–1918.

- Yu, T.-S., Zeeman, S.C., Thorneycroft, D., Fulton, D.C., Dunstan, H., Lue, W.-L., Hegemann, B., Tung, S.-Y., Umemoto, T., Chapple, A., Tsai, D.-L., Wang, S.-M., Smith, A.M., Chen, J., and Smith, S.M. (2005). α -Amylase Is Not Required for Breakdown of Transitory Starch in Arabidopsis Leaves. *The Journal of biological chemistry*, 280(11), 9773–9779.
- Zeeman, S.C., Thorneycroft, D., Schupp, N., Chapple, A., Weck, M., Dunstan, H., Haldimann, P., Bechtold, N., Smith, A.M., and Smith, S.M. (2004). Plastidial α -Glucan Phosphorylase Is Not Required for Starch Degradation in Arabidopsis Leaves But Has a Role in the Tolerance of Abiotic Stress. *Plant physiology*, 135(2), 849–858.
- Zhang, X., Szydlowski, N., Delvallé, D., D’Hulst, C., James, M.G., and Myers, A.M. (2008). Overlapping functions of the starch synthases SSII and SSIII in amylopectin biosynthesis in Arabidopsis. *BMC plant biology*, 8, 96.
- Zhan, Y., Marchand, C.H., Maes, A., Mauries, A., Sun, Y., Dhaliwal, J.S., Uniacke, J., Arragain, S., Jiang, H., Gold, N.D., Martin, V.J.J., Lemaire, S.D., and Zerges, W. (2018). Pyrenoid functions revealed by proteomics in *Chlamydomonas reinhardtii*. *PLoS one*, 13(2), e0185039.
- Zimmermann, L., Stephens, A., Nam, S.-Z., Rau, D., Kübler, J., Lozajic, M., Gabler, F., Söding, J., Lupas, A.N., and Alva, V. (2018). A Completely Reimplemented MPI Bioinformatics Toolkit with a New HHpred Server at its Core. *Journal of molecular biology*, 430(15), 2237–2243.
- Zones, J.M., Blaby, I.K., Merchant, S.S., and Umen, J.G. (2015). High-Resolution Profiling of a Synchronized Diurnal Transcriptome from *Chlamydomonas reinhardtii* Reveals Continuous Cell and Metabolic Differentiation. *The Plant cell*, 27(10), 2743–2769.